

[Zur Homepage der Dissertation](#)

Neural models of modulation frequency analysis in the auditory system

Von der Fakultät für Mathematik und Naturwissenschaften
der Carl von Ossietzky Universität Oldenburg
zur Erlangung des Grades, Titels und der Würde einer
Doktorin der Naturwissenschaften (Dr. rer. nat.)
angenommene Dissertation

Ulrike Dicke

Erstreferent: Prof. Dr. Dr. Birger Kollmeier

Korreferent: Prof. Dr. Volker Mellert

Tag der Disputation: 17. Dezember 2003

Pongileoni's blowing and the scraping of the anonymous fiddlers had shaken the air in the great hall, had set the glass of the windows looking on to it vibrating; and this in turn had shaken the air in Lord Edward's apartment on the further side. The shaking air rattled Lord Edward's membrana tympani; the interlocked malleus, incus and stirrup bones were set in motion infinitesimal storm in the fluid of the labyrinth. The hairy endings of the auditory nerve shuddered like weeds in a rough sea; a vast number of obscure miracles were performed in the brain, and Lord Edwards ecstatically whispered 'Bach'!

[Aldous Huxley, *Point Counter Point*, 1928]

CONTENTS

1	GENERAL INTRODUCTION	7
2	A FUNCTIONAL POINT-NEURON MODEL SIMULATING COCHLEAR NUCLEUS O_I-UNIT RESPONSES	11
2.1	INTRODUCTION	12
2.2	MODEL STRUCTURE	16
2.2.1	Auditory periphery	16
2.2.2	Model dynamics	17
2.3	SIMULATIONS AND DATA ANALYSIS	19
2.3.1	Pure-tone stimuli	20
2.3.2	Current stimulation	22
2.3.3	Amplitude modulated stimuli	25
2.3.4	Harmonic tone complexes	27
2.4	DISCUSSION	28
2.4.1	Alternative mechanisms suggested to account for octopus cell response properties	28
2.4.2	Intracellular properties of octopus cells	29
2.4.3	Simplifications made in the present model	30
2.5	SUMMARY AND CONCLUSION	33
3	A NEURAL CIRCUIT OF MODULATION BANDPASS FILTERS IN THE IC BASED ON O_I-UNIT RESPONSES OF THE CN: PROCESSING OF SAM TONES	35
3.1	INTRODUCTION	37
3.2	MODEL STRUCTURE	41
3.2.1	Auditory periphery	43
3.2.2	Neuron dynamics	44
3.3	SIMULATIONS AND DATA ANALYSIS	48
3.3.1	EN unit responses	48
3.3.2	CR unit responses	49

3.3.3	LP unit responses	52
3.3.4	BP unit responses	53
3.3.5	Simulation of amplitude modulation filters	54
3.3.6	Level dependence and modulation depth	55
3.4	DISCUSSION	57
3.4.1	Biological plausibility of the present model	57
3.4.2	Alternative mechanisms	58
3.4.3	Implications of the present model	59
3.5	SUMMARY AND CONCLUSION	61
4	AN ADVANCED NEURAL MODEL FOR THE PERIODICITY ANALYSIS OF COMPLEX SOUNDS	63
4.1	INTRODUCTION	65
4.2	MODEL STRUCTURE	68
4.2.1	Auditory periphery and Neuron dynamics	70
4.3	SIMULATIONS AND DATA ANALYSIS	72
4.3.1	The EN model units	73
4.3.2	Characteristics of bandpass modulation filters	75
4.3.3	Coding of modulation depth	76
4.3.4	Processing of complex envelope waveforms	77
4.3.5	Processing of two-component AM	78
4.3.6	Processing of narrowband noise	80
4.3.7	Processing of iterated rippled noise	82
4.4	DISCUSSION	84
4.4.1	The model EN units	84
4.4.2	The modulation filters of the present model	85
4.4.3	Restrictions of the present model	86
4.4.4	Suggestions for physiological experiments	88
4.5	SUMMARY AND CONCLUSION	89
5	SUMMARY AND CONCLUSION	91
	REFERENCES	95
	CURRICULUM VITAE	103
	DANKSAGUNG	105
	ERKLÄRUNG	107

CHAPTER 1

GENERAL INTRODUCTION

The mammalian auditory system is a highly complex processing pathway that extracts perceptually relevant information from acoustic signals in order to achieve a meaningful representation of the acoustic environment. Periodic amplitude modulations (AM) are a physical sound feature produced by many natural sound sources. They can be used by the auditory system in a variety of higher-order auditory tasks, including speech perception (e.g. [Rosen, 1992](#)), pitch perception (e.g. [Schouten *et al.*, 1962](#); [De Boer, 1976](#)) and auditory scene analysis ([Bregman, 1990](#)). Thus, knowledge about how the auditory system extracts, encodes and processes AM information would allow for a better understanding of such complex auditory processes. Electrophysiological recordings and psychophysical experiments represent two fundamentally different approaches towards an understanding of how acoustic information is processed by the auditory system. While electrophysiological recordings provide detailed information about the responses of distinct neuron types to AM stimuli, psychophysical experiments reveal information about possible functional AM processing strategies of the auditory system. The gap between experimental findings from these two approaches might be bridged by neural models that employ biologically motivated neural response types in order to perform a functional processing of perceptually relevant information. The present modeling study may thus help to characterize the information processing strategies of the auditory system.

Besides gaining further insight into how the auditory system extracts and encodes perceptually relevant information, biologically motivated models might also supply future architectures for technical applications as, for example, speech recognition systems, digital hearing aids, or audio coding schemes. Since there is no man-made system performing auditory processing more successfully and robustly than the auditory system, it presumably provides the best target system for developing technical solutions for the processing of acoustic information.

The present modeling study suggests a biologically motivated neural mechanism of how amplitude modulation information might be extracted and encoded by the auditory system. The model is motivated by findings from electrophysiological experiments suggesting that AM information is encoded temporally by neural activity patterns at early processing stages and transformed into a rate-based representation of AM information at higher processing stages. Auditory-nerve (AN) fibers are not selective to a certain modulation frequency in terms of their spike rate (e.g. [Rose and Capranica, 1985](#); [Joris and Yin, 1992](#)). Instead, AM information is inherent in their interspike intervals (ISI) ([Rose, 1970](#); [Evans, 1978](#)) and thus encoded in temporal activity patterns at this stage. Neurons at the level of the cochlear nucleus (CN) exhibit a similar AM information encoding strategy. While the majority of neurons in the CN display flat or low-pass shaped rate modulation transfer functions (rMTF), reflecting the spike rate as a function of the stimulus modulation frequency (e.g. [Kim *et al.*, 1990](#); [Backoff *et al.*, 1999](#)), the temporal synchronization of CN neurons to AM stimuli even exceeds that of AN fibers. Thus, while CN neurons are not selective to a certain modulation frequency in terms of their spike rate, the temporal AM information present in the AN activity patterns seems to be enhanced by CN neurons (e.g. [Frisina *et al.*, 1990](#); [Kim *et al.*, 1990](#)). This temporal periodicity code is assumed to be transformed into a rate-based representation of periodicities between the level of the CN and the inferior colliculus (IC) based on the following observations: (i) While AN fibers and CN neurons have been found to synchronize to modulation frequencies as high as 1 kHz (e.g. [Javel, 1980](#); [Frisina *et al.*, 1990](#)), there is general agreement among authors, that the ability of neurons to synchronize to fast amplitude modulations decreases along the ascending auditory pathway ([Rees and Møller, 1983](#); [Langner and Schreiner, 1988](#)). (ii) At the level of the IC, neurons have been found that exhibit bandpass shaped rMTFs (e.g. [Langner and Schreiner, 1988](#); [Rees and Palmer, 1989](#)). Thus, these neurons are selective to a certain modulation frequency and respond with a maximum spike rate when stimulated with their so-called best modulation frequency (BMF). (iii) Neurons with different BMFs have been found to be topographically organized in the central nucleus of the IC ([Schreiner and Langner, 1988, 1997](#)).

Such a rate-based representation of AM information is also motivated by the psychophysical concept of amplitude modulation filters ([Dau *et al.*, 1997a,b](#); [Ewert and Dau, 2000](#)). This concept has been suggested to account for the modulation frequency selectivity observed in masking experiments in the modulation-frequency domain ([Bacon and Grantham, 1989](#); [Houtgast, 1989](#); [Dau *et al.*, 1997a,b](#)).

The main goal of the present thesis is to develop a neural model that transforms temporal periodicity information into a rate-based representation between the level

of the CN and the IC. Previous neural models of periodicity coding in the auditory system, as suggested by [Langner \(1981\)](#) and [Hewitt and Meddis \(1994\)](#), are limited in their ability to account for the effects of modulation frequency selectivity when tested with complex stimuli. The present neural model provides a mechanism that allows for the psychophysically observed modulation frequency selectivity while employing unit responses and a neural connectivity that correspond to electrophysiological recordings. The model is thus the first neural periodicity model that aims at bridging the gap between electrophysiological and psychophysical descriptions by suggesting a mechanism of how linear amplitude modulation filters could be shaped by the highly nonlinear auditory system.

In Chap. 2 of the present thesis a new functional point-neuron model is developed that simulates the responses of cochlear nucleus ideal onset (O_I) units. Electrophysiological recordings reveal that O_I units, morphologically associated with octopus cells, entrain to low-frequency pure tones, click trains and AM stimuli presented at repetition/modulation rates < 800 Hz (e.g. [Rhode and Smith, 1986](#); [Rhode, 1994a](#)). Since the robust synchronization of O_I units to AM stimuli is presumably the best among all major cell types in the CN ([Frisina et al., 1990](#); [Rhode, 1994a](#); [Winter and Palmer, 1995](#)), these units are assumed to play a functional role in the processing of AM information ([Golding et al., 1995](#); [Evans and Zhao, 1997](#); [Cai et al., 2001](#)). By using a biphasic postsynaptic potential in combination with a dynamic spike-blocking mechanism, the new functional O_I -unit model allows for simulating O_I -unit entrainment to a wide range of AM frequencies. The O_I -unit model that follows an integrate-to-threshold dynamic and requires only the small set of 7 parameters also allows for simulating recorded O_I -unit responses to a large set of different stimuli.

In Chap. 3, a neural circuit is described that transforms temporal periodicity information into a rate-based periodicity code between the CN and the IC. In addition to well established peripheral processing stages describing basilar membrane filtering ([Patterson et al., 1988](#)) and inner hair cell transduction (e.g. [Meddis, 1986](#)), the neural circuit consists of a CN and an IC stage. The CN stage of the model contains two different unit types, an entrainment unit, represented by the functional O_I -unit model developed in Chap. 2, and a set of units revealing flat rMTFs. Due to the neural response properties of the CN model units and the neural connectivity within the model bandpass shaped rMTFs are obtained in units of the IC model stage. Different BMFs hereby result from varying the number of CN model units projecting onto different IC model units. This mechanism fundamentally differs from the mechanisms suggested in previous neural models describing periodicity coding ([Langner, 1981](#); [Hewitt and Meddis, 1994](#)) all of which employ systematically varying temporal parameters among different model units in order to reveal different

BMFs. In contrast to previous models the range of modulation frequencies encoded by the present neural model is not limited by the biological relevance of the range of its temporal parameters.

In Chap. 4 an extended version of the neural model of periodicity coding is presented which is based on the neural circuit presented in Chap. 3. The model alterations are motivated by the limited dynamic range of modulation depths encoded by the original neural circuit which does not allow for a correct description of the processing of more complex stimuli than SAM tones. In order to allow for the increased dynamic range, a set of entrainment units is introduced whose threshold potentials are systematically varied. These threshold variations result in differences in sensitivity for entrainment model units to different modulation depths. Due to this extension, a linear dependency of the output spike rate on the modulation depths of SAM stimuli is obtained within the modulation filters of the model. Simulated responses to complex envelope waveforms are compared to results according to the psychophysically motivated envelope-power spectrum model (EPSM) that explains a large set of psychophysical findings in the modulation frequency domain (Dau *et al.*, 1999; Ewert and Dau, 2000). These comparisons reveal that the neural model accounts for a modulation frequency selectivity to complex envelope waveforms as observed in psychophysical experiments.

CHAPTER 2

A FUNCTIONAL POINT-NEURON MODEL SIMULATING COCHLEAR NUCLEUS O_I -UNIT RESPONSES

ABSTRACT

Cochlear nucleus neurons revealing ideal onset O_I -type peri-stimulus time histograms (PSTH) encode temporal features of acoustic stimuli with very high precision. These neurons may therefore be involved in the recognition of natural sounds with temporally strongly varying envelopes such as speech. A new functional point-neuron model is presented here for the simulation of O_I -unit responses. The model includes an integrate-to-threshold dynamic, an “effective” postsynaptic potential (PSP) revealing a biphasic shape, and a dynamic spike-blocking mechanism. The model is tested and compared to recordings from the literature using a variety of stimuli, including pure tones at low and high frequencies, amplitude modulated stimuli covering a wide range of modulation frequencies and levels, harmonic tone complexes, as well as depolarizing and hyperpolarizing current pulses. The model can account for the main characteristics in the data using the same small set of 7 parameters for each experimental condition. In particular, it is shown that the biphasic shape of the “effectivePSP allows for a description of the main characteristics of O_I -unit responses that can not be accounted for if coincidence detection is assumed as the basis for the observed onset response properties. The presented functional model can be used as a processing module within more complex models of auditory processing and provides a means of investigating the role of O_I units in higher-order auditory processing and perception.

2.1 INTRODUCTION

The cochlear nucleus (CN) is the first nucleus along the ascending auditory pathway in mammals, where the auditory-nerve (AN) fibers synapse on a variety of neurons with different response properties. Cochlear nucleus onset units reveal temporal response properties that differ remarkably from their auditory-nerve input. While all onset units exhibit a strong response at stimulus onset, their sustained response differs among the different unit types. Thus, onset units of the ventral cochlear nucleus (VCN) are commonly divided into three groups based on their peri-stimulus time histograms (PSTH) in response to high-frequency tone bursts: onset with late or long-lasting activity (O_L), onset with chopping (O_C), revealing two or more onset peaks, and ideal onset (O_I) (Godfrey *et al.*, 1975; Rhode and Smith, 1986; Winter and Palmer, 1995). Despite the ongoing stimulation provided by the AN fibers, O_I units show one precisely timed action potential at the tone onset followed by no or little (< 10 spikes/s) subsequent activity when stimulated at their characteristic frequency (CF) (e.g. Godfrey *et al.*, 1975; Rhode and Smith, 1986). Another remarkable feature of O_I units is their entrainment, i.e., the generation of exactly one spike per stimulus period, in response to low-frequency pure tones, click trains and amplitude modulated (AM) stimuli presented at repetition/modulation rates < 800 Hz (e.g. Rhode and Smith, 1986; Rhode, 1994a; Oertel *et al.*, 2000). The robust synchronization of O_I units in response to AM stimuli is presumably the best among all major cell types in the CN (Frisina *et al.*, 1990; Rhode, 1994a; Winter and Palmer, 1995). O_I -type PSTHs are associated with octopus cells (Kane, 1973; Godfrey *et al.*, 1975), that occupy a distinct region in the posteroventral cochlear nucleus (PVCN), called the octopus cell area. The general ability of these cells to entrain to periodic stimuli has led to the assumption that octopus cells may play an important role in the processing of amplitude modulation and pitch information (Frisina *et al.*, 1990; Golding *et al.*, 1995; Evans and Zhao, 1997; Cai *et al.*, 2001). Moreover, since octopus cells emphasize transient stimulus features like gaps and onsets, known to be important in speech processing (e.g. Stevens, 1995) as well as in auditory binding (e.g. Bregman, 1990), it has been suggested that they are also involved in these auditory tasks.

Previous models simulating octopus cell response properties suggested a number of different mechanisms that might account for octopus cell response properties. Cai *et al.* (1997, 2000, 2001) suggested a compartmental octopus cell model, that focuses on a detailed description of individual ion conductances, including a low-threshold potassium conductance as well as an inward rectifying mixed cation conductance. Both conductances have been observed in octopus cells (Golding *et al.*, 1999) and are presumed to shape their response properties. However, as mentioned by

Kalluri and Delgutte (2003b), the model appears hard to evaluate because its entrainment has not been tested in detail. Another compartmental octopus cell model, suggested by Levy and Kipke (1997) (see also Kipke and Levy, 1997; Levy and Kipke, 1998), includes morphological and electrophysiological octopus cell properties in order to investigate their role in shaping octopus cell responses. They found two inherent features dominating their model's onset response: dynamic changes in synaptic effectiveness and a dynamically changing spike threshold. Although such detailed biophysical models, with a sufficiently large number of parameters, may allow for investigating the possible mechanisms that shape the responses of octopus cells, their ability to entrain to periodic stimuli or to simulate octopus cell responses to complex stimuli is limited. Also, due to their very complex dynamics and the extensive computational load, they can probably not easily be integrated in more general auditory processing models.

In contrast to compartmental neuron models that include detailed descriptions of biophysical cell properties, the class of point-neuron models provides a more abstract description of biological neurons. Kalluri and Delgutte (2003a,b) recently presented a point-neuron model where possible common properties among neurons with O_I , O_L and O_C types of onset responses were investigated. Their model is compatible with a coincidence detector across the respective AN input fibers as it is based on short time constants together with a large number of weak synaptic inputs. Viewing octopus cells as coincidence detectors across AN input fibers became popular (i) due to the large number of high-spontaneous rate AN fibers (Liberman, 1993) that provide across-frequency excitatory AN input to octopus cells and (ii) due to their rapid membrane time constant ($< 200\mu s$) (Golding *et al.*, 1995, 1999). Moreover, it has been found that an octopus cell is activated only, if a sufficient number of AN fibers, causing small and rapid excitatory postsynaptic potentials (EPSP), are activated within a small time window of approximately 1 ms (Oertel *et al.*, 2000). Kalluri and Delgutte (2003a) found that their point-neuron coincidence-detector model produces O_L and O_C responses, depending on the choice of particular model parameters, while O_I unit responses can not be accounted for. In particular, the entrainment to low frequencies found in octopus cells can not be described by using a coincidence detector model, as hyper-entrainment (i.e, the generation of more than one spike per stimulus cycle) can not be avoided. In order to avoid hyper-entrainment, Kalluri and Delgutte extended their coincidence detector model by a spike-blocking mechanism (Kalluri and Delgutte, 2003b). Such a mechanism was originally suggested by Romand (1978) as a possible mechanism to account for O_I responses. The spike-blocking mechanism developed by Kalluri and Delgutte is activated after each spike of the neuron, preventing the generation of further spikes. This blocked state

lasts until the membrane potential (which is modeled without including a refractory potential) falls below a so-called reactivation threshold and releases the neuron from spike blocking. Kalluri and Delgutte (2003b) showed that their point neuron coincidence detector in combination with a spike-blocking mechanism accounts for most of the temporal discharge patterns for tones in O_I units, indicating that many response properties can be understood from relatively simple principles. However, pure tones probably do not reveal the true extent to which O_I units are capable of entraining to, for example, low-frequency modulations of stimuli with a broader spectrum. Thus, click trains, AM tones or harmonic tone complexes may be a better choice than pure tones for revealing the capacity for entrainment in O_I units. Moreover, due to the fixed reactivation threshold of the model by Kalluri and Delgutte, problems are likely to occur if the same range of frequencies and levels are used with these more complex stimuli.

The functional point-neuron model presented here is similar to the model by Kalluri and Delgutte (2003b) as it also uses a spike-blocking mechanism (Romand, 1978) with a fixed spike blocking release threshold. In contrast to the model by Kalluri and Delgutte (2003b), however, the model assumes a *biphasic* postsynaptic potential, referred to here as the “effective” PSP. Due to the effective PSP the stimulus is essentially high-pass filtered by the model, i.e., stimulus transients are enhanced and sustained stimulus portions are attenuated. Due to the high-pass filtering of the stimulus the model membrane potential essentially acts on the stimulus slope. In response to an AM stimulus, for example, the model membrane potential is driven towards the (fixed) spike blocking release threshold within each period of the stimulus, even if high stimulus frequencies and high levels are used. This is in contrast to a coincidence detector in combination with a spike-blocking mechanism, where the membrane potential mimics the stimulus waveforms itself, such that high stimulus frequencies or high levels might prevent the membrane potential from falling below its spike blocking release threshold within each stimulus period. However, the shape of the effective PSP is not motivated by biophysical octopus cell properties, instead it is suggested to allow for the simulation of a large variety of different O_I -unit responses.

In contrast to the octopus cell models that focus on possible biophysical mechanisms underlying the octopus cell responses, the modeling approach presented here reflects a much less detailed functional description. As the model by Kalluri and Delgutte (2003a,b), it reflects an abstract model with no direct correspondence to biophysical processes. Nevertheless, the present model attempts to cover the experimental results obtained for a variety of simple and complex stimuli that will be shown to be accounted for by the shape of the effective PSP. In the first part

of the present paper, the structure of the model and its dynamics are described. It follows an analysis of the model's capabilities when tested with pure tones, polarizing current pulses, amplitude modulated tones and harmonic tone complexes. The simulated results are compared with corresponding experimental data from the literature.

2.2 MODEL STRUCTURE

A schematic visualization of the model is shown in Fig. 2.2.

2.2.1 Auditory periphery

Basilar-membrane filtering is simulated using a bank of 128 fourth-order gammatone filters (Patterson *et al.*, 1988), with center frequencies ranging from 80 Hz to 25 kHz spaced according to the equivalent rectangular bandwidth (ERB) scale. The output of each gammatone filter serves as input to Meddis' hair-cell model (Meddis, 1986, 1988; Meddis *et al.*, 1990) that computes deterministic spike probability functions for the corresponding AN fibers in response to arbitrary stimuli¹. The current model assumes a large - but limited - number of stochastically firing AN fibers to converge on an O_I unit. Such a convergent input from a large number of AN fibers has been reported by Liberman (1993) and Oertel *et al.* (2000). The time-dependent AN input to the model is obtained from the deterministic hair-cell probability function for computational reasons. While the hair-cell probability function is assumed to reflect the summed spike activity of an *infinite* number of AN fibers a more realistic model input is obtained from applying noise to hair cell spike probability. Thus, the hair-cell probability function was multiplied, on a sample by sample basis, by a random variable equally distributed in the range [0.5...1.5]². In order to account for the wide range of across-frequency input that octopus cells receive, the simulated AN activity is summed across a range of cochlear frequency channels, such that each model unit receives equally weighted input from a frequency range spanning about half an octave around the unit's CF. The exact choice of the input frequency range is not critical for the model performance (see below).

¹Despite the existence of a revised version of Meddis' hair-cell model (Sumner *et al.*, 2002, 2003), the original model was chosen here because of its well known structure. However, the peripheral preprocessing steps of this model can easily be exchanged by arbitrary peripheral neural models, that provide a means of reproducing the basic features of cochlear and inner hair cell filtering.

²An analysis of the mean spike rate and the variance in the activity of individual AN fibers (CF = 10.08 kHz) stimulated with a 10-kHz tone burst revealed that the assumed noise would correspond to a number of approximately 5000 statistically independent AN fibers. Simulation results assuming a physiologically more realistic total number of 700 AN fibers, whose spike trains are simulated individually, have been obtained using low and high-frequency pure tones. A comparison between these results and those obtained from using the hair-cell probability function revealed that although the assumed noise is too small to describe the variance of 700 independently spiking AN fibers, the simulation results are in good qualitative agreement.

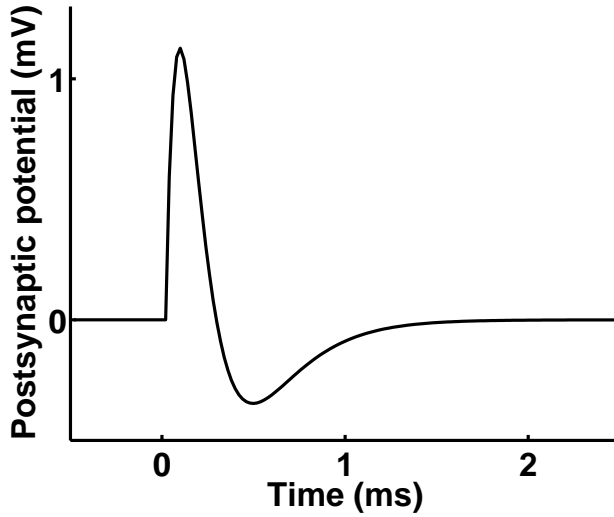


FIG. 2.1: The effective postsynaptic potential (PSP) used in the present model.

2.2.2 Model dynamics

The functional octopus cell module is modeled as a point neuron, with an integrate-to-threshold model dynamic. Compared to compartmental octopus cell models (Cai *et al.*, 1997, 2000, 2001; Levy and Kipke, 1997; Kipke and Levy, 1997; Levy and Kipke, 1998), a point neuron does not consider any spatial properties of the neuron, i.e., it assumes the same membrane potential everywhere inside the cell. Each presynaptic spike that is delivered to an integrate-to-threshold unit causes a postsynaptic potential that contributes to the unit’s membrane potential. The postsynaptic potential, caused by a presynaptic spike at time $t = 0$, is chosen as

$$\epsilon(t) = \begin{cases} t \left[e^{(-\frac{t}{\tau_a})} - ce^{(-\frac{t}{\tau_b})} \right] & \text{for } t > 0 \\ 0 & \text{otherwise} \end{cases} \quad (2.1)$$

with τ_a and τ_b being time constants and c denoting a constant factor. Figure 2.1 shows the postsynaptic potential, in the following referred to as the “effective PSP”. The shape of the effective PSP is assumed to be identical at all synapses in the present model.

Each presynaptic spike i arriving at a time t_i causes a postsynaptic potential that contributes to the membrane potential $V_m(t)$ of the model unit. The model unit is modeled as a leaky-integrator with time constant τ_m

$$\tau_m \frac{dV_m(t)}{dt} = -V_m(t) + \sum_{t_i} \epsilon(t - t_i). \quad (2.2)$$

Finally the output potential $V(t)$ of the unit is expressed with respect to its resting potential V_{rest}

$$V(t) = V_{rest} + V_m(t). \quad (2.3)$$

The latter term in equation 2.2 essentially represents the convolution sum of the presynaptic spike train with the postsynaptic potential $\epsilon(t)$. While the cell’s poten-

TABLE 2.1: Simulation parameters.

Parameter	Description	EN
V_{rest}	membrane equilibrium potential	$-60mV$
τ_m	membrane time constant	$1ms$
Θ_{act}	spike threshold	$-45mV$
τ_a	effective PSP time constant	$0.1ms$
τ_b	effective PSP time constant	$0.2ms$
c	constant PSP factor	0.25
Θ_{rel}	spike blocking release threshold	$-59mV$

tial, $V(t)$, is below its spike threshold Θ_{act} , the unit's state variable s is set to zero. If the membrane potential of the model unit exceeds the unit's spike threshold, the neuron emits a spike, i.e., its state variable is set to one:

$$s = \begin{cases} 0 & : V(t) \leq \Theta_{act} \\ 1 & : V(t) > \Theta_{act} \end{cases}$$

After the neuron has emitted a spike it remains in an absolute refractory period with a duration of 0.8 ms, preventing it from emitting further action potentials ($s = 0$). In addition, a spike-blocking mechanism is activated following each spike, which also prevents the unit from emitting further spikes unless its membrane potential falls below the release potential Θ_{rel} . All simulations of the present study were performed at a sampling rate of 50 kHz. The model-specific parameters are shown in Table 2.1.

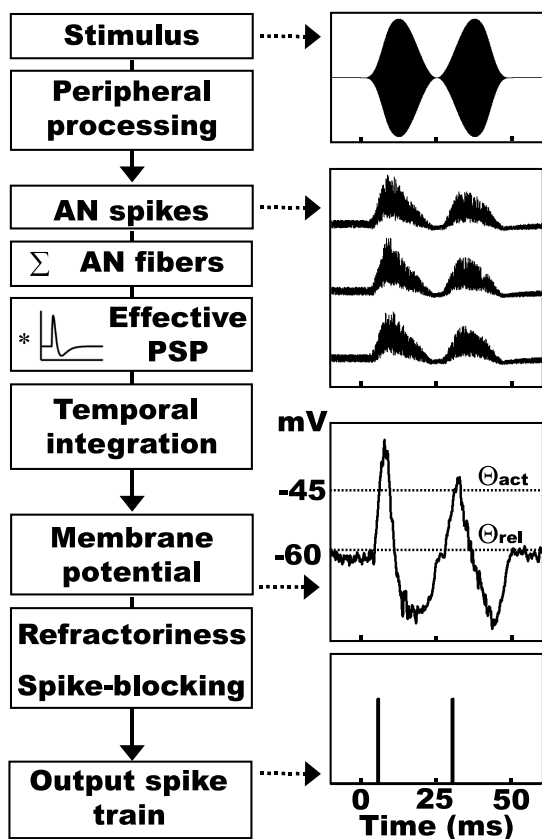


FIG. 2.2: Model processing scheme: An acoustic stimulus (right panel, top) traverses the peripheral processing models resulting in simulated AN activity (the corresponding activity of three exemplary AN fibers is shown in the upper middle of the right panel). AN activity is summed across peripheral filters and convolved with the effective PSP to describe the synaptic input provided to the model unit. The model integrates its synaptic input and generates a spike, if its membrane potential exceeds its spike threshold Θ_{act} (right panel, lower middle). Following a spike the model enters its refractory period and its spike-blocking mechanism becomes activated. The spike-blocking mechanism remains active until the model membrane potential falls below the model's spike-blocking release threshold Θ_{rel} . The model's output spike train in response to the acoustic stimulus (right panel, top) is shown at the bottom of the right panel.

2.3 SIMULATIONS AND DATA ANALYSIS

The presented octopus cell model is tested using a variety of stimuli. Results from the simulations are compared to literature data from octopus cell recordings, if available. Stimuli include pure tones, polarizing currents, amplitude modulated (AM) tones, and harmonic tone complexes. Model responses to pure-tone stimuli are analyzed in terms of their peri-stimulus time histograms (PSTH). An interspike interval (ISI) histogram is used in the case of the harmonic tone complex. If not stated otherwise, histograms are gained from 250 repetitions of a 50-ms stimulus with 10-ms ramps, using a bin width of 0.2 ms. The degree of synchronization of the model response to AM stimuli is analyzed using the synchronization coefficient (SC) (Goldberg and Brown, 1969), computed as the vector strength of the distribution of spikes. $SC=1$ indicates perfect synchronization to the stimulus modulation while $SC=0$ represents no synchronization at all. Additionally, the rate modulation transfer function (rMTF), where the spike rate is plotted as a function of the modulation frequency, is computed in response to AM stimuli. AM stimuli are presented with a duration of 1.05 s with the first 50 ms being excluded from the analysis in order to avoid onset effects. Stimulus levels are given in dB above the model's individual CF pure-tone response threshold (mTh).

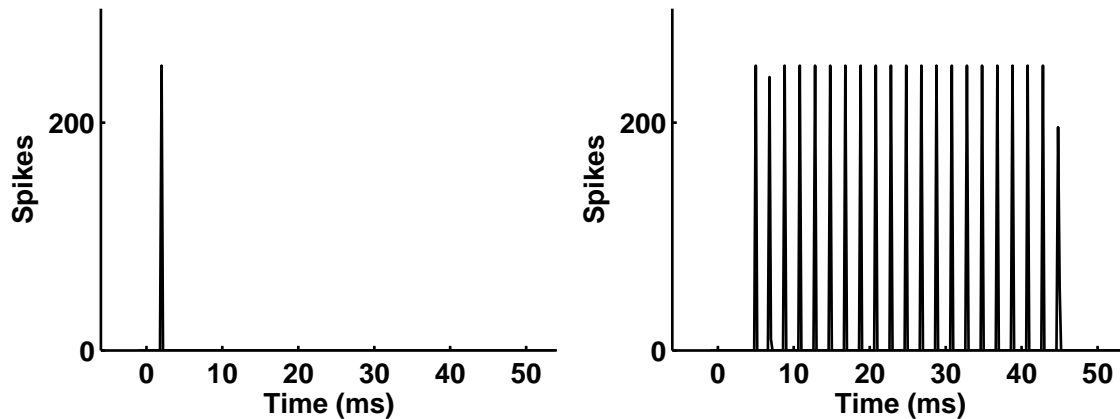


FIG. 2.3: Left: PSTH of a model unit (CF=3.98 kHz) in response to a 4-kHz tone presented at 50 dB (mTh). Right: PSTH of the same model unit in response to a 500-Hz tone presented at 50 dB (mTh). Note that the same model unit reveals both, an onset response when stimulated with high-frequency tones and entrainment when stimulated with low-frequency tones.

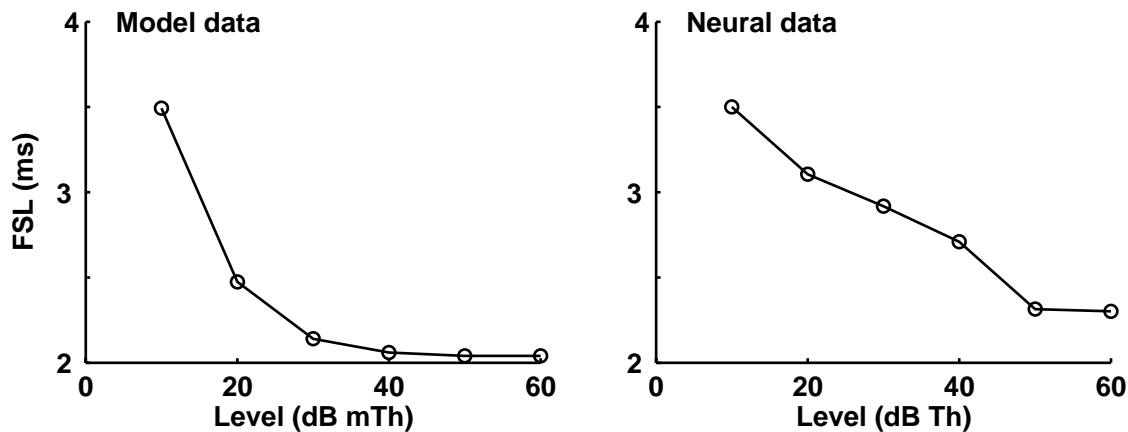


FIG. 2.4: Left: FSL of the model unit (CF=3.98 kHz) as a function of different stimulus levels. Right: Recorded FSL of an octopus cell (CF=7.96 kHz) when stimulated with pure tones at CF presented at different levels (stimulus level is given with respect to the unit's pure-tone threshold). Replot with permission from [Winter and Palmer \(1995\)](#).

2.3.1 Pure-tone stimuli

[Godfrey *et al.* \(1975\)](#) found that octopus cells in cats respond to pure-tone stimuli ($f > 2$ kHz) revealing one sharply timed action potential at stimulus onset followed by no or little (< 10 spikes/s) subsequent activity during the sustained portion of the tone. Such an O_I -type response was confirmed in a number of subsequent studies (e.g. [Rhode and Smith, 1986](#); [Winter and Palmer, 1995](#)) investigating the responses of PVCN octopus cells. The first spike latency (FSL) of octopus cells ranges from 2-4 ms at intermediate stimulus levels and decreases with increasing stimulus level ([Rhode and Smith, 1986](#); [Winter and Palmer, 1995](#)). In contrast to their onset response at high stimulus frequencies, octopus cells can entrain to low-frequency pure tones ($f < 800$ Hz), where they emit exactly one spike at each stimulus cycle

(e.g. Rhode and Smith, 1986), if the stimulus frequency is included in the cell's frequency-response area. The synchronization coefficient of low-frequency pure-tone entrainment lies between 0.9 and 0.99 (Rhode and Smith, 1986), indicating a nearly perfect synchronization of the cell's response to the stimulus frequency.

The left panel of Fig. 2.3 shows, as an example, the PSTH of a model cell (CF=3.98 Hz) in response to a 4-kHz pure tone presented at 50 dB (mTh). Such reliable onset responses are produced by the model for all tested stimulus levels. Due to the spike-blocking mechanism, multiple spikes do not occur at stimulus onset, even not at the highest stimulation level tested (90 dB (mTh)). The right panel of Fig. 2.4 displays the recorded FSL of an octopus cell (CF=7.96 kHz) when it is stimulated with pure-tones at its CF as a function of the stimulus level, replotted from Winter and Palmer (1995). The FSL decreases from 3.5 to 2.3 ms as the stimulus level is increased from 10 to 60 dB (level above the unit's threshold). The left panel of Fig. 2.4 displays the FSL of the same model cell (CF=3.98 kHz) as shown in Fig. 2.3, as a function of the stimulation level of a 4-kHz pure tone. The simulated FSL decreases from 3.4 to 2.0 ms when the stimulus level is increased from 10 to 60 dB (mTh), which is in good agreement with the recorded octopus cell data. If the same model unit is stimulated with a low-frequency pure tone it entrains to the stimulus frequency. This is shown in the right panel of Fig. 2.3 where the simulated PSTH of the model unit (CF=3.98 kHz) is given in response to a 500-Hz tone presented at 50 dB (mTh). The synchronization coefficient, calculated from the model PSTH, is 0.99, thus being in good agreement with recorded octopus cell synchronization coefficients.

A more general view is obtained from the frequency-response area of a neuron where the spike rate of the neuron is computed in response to pure-tones presented at different frequencies and levels. The right panel of Fig. 2.5 shows a recorded frequency-response area of an octopus cell (CF=2.2 kHz, CF pure-tone threshold 30 dB, stimulus levels are increased in 10dB steps from 30 to 90 dB SPL), replotted from Rhode and Smith (1986). The frequency-response area is broad, due to the wide across-frequency range spanned by the AN fibers that terminate on an octopus cell, and reveals an asymmetric shape with respect to the unit's CF. The simulated frequency-response area of a model neuron with CF = 1.96 kHz in response to pure tone stimuli presented at 10, 20, 30 and 60 dB (mTh) is shown in the left panel of Fig. 2.5. The simulated frequency-response area agrees with the recorded data in its broad shape and in its asymmetry. The asymmetric shape of the frequency response area is a particular feature of octopus cells that receive AN input coming from low-frequency cochlear filter channels. This can be understood from the pure-tone PSTHs shown in Fig. 2.3. While the simulated cell reveals purely an onset response

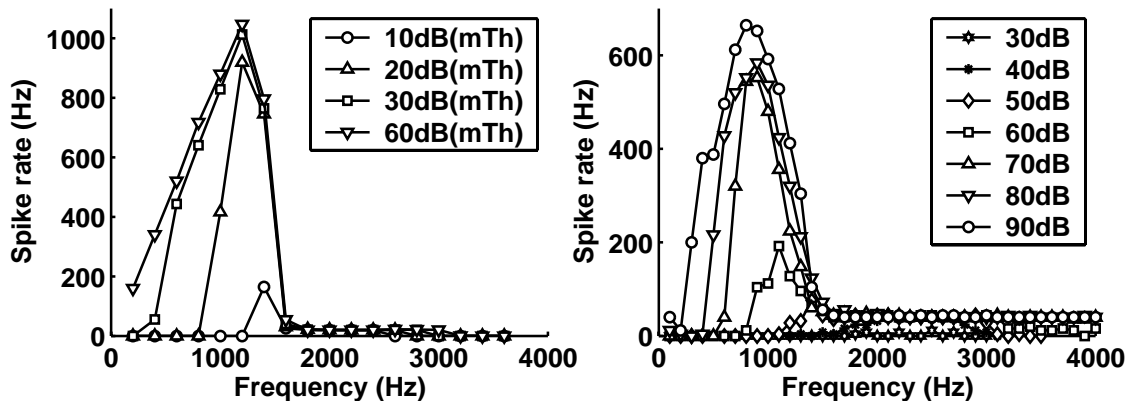


FIG. 2.5: Left: Frequency-response area of a model unit (CF=1.96 kHz) for different stimulus presentation levels of 10, 20, 30 and 60 dB (mTh) (100 stimulus repetitions). Right: Recorded O_I -unit response area (CF=2.2kHz, response threshold at CF=30 dB SPL, stimulus duration 25 ms, 250 stimulus repetitions). Replot with permission from [Rhode and Smith \(1986\)](#).

at high stimulus frequencies (left panel of Fig. 2.3) it entrains to low-frequency pure tones (right panel of Fig. 2.3) with a spike rate that reflects the stimulus frequency. The cell's entrainment leads to an enhanced spike rate in response to low-frequency tones, in contrast to the onset spike the cell exhibits in response to high-frequency tones and thus causes the asymmetric shape of the frequency-response area. The left panel of Fig. 2.5 also indicates that when the stimulus frequency equals the neuron's CF (1.96 kHz), essentially no changes occur in its spike rate when the stimulus level is varied within 10 to 60 dB (mTh). This indicates that the dynamic range of the model neuron (at CF) must be smaller than 10 dB. Such a small dynamic range is in good agreement with experimental octopus cell data, revealing a dynamic range of only 10 dB to 25 dB ([Rhode and Smith, 1986](#)). However, at stimulus frequencies at which entrainment occurs, the dynamic range increases. This is due to the basal spread of excitation, that causes an increasing number of AN fibers to follow the stimulus.

2.3.2 Current stimulation

The right panel of Fig. 2.6 shows recorded octopus cell data in response to steps of current between 5 and -3.5 nA in 0.5 nA increments, reprinted from [Oertel et al. \(2000\)](#). When stimulated with depolarizing currents of sufficient magnitude, octopus cells exhibit an action potential at stimulus onset that is followed by a low sustained depolarization during the sustained portion of the stimulus. Moreover, [Golding et al. \(1999\)](#) reported that repetitive firing is never observed even if very high current pulses are used. After the depolarizing current has terminated the cell becomes hyperpolarized, i.e., the membrane potential falls below its resting value. When stimulated with hyperpolarizing currents of sufficient magnitude, octopus cells are

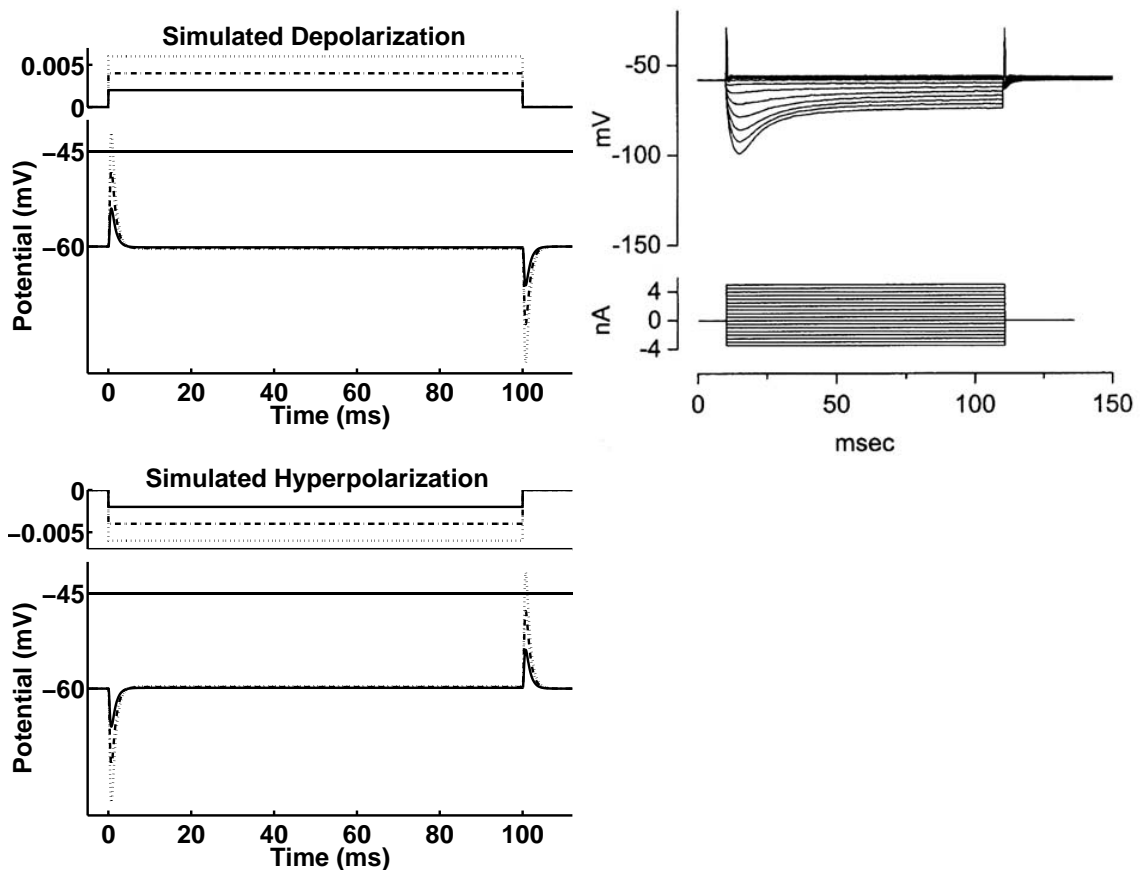


FIG. 2.6: Upper left panel: Simulated depolarizing currents of different strengths (top) and the corresponding model membrane potential (bottom). Lower left panel: Simulated hyperpolarizing currents of different strengths (top) and the corresponding model membrane potential (bottom). The solid line in the bottom panel of each figure indicates the spike threshold of the model unit. Right: Recorded octopus cell potentials (top) in response to current steps between 5 and -3.5 nA in 0.5 nA increments (bottom). The cell evokes an action potential at the onset and offset of large depolarizing and hyperpolarizing currents, respectively. Reprint from [Oertel *et al.* \(2000\)](#) (Copyright (2000) National Academy of Sciences, U.S.A.).

hyperpolarized throughout the whole stimulus and generate an offset action potential after the hyperpolarizing current has terminated.

Simulation results are shown in the left panel of Fig. 2.6. The simulated depolarizing stimulus is presented at three different magnitudes (upper left panel, top). The corresponding model membrane potential, shown in the bottom panel, only exceeds the model spike threshold (solid line), when the strongest stimulus is presented. Following the onset depolarization the membrane potential remains at a low sustained depolarization and finally becomes hyperpolarized after the depolarizing stimulus has terminated. The lower left panel of Fig. 2.6 displays the simulated hyperpolarizing stimulus presented at three different magnitudes (top) and the corresponding model membrane potential (bottom). The strong hyperpolarization of the model membrane potential at stimulus onset is reduced during the sustained

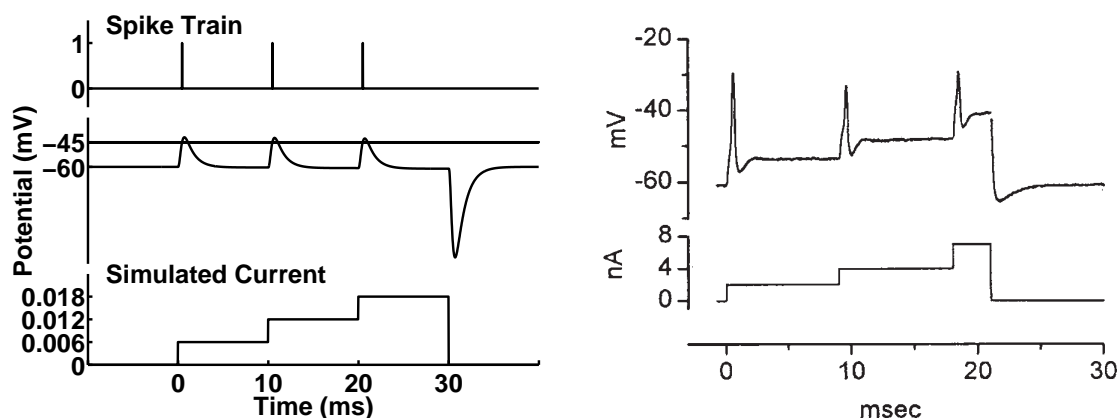


FIG. 2.7: Left: Model output spike train (top) and the corresponding model membrane potential (middle). The vertical line indicates the spike threshold of the model unit. The simulated staircase current stimulus is shown at the bottom. Right: Recorded octopus cell data. The octopus cell potential is shown in the top panel and the staircase current stimulus in the bottom panel. Both, the recorded and the simulated, data reveal that if the cell is depolarized with increasing current steps it emits an action potential with each current increment. At the offset of the current pulse the cell potential falls below its resting potential. Reprint from [Oertel *et al.* \(2000\)](#) (Copyright (2000) National Academy of Sciences, U.S.A.).

stimulus portions. In case that the hyperpolarization is strong enough, the membrane potential exceeds its spike threshold after the stimulus has ended, such that an offset action potential is generated. Thus, the model responses to depolarizing and hyperpolarizing stimuli show the main characteristics of the recorded cell potentials.

The right panel of Fig. 2.7 shows recorded octopus cell data in response to increasing current steps, reprinted from [Oertel *et al.* \(2000\)](#). When the cell is depolarized with a current pulse of 2 nA it generates an action potential at the onset of the current pulse and remains at a low depolarization during the sustained portion of the current. Further increments of the depolarizing current pulse from 2 to 4 nA and from 4 to 7 nA cause the octopus cell to exhibit further action potentials. After the current stimulus has ended a hyperpolarization of the octopus cell is observed. The left panel of Fig. 2.7 shows the model membrane potential (middle) and the corresponding output spike train (top) in response to a simulated staircase stimulus, increased in three steps (bottom). The model membrane potential exceeds its spike threshold at the beginning of each step, thus emitting a spike with each increment, while it approaches its resting potential during the sustained stimulus portions. Even though the simulated membrane potential differs from the recorded octopus cell potential, in that the low sustained depolarization of the recorded potential increases with each current increment, it resembles the latter in its key features including the strong hyperpolarization occurring after stimulus offset.

Due to the shape of the effective PSP within the present model it allows for simulating the recorded octopus cell data shown in the right panels of Fig. 2.6 and Fig. 2.7. Octopus cell responses to current stimuli would not be obtained if coincidence detection was used as a mechanism for modeling an octopus cell, which would imply the use of a monophasic PSP. This is further discussed in Sec. 2.4.1.1.

2.3.3 Amplitude modulated stimuli

Octopus cells are presumably the best AM encoders among all major CN cell types (Frisina *et al.*, 1990; Rhode, 1994a; Winter and Palmer, 1995). Entrainment of a model unit (CF=10.08 kHz) to 100% amplitude modulated stimuli can be seen in Fig. 2.8, where the synchronization coefficient (left scale, circles) is plotted versus modulation frequency in response to an 10-kHz SAM tone presented at 30 dB (mTh). An example stimulus with a modulation frequency of 500 Hz is shown in the inset of Fig. 2.8. The resulting synchronization coefficients have values between 0.98-1.0. Since the synchronization coefficient does not reveal whether the cell fires at each stimulus cycle, or misses out some cycles, the corresponding rate modulation transfer function (rMTF) is also shown in Fig. 2.8 (right scale, triangles). A spike rate approximately equaling the modulation frequency and a high vector strength indicate a nearly perfect entrainment of the model unit to the AM stimulus. At a modulation frequency of 500 Hz, for example, the cell exhibits 502 spikes/s and a synchronization coefficient of 0.98 thus revealing nearly perfect entrainment. At a modulation frequency of 600 Hz, the rate is strongly decreased, as the cell can not follow the fast fluctuations of the modulated input anymore. However, since the remaining spikes are still phase-locked to the stimulus modulation the synchronization coefficient remains at a high value (SC=0.98). If the stimulus modulation frequency exceeds 800 Hz, the cell exhibits an onset response instead of entraining to the stimulus. A direct comparison of simulated and experimental 100% AM responses for O_I units is not possible due to the paucity of recorded data for these units.

Although recorded data from octopus cells are limited, responses to 200% amplitude modulated tones have been investigated relatively extensively, since they resemble natural vocalizations more closely than 100% SAM tones (Rhode, 1994a). The right panel of Fig. 2.9 shows recorded data of an O_I unit with CF=6.7 kHz (pure-tone threshold at CF is 13 dB SPL) in response to a 200% amplitude modulated carrier, replot from Rhode (1994a). The stimulus was presented at 50 dB SPL and the carrier frequency of the 200% amplitude modulated tone was chosen to equal the unit's CF. The left panel of Fig. 2.9 shows the synchronization coefficient of the model unit (CF=10.08 kHz) in response to a 200% amplitude modulated 10-kHz tone presented at 20 dB (mTh). The stimulus corresponding to the modulation

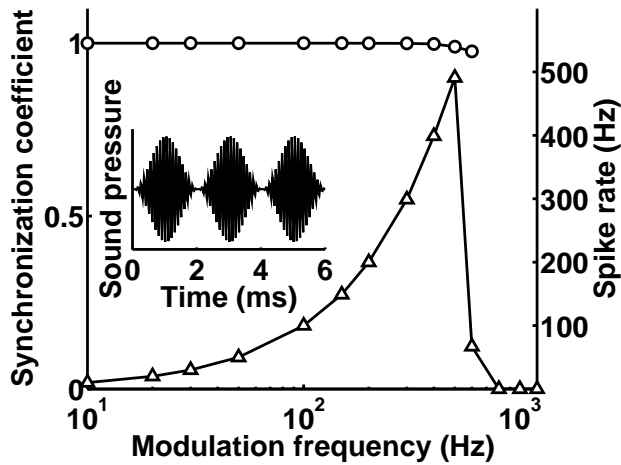


FIG. 2.8: Synchronization coefficient (left scale, circles) and spike rate (right scale, triangles) of a model unit ($CF=10.08$ kHz) as a function of the modulation frequency of an 100% amplitude modulated pure tone ($f=10$ kHz) presented at 30 dB (mTh). The inset shows an exemplary stimulus modulated at a rate of 500 Hz.

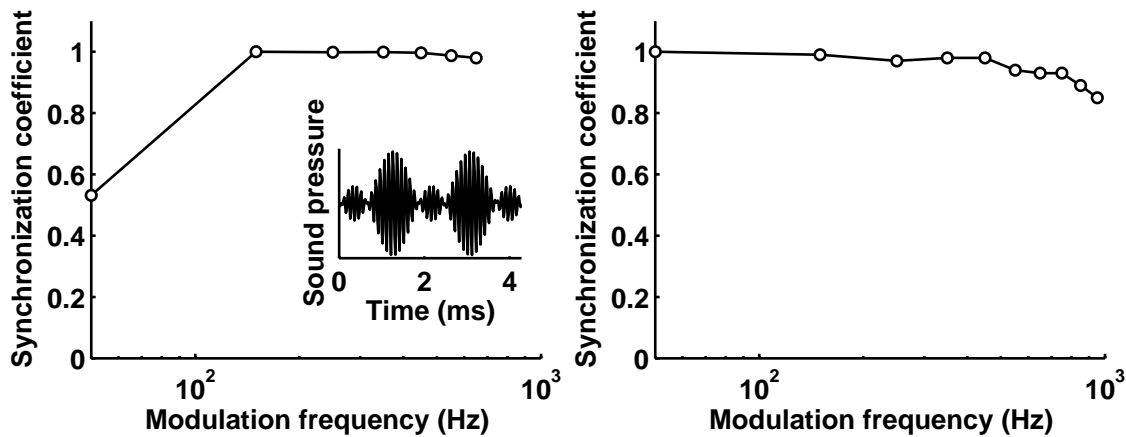


FIG. 2.9: Left: Synchronization coefficient of the model unit ($CF=10.08$ kHz) as a function of the modulation frequency of a 200% amplitude modulated 10-kHz tone presented at 20 dB (mTh). The inset displays an exemplary stimulus modulated at a rate of 550 Hz. Right: Recorded synchronization coefficient of an octopus cell in response to 200% amplitude modulated pure tones presented at 37 dB above the unit's pure tone threshold. The stimulus carrier frequency was chosen to equal the unit's CF (stimulus duration 100 ms). Replot with permission from [Rhode \(1994a\)](#).

frequency of 550 Hz is shown as an example in the inset of Fig. 2.9 (left). The model entrains to the stimulus modulation revealing synchronization coefficients that lie between 0.98-0.99, being in good agreement with the recorded data shown in the right panel of Fig. 2.9. However, at the lowest modulation rate, 50 Hz, the simulation results deviate from the recorded data, in that the model entrains not only to the center peak, but also to the small lobe of the 200% AM stimulus (see example stimulus in the inset of Fig. 2.9 (left)). This results in a doubled model spike rate and thus to a synchronization coefficient that is reduced compared to the synchronization coefficients obtained at higher modulation frequencies. Thus, at this low modulation frequency the model is more sensitive to onset transients than the octopus cell used in the recordings.

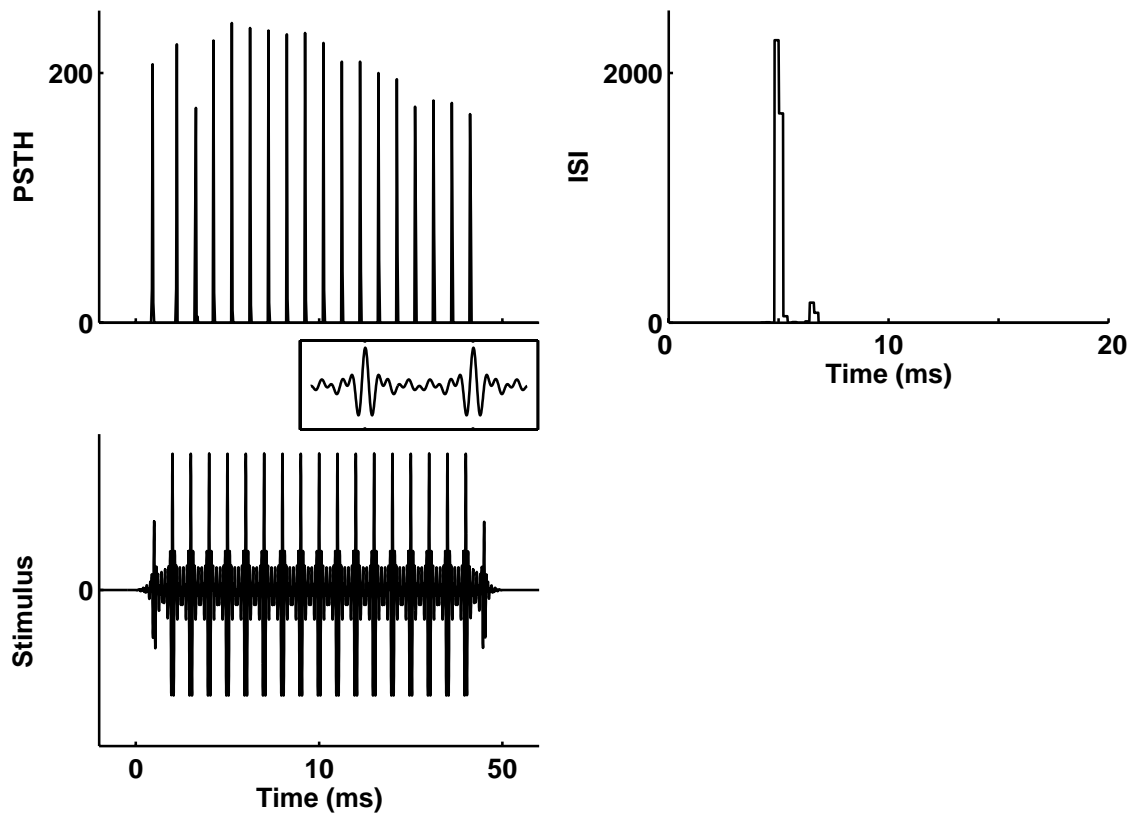


FIG. 2.10: PSTH (left panel, top) and ISI histogram (right panel) of a model unit (CF=2.04 kHz) in response to a harmonic tone complex consisting of 6 components equally spaced between 1 kHz and 2 kHz presented at 20 dB (mTh). The stimulus shown in the lower left panel is presented for 100 ms (the inset displays a magnified version of one stimulus period). The PSTH shows that the model responds with each stimulus cycle such that the ISI histogram exhibits a peak at interspike intervals (5 ms) that correspond to the missing fundamental of the tone complex (200 Hz).

2.3.4 Harmonic tone complexes

Octopus cells are found to entrain to the fundamental frequency of a harmonic tone complex, even if the fundamental frequency itself is missing (Cai *et al.*, 2001; Evans and Zhao, 1998; Palmer and Winter, 1993).

Figure 2.10 shows the PSTH (left panel, top) and ISI histogram (right panel) of a model unit (CF=2.04 kHz) in response to a harmonic tone complex with a (missing) fundamental frequency of 200 Hz consisting of six frequency components spaced between 1 kHz and 2 kHz. The simulation level was 20 dB (mTh). The temporal waveform of the harmonic tone complex is shown in the lower left panel of Fig. 2.10 and the inset shows one magnified period of the stimulus. The simulated PSTH shown in Fig. 2.10 (left panel, top) reveals that the model responds at each cycle of the harmonic tone complex. This results in interspike intervals that correspond to the period time of the missing fundamental frequency of the harmonic tone complex (5 ms). Thus, the simulated responses correspond well to the responses reported from octopus cells (Cai *et al.*, 2001; Evans and Zhao, 1998).

2.4 DISCUSSION

2.4.1 Alternative mechanisms suggested to account for octopus cell response properties

2.4.1.1 Coincidence detection

Even though octopus cells are often assumed to act as coincidence detectors, coincidence detection itself is not sufficient to account for the entrainment found in these cells, as has been recently shown in [Kalluri and Delgutte \(2003a\)](#). Two additional features observed in octopus cell recordings using depolarizing and hyperpolarizing current pulses ([Golding *et al.*, 1999](#)) also indicate that coincidence detection is not sufficient for modeling an octopus cell: the offset action potential observed in response to hyperpolarizing currents of sufficient strength (Fig. 2.6, right) and the hyperpolarization of the cell following a depolarizing current (right panels of Fig. 2.6 and Fig. 2.7). As a pure coincidence detector uses a monophasic PSP, such that its membrane potential mimics the stimulus waveform, it lacks a mechanism that allows for detecting a stimulus offset as well as a hyperpolarizing mechanism, that is not related to its refractoriness. Even if combined with a spike-blocking mechanism ([Kalluri and Delgutte, 2003b](#)) coincidence detection is not appropriate to model octopus cell responses, a conclusion that can be drawn from octopus cell recordings in response to increasing current steps (Fig. 2.7, right). If a coincidence detector in combination with a spike-blocking mechanism was stimulated by a simulated staircase current, it would only generate one action potential at the stimulus onset. After emitting the initial action potential, the spike-blocking mechanism would be activated and remained activated throughout the entire stimulus, as the membrane potential did not fall below the release threshold, that releases the cell from spike blocking.

In contrast, the simulation results of this study reveal that, if a biphasic PSP is used instead of a monophasic PSP, octopus cell responses can be simulated using a variety of stimuli, including current steps. The shape of the effective PSP used in this study essentially represents a high-pass filtering process of the stimulus, i.e., it enhances stimulus transients and attenuates sustained stimulus portions. Thus, when stimulated with a staircase current, the membrane potential of the present model falls below the release threshold during the sustained stimulus portions, such that the cell is released from spike blocking and can generate further action potentials (left panel of Fig. 2.7).

The present model corresponds to all previous octopus cell models in terms of its fast time constants. However, the fast time constants in the present model are

not associated with a coincidence detection mechanism, but are required to allow for an entrainment to high input frequencies.

2.4.1.2 Dynamic changes in synaptic effectiveness and inhibitory mechanisms

Dynamical changes in synaptic effectiveness, suggested to account for octopus cell responses in the model by Levy and Kipke (1997) (see also Kipke and Levy, 1997; Levy and Kipke, 1998), could not be confirmed in octopus cell recordings. Although signs of depression, possibly indicating a decreased synaptic effectiveness, were observed in octopus cell recordings (Golding *et al.*, 1995; Oertel *et al.*, 2000), their effects were small and occurred only under unphysiological stimulus conditions.

Inhibitory circuits or inhibitory interneurons, suggested to account for octopus cell responses (Godfrey *et al.*, 1975; Kane, 1973), are unlikely to shape the response properties of octopus cells for several reasons. Inhibitory interneurons are unlikely to be involved in octopus cell responses due to the short FSLs observed in octopus cells (2-4 ms) (Rhode and Smith, 1986; Winter and Palmer, 1995). Moreover, while blocking inhibition by applying a GABA_A receptor antagonist largely affects the responses of O_L and O_C units, it does not affect the response properties of O_I units (Palombi and Caspary, 1992; Evans and Zhao, 1998). Additionally, immunostaining studies revealed only a weak influence of inhibition on octopus cells compared to other CN cell types (Wenthhold *et al.*, 1986, 1987). Thus, it can be assumed that neither dynamic changes in synaptic effectiveness nor inhibitory mechanisms play a critical role in shaping octopus cell response properties.

2.4.2 Intracellular properties of octopus cells

Recent studies focusing on the intracellular properties of octopus cells revealed two voltage-sensitive conductances inherent in octopus cells: an outward rectifying low-threshold, depolarization-activated potassium conductance and an inward rectifying hyperpolarization-activated mixed-cation conductance (Golding *et al.*, 1995, 1999). The inward rectifying current is found to act mainly in the hyperpolarized voltage range, having no major effect on the response properties of octopus cells. However, blocking the outward rectifying conductance leads to repetitive firing and broadened action potentials (Golding *et al.*, 1999), indicating that the low-threshold potassium conductance plays a critical role in shaping octopus cell response properties. The octopus cell model by Cai *et al.* (1997, 2000, 2001), that includes these two conductances, thus presumably employs a biologically plausible mechanism for simulating octopus cell responses. However, entrainment of their model has not been tested using a wide range of frequencies and levels. Thus, the usability of their model ap-

pears limited in this respect. It is not possible to correlate the shape of the effective PSP used in this model with distinct ion conductances. However, the effective PSP reflects an intracellular model property that might result from combined fast inwardly directed currents and slower outwardly directed currents, in response to a presynaptic spike. Whether these outwardly directed currents reflect the effective contribution of the low-threshold potassium conductances can not be decided here.

Since the different types of onset units differ in both their morphological and their physiological properties, the present model exclusively focuses on O_I -unit responses. While O_C responses have been associated with multipolar stellate cells (Rhode *et al.*, 1983; Smith and Rhode, 1989) and O_I responses with octopus cells (Kane, 1973; Godfrey *et al.*, 1975), the morphological basis of O_L units is uncertain. Few O_L units have been identified as octopus cells (Rhode *et al.*, 1983; Winter and Palmer, 1995), but O_L responses are also associated with bushy cells. Beside these morphological differences, onset units also differ in their physiological properties, for example, in terms of their dynamic ranges, frequency selectivity, and ISI histograms (Rhode *et al.*, 1983; Winter and Palmer, 1995). Moreover, the responses of O_L and O_C units are strongly affected if inhibition is blocked by applying a GABA_A receptor antagonist, while responses of O_I units are not (Palombi and Caspary, 1992; Evans and Zhao, 1998). The strong influence of inhibition on the responses of O_L and O_C units indicates that their responses result from inhibitory mechanisms, in contrast to the responses of O_I units that are assumed to be shaped by membrane-based mechanisms (Evans and Zhao, 1998). Due to these fundamental differences between the different types of onset units, we decided to model exclusively O_I -unit responses, in contrast to the coincidence detector model by Kalluri and Delgutte (2003a,b).

2.4.3 Simplifications made in the present model

2.4.3.1 The model membrane potential

A number of simplifying assumptions have been made in order to limit the model's complexity. The membrane potential of the presented model differs from recorded octopus cell potentials in that it is not affected by refractoriness. Refractoriness is implemented in the presented model by preventing the cell from generating action potentials during its refractory period, without being reflected in the cell's membrane potential. Otherwise the spike-blocking mechanism, that is driven by the membrane potential, would be disturbed by the refractoriness of the cell. If the spike-blocking mechanism would be driven by an internal copy of the membrane potential, that is not affected by refractoriness, the model membrane potential could be simulated having a biologically more plausible shape. However, we decided not to implement

such an extra “spike-blocker potential” as the structure of the present model was intended to be as simple as possible and as it does not affect any other model response property except the shape of its membrane potential.

The model membrane potential also differs from recorded octopus cell potentials in that the strength of its hyperpolarization following a depolarizing stimulus exceeds the hyperpolarization observed in octopus cell recordings (see for example Fig. 2.7). However, the model hyperpolarization can be reduced by including an inward rectifying mixed cation current. Such a current has been found in octopus cells to act in the hyperpolarization range, without revealing a strong influence on the shape of octopus cell PSTHs (Golding *et al.*, 1995, 1999). An inward rectifier current is not included in the model as it does not affect the basic response properties of the model. If the presented model, which is attempted to possess an as simple as possible structure, was supposed to simulate octopus cell potentials in detail, this could be obtained by introducing both, an extra membrane potential driving the spike-blocking mechanism as well as an inward rectifying mixed cation conductance that acts in the hyperpolarization range.

2.4.3.2 The spike-blocking mechanism

The spike-blocking mechanism of the present model resembles the one implemented by Kalluri and Delgutte (2003b). Although little is known about the biophysical basis of such a mechanism, it might be associated with an inactivation of Na^+ channels, as these channels are among the principal channels underlying fast spiking in neurons. The inactivation of Na^+ channels (depolarization block) has been originally suggested by Romand (1978) as a mechanism shaping onset responses. However, in contrast to the model by Kalluri and Delgutte (2003b), where the spike-blocking mechanism is driven by the stimulus, the mechanism used in the present model is effectively driven by the stimulus slope since the effective PSP yields the slope of the stimulus. Thus, the present model allows, for example, to account for octopus cell responses to increasing current steps (Fig. 2.7), which can not be obtained when the spike-blocking mechanism is driven by the stimulus itself (Kalluri and Delgutte, 2003b). However, since little is known about the biophysical properties that might reflect such a mechanism, we can not clearly associate the spike-blocking mechanism with distinct octopus cell properties.

2.4.3.3 The input provided by AN fibers

Although the actual number of high-spontaneous rate ($> 60\text{spikes/s}$) AN fibers projecting onto an octopus cell is difficult to quantify, Liberman (1993) estimated that approx. 63 AN fibers project onto the soma of an octopus cell. This is less

than the number of AN input used in this model. However, the total number of AN fibers terminating on an octopus cell is presumably several times that high as AN fiber synapses are also located on the dendrites of octopus cells (Kane, 1973; Smith and Rhode, 1989; Oertel *et al.*, 2000). Based on the fraction of the somatic and dendritic surface area of octopus cells that is covered by synaptic terminals and the average size of synaptic terminals on octopus cells, Kalluri and Delgutte (2003a,b) estimated a number of up to 600 AN fiber synapses per octopus cell. The large number of inputs that is simulated by the noisy version of the hair-cell spike probability in the present study is thus justified by the large number of AN synapses observed on octopus cells.

Although the actual frequency range of AN fibers providing input to one octopus cell is also not known so far, the present model unit presumably receives input from a smaller frequency range than octopus cells. Extending the across frequency range of the model input, especially for units having a low CF, is restricted by the different traveling wave delays on the basilar membrane. Large differences in the traveling wave delays between channels that provide input to the same octopus cell disturb the input shape and thus might lead to inappropriate model responses. However, octopus cells are found to receive input from AN fibers that encode low frequencies near the cell body and from those that encode higher frequencies progressively more distally on their dendrites (Oertel *et al.*, 2000). This ordered spatial arrangement has been suggested to compensate for the traveling wave “distortion” along the cochlea and to increase the synchronization of across-frequency input (Golding *et al.*, 1999). Extending the present model by such a traveling wave compensation would provide a simple way of extending the across frequency range of AN inputs, without disturbing the input shape by the differences in basilar membrane delays.

2.5 SUMMARY AND CONCLUSION

A functional point-neuron module was presented that allows for simulating O_I -unit responses found in cochlear nucleus octopus cells. The PSTH of O_I units reveals one single spike at the onset of a high-frequency tone burst and no further activity during the ongoing stimulus. Thus, short ISIs do not occur in the responses of O_I units to high-frequency tones. In contrast, the same units entrain to a wide range of low-frequency tones, revealing exactly one spike per stimulus cycle and thus exhibit ISIs that are in the range of 1 ms. The present model accounts for this diversity of O_I unit's pure-tone responses by using a biphasic "effective" PSP in combination with a spike-blocking mechanism. The same model was also tested using more complex stimuli, including depolarizing and hyperpolarizing current steps, amplitude modulated stimuli and harmonic tone complexes. It accounts for the main response characteristics of O_I -unit responses found in the recorded data (from the literature). Thus, the present model actually provides a useful means of simulating O_I -unit responses without the need of describing the dynamic properties of octopus cells in detail. Moreover, it was shown that the model can account for O_I -unit responses that can not be simulated if a coincidence-detector model was used instead. Due to its plain structure and the small set of simulation parameters, the present functional model can easily be integrated in complex models of higher auditory function, in order to investigate the role of octopus cells in higher-order auditory processing.

CHAPTER 3

A NEURAL CIRCUIT OF MODULATION BANDPASS FILTERS IN THE IC BASED ON O_I -UNIT RESPONSES OF THE CN: PROCESSING OF SAM TONES

ABSTRACT

Periodic amplitude modulations (AM) of an acoustic stimulus are presumed to be encoded in temporal activity patterns of neurons at the early stages of the auditory system. Physiological recordings indicate, that this temporal AM code is transformed into a rate-based periodicity representation at the higher auditory processing stages. Especially, the bandpass shaped rate modulation transfer functions (rMTF) found in neurons at the level of the inferior colliculus (IC) (Rees and Møller, 1983; Langner and Schreiner, 1988; Rees and Palmer, 1989; Krishna and Semple, 2000) can be assumed to represent a rate-based code of AM information, arising between the level of the cochlear nucleus (CN) and the IC. The assumption that AM information is represented by a rate-based code at the higher auditory processing stages is also supported by the psychophysical concept of amplitude modulation filters (Dau *et al.*, 1997a,b; Ewert and Dau, 2000). The present model provides a neural circuit that transforms temporal periodicity information, provided by ideal onset O_I units in the CN, into a rate-based periodicity representation at the level of the IC. Due to the neural connectivity of the present model, bandpass shaped rMTFs with different best modulation frequencies (BMF) are obtained that correspond to recorded rMTFs of IC neurons. The suggested neural circuit thus offers a possible neural cor-

relate to the psychophysically postulated AM filters. The model may also explain how rMTFs with a region of suppression, a further rMTF-type observed in the IC ([Krishna and Semple, 2000](#)), result from neural connectivity within the auditory system. In contrast to previous modeling studies describing the formation of bandpass modulation filters in the IC, the present neural circuit employs no temporal delay lines, as well as no other continuously changing temporal parameter.

3.1 INTRODUCTION

Periodic amplitude modulations are a common physical feature of sounds produced by many natural sound sources, among which are vocal chords, strings, pipes and tubes. Amplitude modulation (AM) information is utilized by the auditory system in a variety of complex auditory tasks, including speech perception (e.g. [Rosen, 1992](#)), pitch perception (e.g. [Schouten *et al.*, 1962](#); [De Boer, 1976](#)) and auditory scene analysis ([Bregman, 1990](#)). Thus, knowledge about how the auditory system extracts, encodes and processes AM information would provide an important step towards a better understanding of the higher-order auditory processes listed above. While AM information is encoded in temporal activity patterns of neurons at the early stages of the auditory system, it is generally believed that this temporal periodicity code is transformed into a rate-based code at some higher stage of auditory processing. Such a rate-based periodicity code would correspond to the psychophysical concept of amplitude modulation filters suggested to account for the frequency selectivity in the modulation domain observed in psychophysical experiments ([Bacon and Grantham, 1989](#); [Houtgast, 1989](#); [Dau *et al.*, 1997a,b](#); [Ewert and Dau, 2000](#)). However, while psychophysical experiments may provide a way of characterizing effective amplitude modulation filters, the question how such filters are represented neurally in the auditory system remains.

Physiological experiments reveal that the average spike rates of auditory-nerve (AN) fibers are largely independent of stimulus modulation ([Rose and Capranica, 1985](#); [Joris and Yin, 1992](#); [Rhode and Greenberg, 1994b](#)), such that AN fibers are not selective to certain modulation frequencies in terms of their spike rate. The temporal modulation transfer functions (tMTF) of AN fibers, where modulation gain is computed in response to different modulation frequencies, have a low-pass shape with cutoff frequencies below 1 kHz ([Javel, 1980](#); [Palmer, 1982](#); [Kim *et al.*, 1990](#); [Joris and Yin, 1992](#); [Rhode and Greenberg, 1994b](#)). Moreover, AM information is inherent in the interspike intervals (ISI) of AN fibers ([Rose, 1970](#); [Evans, 1978](#)), indicating that AMs are encoded in the temporal activity patterns of AN fibers. The majority of neurons in the cochlear nuclei (CN) are found to display flat or low pass rate modulation transfer functions (rMTF), where spike rate is computed in response to different stimuli ([Kim *et al.*, 1990](#); [Rhode, 1994a](#); [Backoff *et al.*, 1999](#)). Since the temporal synchronization of CN neurons to AM stimuli exceeds that of AN fibers, temporal AM information present in the activity patterns of AN fibers seems to be enhanced by CN neurons ([Frisina *et al.*, 1990](#); [Kim *et al.*, 1990](#); [Rhode, 1994a](#); [Rhode and Greenberg, 1994b](#)). Thus, since CN neurons are not selective to a certain modulation frequency in terms of their spike rate, AM information can be assumed to be encoded in their temporal pattern. While AN fibers and CN

neurons have been found to synchronize to modulation frequencies as high as 1 kHz (Javel, 1980; Frisina *et al.*, 1990; Rhode and Smith, 1986; Backoff *et al.*, 1999), the highest modulation frequency for which temporal synchronization is observed in the auditory midbrain differs from below 120-150 Hz (Rees and Møller, 1983; Krishna and Semple, 2000) up to 1000 Hz (Langner, 1981). Despite this diversity, which presumably results from differences in the experimental conditions of the studies, there is general agreement among authors, that the ability of neurons to synchronize to fast amplitude modulations decreases along the ascending auditory pathway (Rees and Møller, 1983; Langner and Schreiner, 1988). Thus, if the temporal information about fast AMs is not lost as it ascends the auditory pathway, it needs to be transformed into some other kind of representation. At the level of the IC, neurons have been found that exhibit bandpass shaped rMTFs (Rees and Møller, 1983; Langner and Schreiner, 1988; Rees and Palmer, 1989; Krishna and Semple, 2000). Thus, in contrast to CN neurons, these neurons are selective to a certain modulation frequency and respond with a maximum spike rate when stimulated with their so-called best modulation frequency (BMF). Moreover, rate BMFs have been found to be topographically organized in the central nucleus of the IC and cover a BMF range of 10-1000Hz (Schreiner and Langner, 1988, 1997). Based on these findings it can be assumed that temporal information about AMs present in the activity of CN neurons is transformed into rate-based information represented by bandpass shaped rMTFs with different BMFs between the level of the CN and the IC. Such a rate-based representation of AM information is also motivated by the psychophysical concept of amplitude modulation filters (Dau *et al.*, 1997a,b; Ewert and Dau, 2000).

Two biologically motivated models have been suggested previously, both suggesting a mechanism of how temporal AM information can be transformed into a rate-based representation between CN and IC. The neural circuit suggested by Langner (1981) (see also Langner and Schreiner, 1988; Langner, 1997a,b) consists of three functional units at the model CN stage, a trigger unit, a buildup circuit and an oscillator circuit, with each of these units being associated with a neural response type in the CN. At the model IC stage a coincidence detector unit is located that represents the model output unit. According to Langner, the response types and the neural connectivity of his model units result in a bandpass shaped rMTF of the IC coincidence detector unit. In order to yield a number of bandpass rMTFs with different BMFs, a number of such neural circuits are needed that differ in the integration time constant of the CN buildup circuit. Based on the specific assumptions in his model, Langner (1997a,b) predicts that the IC bandpass units can only reveal BMFs that are multiples of the stimulus carrier frequency. Such a relationship could

not be confirmed in electrophysiological recordings, where no relationship between the BMFs of bandpass IC neurons and the stimulus carrier frequency was observed (Krishna and Semple, 2000). Moreover, since the model has not been tested extensively, it is difficult to predict whether a biologically plausible range of integration time constants in the model buildup circuit would allow for covering a plausible range of BMFs.

The second biologically motivated model describing the transformation of temporal periodicity information into a rate-based representation was suggested by Hewitt and Meddis (1994). The CN stage of their model employs populations of simulated chopper units (Hewitt *et al.*, 1992), that are morphologically associated with stellate cells in the ventral cochlear nucleus (VCN) (Rhode *et al.*, 1983; Smith and Rhode, 1989). While the chopping frequencies of units within one population are identical, the chopping frequencies among different populations of chopper units differ. Coincidence detector units are located at the model IC stage, with each coincidence detector receiving convergent input from one population of chopper units. If an amplitude modulated stimulus is presented to the model, the chopper units whose chopping frequencies resemble the modulation frequency of the stimulus synchronize best to the stimulus modulation. Thus, this population of chopper units provides a highly synchronized input to its subsequent IC coincidence detector. In contrast, the activity within populations of units whose chopping frequencies differ from the stimulus modulation is less synchronized. The IC coincidence detectors that are driven by these populations receive less synchronized input and respond with a smaller spike rate. Thus the model by Hewitt and Meddis (1994) transforms the bandpass shaped tMTFs observed in VCN chopper units into bandpass shaped rMTFs. The different BMFs of different IC coincidence detector units hereby result from the different chopping frequencies among different populations of chopper units. Thus, similar to the model by Langner (1981), different BMFs are gained from changing a temporal model parameter. Since electrophysiological studies have reported natural chopping frequencies of 50 to 400 Hz in VCN stellate cells (e.g. Frisina *et al.*, 1990; Kim *et al.*, 1990) it is not clear whether modulation frequencies below 50 Hz and modulation frequencies exceeding 400 Hz could be encoded by this model. Moreover, the shape of VCN stellate cell tMTFs becomes increasingly more low pass with decreasing stimulus level (e.g. Frisina *et al.*, 1990), such that the required bandpass shaped rMTFs would not be obtained at low stimulus levels.

In contrast to these two models where temporal model parameters are changed in order to obtain different BMFs within different model units, the modeling approach presented here employs a non-temporal mechanism. As the previous modeling studies, the presented model reflects a biologically motivated circuit based

on simulated unit responses that can be associated with neural response types. For example, simulated responses of ideal onset O_I units, a response type observed in the posteroventral cochlear nucleus (PVCN), are chosen to provide the temporal information in the present model. PVCN O_I units are found to entrain to periodic stimuli, i.e., they emit exactly one spike per stimulus period (e.g. Rhode and Smith, 1986; Rhode, 1994a) with a remarkable temporal precision.

In the first part of the present paper, the structure of the model and its dynamics are described. Subsequently an analysis of the response properties of the model units is presented, when tested with amplitude-modulated pure tones covering a wide range of modulation frequencies, levels and modulation depths, and high-frequency tone bursts. The simulation results are compared with corresponding experimental data from the literature.

3.2 MODEL STRUCTURE

Figure 3.1 displays a schematic representation of the neural model circuit. The model is a cascade of three stages: (i) the peripheral processing stages that include basilar membrane filtering, inner hair cell transduction and a simulation of AN activity (bottom), (ii) the CN stage (middle) and (iii) the IC stage of the model (top). Excitatory synaptic connections are represented by arrows and inhibitory synaptic connections are represented by filled circles. The model CN stage contains three neurons, each of which receives excitatory input from the ascending AN fibers: an entrainment (EN) neuron and two constant-rate (CR) neurons. The schematic rMTFs of each model unit, that would be ideally obtained in response to 100% amplitude modulated high-frequency tones, are shown in Fig. 3.2. The rMTF of the EN model unit, displayed in the lower left panel of Fig. 3.2, reveals that the spike rate of the EN unit corresponds to the stimulus modulation frequency up to a modulation frequency of 600 Hz. Thus, in response to modulation frequencies < 600 Hz the EN unit entrains to the stimulus modulation, emitting exactly one spike per stimulus period. If the modulation frequency exceeds 600 Hz, the EN unit can no longer follow the fast stimulus modulation. In this case the unit generates only one spike at stimulus onset. The lower right panel of Fig. 3.2 displays the schematic rMTFs of two CR units in the CN stage. Both CR units exhibit a flat rMTF, i.e., their spike rate of about 100 Hz does not depend on the stimulus modulation frequency.

All model CN units project onto the IC stage of the model, that consists of three different neurons, two low-pass (LP) units and one bandpass (BP) unit (Fig. 3.1). Each LP unit of the model IC stage receives inhibitory input provided by the CN entrainment unit and excitatory input from a different number of CR units of the CN stage, such that one LP neuron receives input from one CR unit and the other receives input from both CR units. The upper left panel of Fig. 3.2 illustrates the resulting rMTFs of the two LP units, that reveal two regions of enhancement interrupted by a region of suppression. The region of suppression results from the inhibitory contribution of the EN unit of the CN stage. If the spike rate of the EN unit, that reflects the stimulus modulation frequency, exceeds the excitatory input from the CR units, the activity of the LP unit becomes suppressed. Due to the increasing inhibitory contribution provided by the EN unit as the modulation frequency increases, the LP unit remains suppressed until the modulation frequency exceeds 600 Hz. As the EN unit fails to entrain to modulation frequencies > 600 Hz and instead exhibits an onset response, no inhibitory input is delivered to the LP unit at such high modulation frequencies. Thus, the LP neurons become active with a spike rate that reflects the excitatory input from the CR units of the CN stage. The schematic rMTFs of the two LP units shown in the upper left panel of Fig. 3.2 reveal

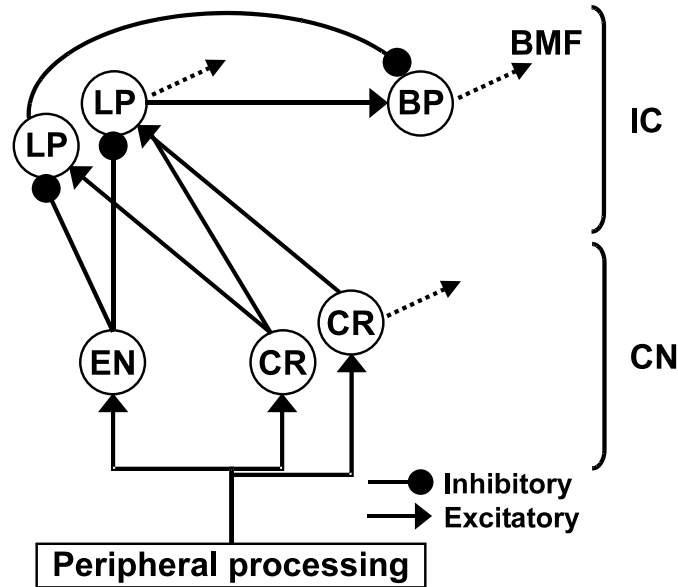


FIG. 3.1: The architecture of the present model. The model is a cascade of three stages: (i) the peripheral processing stages (bottom), (ii) the CN stage that includes an entrainment (EN) unit and a number of constant-rate (CR) units (middle) and (iii) the IC stage of the model (top) that includes low-pass (LP) and bandpass (BP) units. Excitatory synaptic connections between model units are represented by arrows and inhibitory synapses by filled circles. For a detailed description see text.

that the activity of the first LP unit (dashed line), that receives input from only one CR neuron, becomes suppressed if the stimulus modulation exceeds 100 Hz. In contrast the second LP unit (solid line), that receives excitatory input from both CR neurons, is not suppressed before the stimulus modulation frequency exceeds 200 Hz. The model output unit is the BP unit of the IC stage, that receives a strong inhibitory input from the first LP unit (dashed line) and a weak excitatory input from the second LP unit (solid line). The upper right panel of Fig. 3.2 displays the resulting rMTF of the BP unit, exhibiting a bandpass shape with a maximum spike rate at its individual BMF. This bandpass shaped rMTF results from the different modulation frequencies at which the region of suppression occurs in the LP units of the IC model stage. Since the modulation frequency at which the region of suppression occurs in an LP unit, depends on how many CR units project onto that unit, different BMFs of the model BP units are obtained from varying the number of CR input units in the present neural circuit. Thus, a rate-based representation of AMs is obtained by simply varying the number of CR units providing input to the different LP model units. In the present study, 2^n CR units are simulated that project onto $n + 1$ model LP units $n = 5$. The different LP units of the IC model stage receive input from between 2^0 to 2^n CR units and project onto n BP units with n different BMFs.

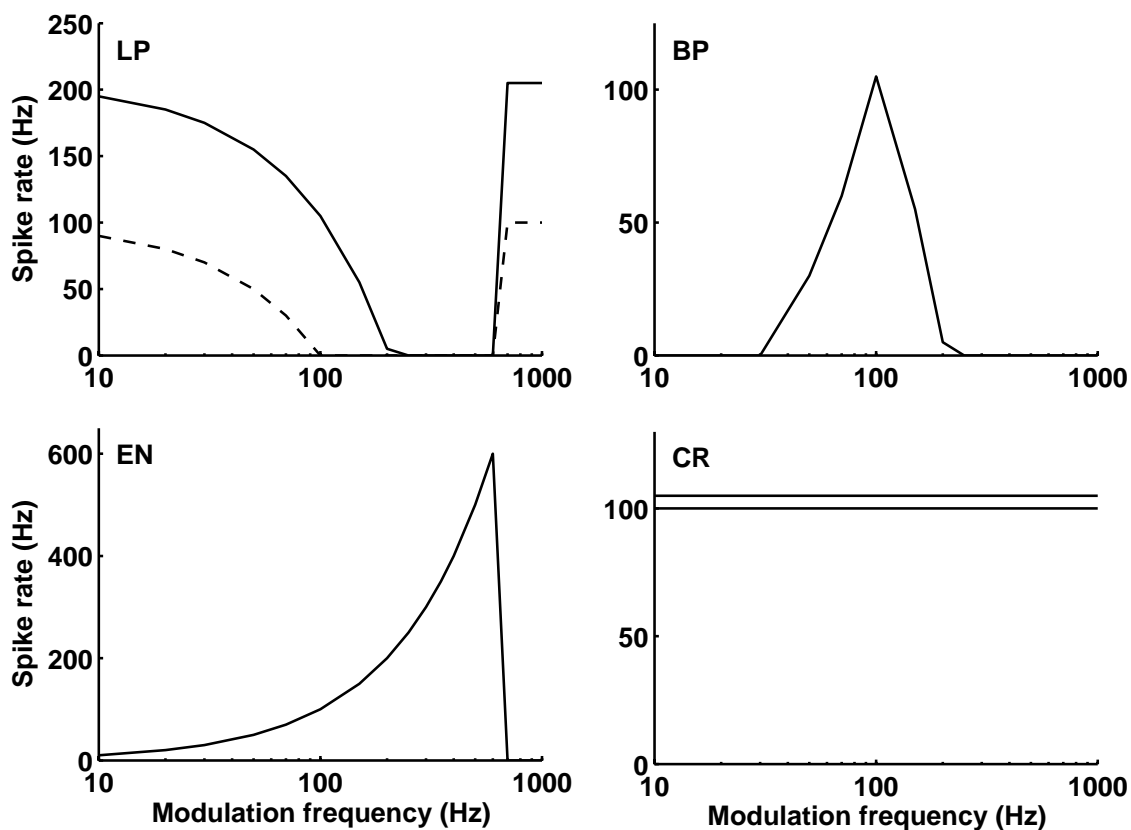


FIG. 3.2: Schematic rMTFs of the different model units: CN entrainment (EN) unit (lower left panel), CN constant-rate (CR) units (lower right panel), IC low-pass (LP) units (upper left panel) and IC bandpass (BP) unit (upper right panel)

Thus, in order to yield bandpass shaped rMTFs at the model IC stage, a precise entrainment of the EN model unit to the stimulus modulation is needed together with a number of neurons whose spike rates are independent of the stimulus modulation. All further response properties, including the bandpass shaped rMTFs at the model IC stage, result from these CN unit responses and the neural connectivity between model units. A detailed description of the model units is given in the following.

3.2.1 Auditory periphery

The frequency decomposition performed by the basilar membrane is simulated using a bank of 128 fourth-order gammatone filters (Patterson *et al.*, 1988), with center frequencies ranging from 80 Hz to 25 kHz spaced according to the equivalent rectangular bandwidth (ERB) scale. The transduction of mechanical energy into neural activity patterns, performed by the hair cells of the inner ear, is simulated by Meddis' hair-cell model (Meddis, 1986, 1988; Meddis *et al.*, 1990)¹. Based on the output

¹Despite the existence of a revised version of Meddis' hair-cell model (Sumner *et al.*, 2002, 2003), the original model was chosen here because of its well known structure. However, the peripheral

of each gammatone filter, the hair-cell model computes a deterministic spike probability function for the corresponding AN fibers in response to arbitrary stimuli. Since the frequency range and the number of AN fibers providing input to the EN and the CR model units differ largely, AN activity is computed separately for the two CN unit types. The CR model units receive input from 50 AN fibers all originating from the same peripheral frequency channel. The individual spike trains of each AN fiber is simulated by comparing the instantaneous hair-cell spike probability with a random number equally distributed in the range [0...1]. If the instantaneous spike probability exceeds the random number, a spike is generated and the AN fiber enters a refractory period of 1 ms. The EN unit of the present model receives input from at least ten times as many AN fibers, such that the AN spike trains are not simulated individually for computational reasons. Since the deterministic hair-cell probability function can be assumed to reflect the summed activity of an *infinite* number of AN fibers, a large - but limited number of AN fibers - is simulated by multiplying the hair-cell probability function, on a sample by sample basis, by a random variable equally distributed in the range [0.5...1.5] (see Sec. 2.2 of Chap. 2). Finally, the simulated AN activity is summed across a number of cochlear frequency channels, such that the EN model unit receives input from a frequency range spanning about half an octave around the unit's characteristic frequency (CF).

3.2.2 Neuron dynamics

Each model unit is simulated by a point neuron model with an integrate-to-threshold dynamic (Tuckwell, 1988). However, in order to simulate the distinct temporal response properties of the model EN unit, this unit differs from the other model units and its dynamics will be described separately. All other model units are simulated by a modified version of the MacGregor point neuron model (MacGregor, 1987; Arle and Kim, 1991). Each presynaptic spike arriving at a model unit causes a postsynaptic potential (PSP), that contributes to the membrane potential V_m of the cell. The postsynaptic potentials can be either excitatory (EPSP) or inhibitory (IPSP), depending on the type of synapse connecting the pre- and the postsynaptic unit. The shape of each postsynaptic potential $\epsilon(t)$, caused by a presynaptic spike at time $t = 0$, is described by an "alpha-function"

$$\epsilon(t) = \begin{cases} \frac{g_{ex/in}}{G} t \left[e^{-\frac{t}{\tau_{ex/in}}} \right] & \text{for } t > 0 \\ 0 & \text{otherwise} \end{cases},$$

preprocessing steps of this model can easily be exchanged by arbitrary peripheral neural models, that provide a means of reproducing the basic features of cochlear and inner hair cell filtering.

with $\tau_{ex/in}$ representing the time constant of the excitatory or inhibitory postsynaptic potential, respectively. The conductance change, $g_{ex/in}$, at an excitatory/inhibitory synapse is normalized by the total resting conductance G and reflects the effectiveness of a given synapse. The change in synaptic conductance is positive for an excitatory synapse $g_{ex} > 0$ (EPSP) and negative in case of an inhibitory synapse $g_{in} < 0$ (IPSP). The PSPs of all presynaptic spikes i arriving at times t_i contribute to the synaptic input potential V_{syn} of a model unit

$$V_{syn}(t) = \sum_{t_i} \epsilon(t - t_i).$$

The model units also possess a dynamically changing potassium conductance g_k , that reflects their refractoriness. Following each spike of a model unit, its potassium conductance is increased by a constant amount b , decaying with the potassium time constant τ_k

$$\tau_k \frac{dg_k(t)}{dt} = -g_k(t) + bs,$$

where s denotes the state variable of the model unit. The spike-induced change in potassium conductance results in a potassium potential V_k

$$V_k(t) = -\frac{g_k(t)}{G} V_m(t).$$

Both, the synaptic input potential V_{syn} and the potassium potential V_k contribute to the membrane potential V_m of the model unit, which is modeled as an integrate-to-threshold unit with membrane time constant τ_m

$$\tau_m \frac{dV_m(t)}{dt} = -V_m(t) + V_k(t) + V_{syn}(t).$$

Finally the output potential $V(t)$ of the unit is expressed with respect to its resting potential V_{rest}

$$V(t) = V_{rest} + V_m(t).$$

While the cell's output potential, $V(t)$, remains below its spike threshold Θ_{act} , the unit's state variable s is set to zero. If the membrane potential of the model unit exceeds the unit's spike threshold, the neuron emits a spike, i.e., its state variable is set to one:

$$s = \begin{cases} 0 & \text{for } V(t) \leq \Theta_{act} \\ 1 & \text{for } V(t) > \Theta_{act} \end{cases}.$$

Besides the relative refractory period of the model units, that is represented by the spike-induced increase in potassium conductance, the unit also incorporates an absolute refractory period of 1.5 ms, during which no further spikes can be emitted by the unit. The specific parameters of the different model units are summarized in Table 3.1.

TABLE 3.1: Simulation parameters of the CR, the LP and the BP model units.

Parameter	Description	CR	LP	BP
V_{rest}	membrane equilibrium potential	-60 mV	-60 mV	-60 mV
τ_m	membrane time constant	3 ms	10 ms	5 ms
τ_k	potassium time constant	1.5 ms	1.5 ms	1.5 ms
G	total resting conductance	50 nS	50 nS	50 nS
b	potassium conductance change	0.1 mS	50 μ S	50 μ S
Θ_{act}	spike threshold	-50 mV	-40 mV	-40 mV
τ_{ex}	excitatory time constant	0.5 ms	0.5 ms	0.5 ms
τ_{in}	inhibitory time constant		1 ms	3 ms
g_{ex}	excitatory conductance change	0.01 nS	0.6 nS	0.6 nS
g_{in}	inhibitory conductance change		0.9 nS	1.2 nS

The EN unit of the present model differs from the other model units in its entrained responses to the modulation frequency of AM stimuli. Thus, the EN unit model is chosen to differ from the other unit models in terms of its PSP and in the way its refractoriness is modeled. In contrast to the monophasic PSPs of the other model units that are described by an “alpha-function”, the EN unit exhibits a biphasic “effective” PSP. Since the shape of the effective PSP is compatible to a high-pass filtering of the stimulus, the EN unit enhances stimulus transients and attenuates sustained stimulus portions. Moreover, the relative refractory period of the EN unit is modeled by a dynamic spike-blocking mechanism. Such a dynamic spike-blocking mechanism in combination with a biphasic effective PSP has been shown to account for entrainment to a wide range of frequencies and levels (see Chap. 2).

The postsynaptic potential $\epsilon(t)$ of the EN model unit caused by a presynaptic spike at time $t = 0$, is chosen as

$$\epsilon(t) = \begin{cases} t \left[e^{-\frac{t}{\tau_a}} - ce^{-\frac{t}{\tau_b}} \right] & \text{for } t > 0 \\ 0 & \text{otherwise} \end{cases},$$

with τ_a and τ_b being time constants and c denoting a constant factor. The PSP of each presynaptic spike i contributes to the membrane potential $V_m(t)$ of the EN model unit. The EN unit is modeled as an integrate-to-threshold neuron with membrane time constant τ_m

$$\tau_m \frac{dV_m(t)}{dt} = -V_m(t) + \sum_{t_i} \epsilon(t - t_i).$$

TABLE 3.2: Simulation parameters of the EN model unit.

Parameter	Description	EN
V_{rest}	membrane equilibrium potential	-60 mV
τ_m	membrane time constant	1 ms
Θ_{act}	spike threshold	-45 mV
τ_a	effective PSP time constant	0.1 ms
τ_b	effective PSP time constant	0.2 ms
c	constant PSP factor	0.25
Θ_{rel}	spike blocking release threshold	-59 mV

The output potential $V(t)$ of the EN unit is, again, expressed with respect to the units resting potential V_{rest}

$$V(t) = V_{rest} + V_m(t).$$

Similar to the other model units, the state variable of the EN unit is set to one, if its potential exceeds its spike threshold Θ_{act} , such that the neuron generates an action potential:

$$s = \begin{cases} 0 & \text{for } V(t) \leq \Theta_{act} \\ 1 & \text{for } V(t) > \Theta_{act} \end{cases}.$$

In contrast to the other units whose relative refractory periods are simulated by changes in the potassium conductances of the units, the relative refractory period of the EN unit is modeled by a dynamic spike-blocking mechanism. A spike-blocking mechanism has originally been suggested by [Romand \(1978\)](#), as a mechanism to shape onset responses. Following each spike, the EN unit enters a spike-blocked state during which it can not exhibit further action potentials. This spike-blocked state lasts until its potential falls below a so-called spike blocking release threshold Θ_{rel} that releases the cell from spike blocking. Additionally, the EN unit possesses an absolute refractory period of 0.8 ms during which the it can not emit further action potentials. A detailed description of the EN unit model and its mechanisms is given in Sec. 2.2 of Chap. 2. The specific parameters of the EN unit are given in Table 3.2. All simulations of the present study are performed at a sampling rate of 50 kHz.

3.3 SIMULATIONS AND DATA ANALYSIS

All simulations are performed within the neural circuit that receives input from the peripheral filter channel centered at 10.087 kHz. If not stated otherwise the neural circuit is tested using 100% sinusoidally amplitude modulated (SAM) 10-kHz tones. Simulation results are compared to recorded data from the literature, if available. The degree of temporal synchronization of the model response to an SAM tone is analyzed using the synchronization coefficient (SC) (Goldberg and Brown, 1969), computed as the vector strength of the distribution of spikes (with SC=1 indicating perfect synchronization to the stimulus modulation and SC=0 representing no synchronization). The rMTF, where spike rate is plotted as a function of modulation frequency, is also computed in order to determine whether the spike rate of an individual model unit is selective to a certain modulation frequency. SAM stimuli are presented for 1.05 s with the initial 50 ms of a unit's response being excluded from the analysis in order to avoid onset effects. The response types of the different model units are characterized by their peri-stimulus time histograms (PSTH) yielded in response to a ramped 10-kHz tone burst with a duration of 100 ms. PSTHs are gained from 250 stimulus representations of the high-frequency tone burst and binned with 0.5 ms (ramp duration 10 ms).

3.3.1 EN unit responses

The EN unit of the model CN stage provides the present neural circuit with periodicity information due to its entrained response to periodic stimuli. This temporal periodicity information is then transformed into a rate-based periodicity representation by the present neural circuit. Thus, the quality of the present model depends crucially on the reliability and temporal precision of the simulated EN unit responses. A detailed description of the EN unit model and its response properties is given in Chap. 2. Figure 3.3 displays the modulation transfer functions of the EN unit in response to an 100% amplitude modulated 10-kHz tone presented at 60 dB SPL. The spike rate in the rMTF (right scale, triangles) of the EN unit corresponds to the stimulus modulation up to modulation frequencies of 600 Hz. At frequencies above 600 Hz, the EN unit can not follow the fast fluctuations of the modulated stimulus anymore and exhibits purely an onset response to the stimulus. Figure 3.3 also displays the synchronization coefficient (left scale, circles) of the EN unit that lies between 0.98 and 1 for modulation frequencies below 600 Hz. Such a high synchronization coefficient, together with a spike rate that reflects the stimulus modulation, indicate a nearly perfect entrainment of the unit to the stimulus modulation. Mo-

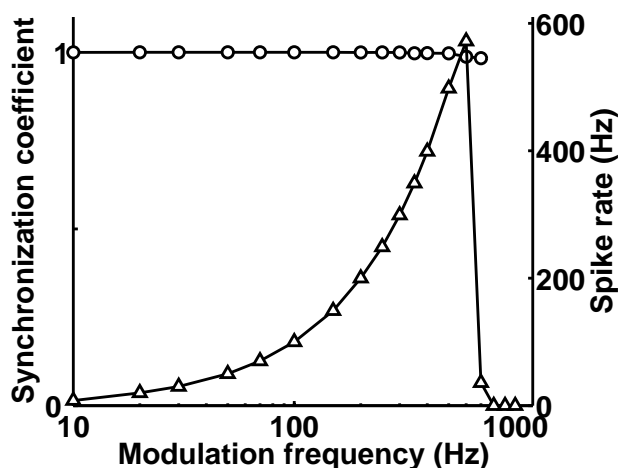


FIG. 3.3: Simulated rMTF (right scale, triangles) and synchronization coefficient (left scale, circles) of the EN model unit in response to 100% amplitude modulated 10-kHz tones with varying modulation frequencies presented at 60 dB SPL. The MTFs of the EN unit indicate a nearly perfect entrainment of the unit to the stimulus modulation.

reover, the entrained responses of the model EN unit are largely independent of stimulus level.

The upper left panel of Fig. 3.4 displays the pure tone PSTH of the EN model unit, when stimulated with a 10-kHz tone burst presented at 50 dB SPL. The unit displays one spike at stimulus onset, that is followed by no further activity during the sustained portion of the stimulus. Such a high-frequency pure-tone PSTH can be associated with a cochlear nucleus O_I (ideal onset) unit. These units have been found to respond to pure-tone stimuli ($f > 2$ kHz) revealing one sharply timed action potential at stimulus onset followed by no or little (< 10 spikes/s) subsequent activity during the sustained portion of the tone (Godfrey *et al.*, 1975; Rhode and Smith, 1986). Morphologically, O_I units are associated with posteroventral cochlear nucleus (PVCN) octopus cells (Kane, 1973; Godfrey *et al.*, 1975). When stimulated with SAM pure tones with modulation frequencies < 800 Hz, octopus cells have been found to entrain to the stimulus modulation (Rhode and Smith, 1986; Rhode, 1994a). Moreover, due to their precisely timed action potentials in response to AM stimuli, these cells have been assumed to be the best temporal encoders of AM stimuli among all major cell types in the cochlear nucleus (Frisina *et al.*, 1990; Rhode, 1994a; Winter and Palmer, 1995). Thus, the response properties of the model EN unit correspond well to the responses observed in PVCN octopus cells.

3.3.2 CR unit responses

The CR units represent another class of neurons located at the CN stage of the present neural circuit. In contrast to the rMTF of the EN unit that reflects the stimulus modulation, the rMTF of a CR unit is independent of the modulation frequency of the stimulus. Thus, while the EN unit provides the model with the AM information, the CR units provide the mechanism by which the selectivity of different IC units to different modulation frequencies is shaped. The left panel of Fig. 3.5 displays

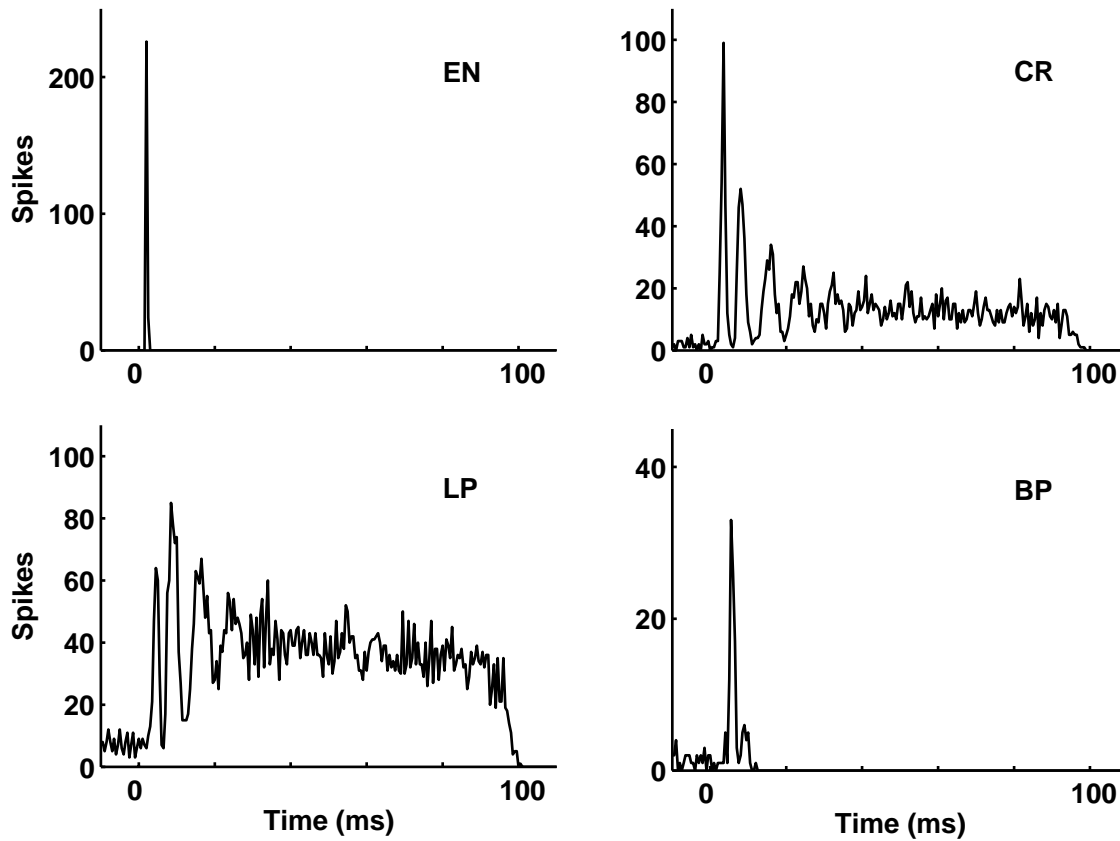


FIG. 3.4: PSTHs of the model units (CF=10.087 kHz) in response to a 10-kHz tone burst presented at 50 dB SPL. The EN model unit (upper panel, left) reveals an onset-type PSTH. In contrast, the PSTH of the CR unit (upper panel, right) reveals a sustained chopping response (CR unit parameters: $\tau_m = 3$ ms, $\Theta_{act} = -48$ mV). The preferred interspike interval of 8 ms of the CR unit corresponds to an individual chopping frequency of about 125 Hz. The PSTH of the LP unit (lower panel, left), receiving excitatory input from 8 CR units and inhibitory input from the EN unit, displays a sustained response. The chopping observed in CR input units is also reflected in the PSTH of the LP unit. The PSTH of the model BP unit (lower panel, right), receiving excitatory input from the LP unit with 8 CR inputs and inhibitory input from the LP unit with 4 CR inputs, reveals an onset response. However, compared to the EN unit, the BP unit responds with a larger first-spike latency and less temporal precision.

the simulated rMTF of one example model CR unit (with membrane time constant $\tau_m = 3$ ms and spike threshold $\Theta_{act} = -48$ mV) in response to 100% amplitude modulated 10-kHz tones presented at three different levels (40, 60 and 80 dB SPL), as a function of the stimulus modulation frequency. Despite small fluctuations in the spike rate resulting from stochastic fluctuations in the AN activity, the rMTF reveals that the spike rate of the CR neuron does not depend on the modulation frequency. However, the spike rate slightly increases with increasing stimulus level. The corresponding synchronization coefficient is shown in the right panel of Fig. 3.5. The tMTF of the CR unit becomes increasingly more bandpass when the stimulus level is increased from 40 to 80 dB SPL.

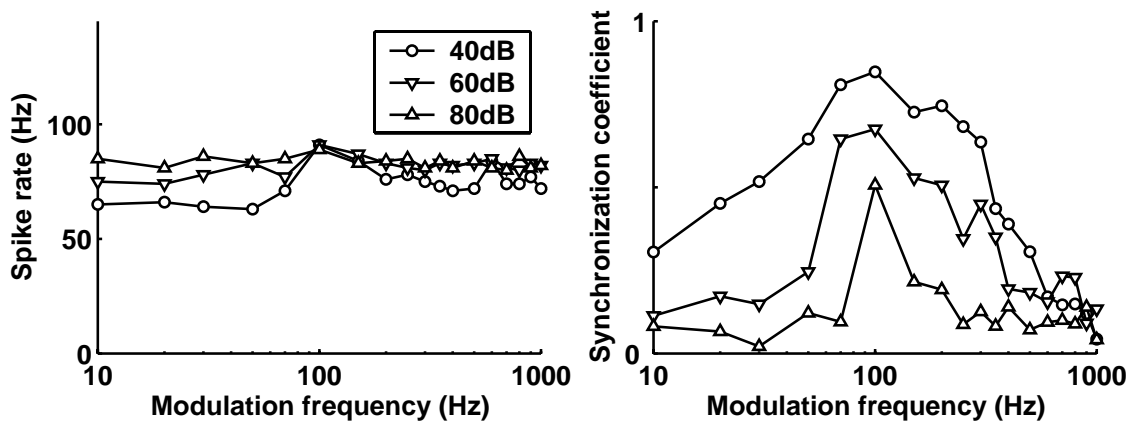


FIG. 3.5: Left: Simulated rMTF of one model CR unit (CR unit parameters: $\tau_m = 3$ ms, $\Theta = -48$ mV) in response to 100% amplitude modulated 10-kHz tones with different modulation frequencies presented at 40, 60 and 80 dB SPL. Right: The synchronization coefficients of the same unit as a function of the modulation frequency of the 10-kHz tone for stimulus presentation levels of 40, 60 and 80 dB SPL.

The upper right panel of Fig. 3.4 displays the PSTH of the CR unit in response to a 10-kHz tone burst presented at 50 dB SPL. The PSTH reveals that the CR unit responds with a preferred interspike interval of approx. 8 ms which is not related to the 10-kHz tone. The model CR unit thus displays a so-called sustained chopping response. Such a response type is morphologically associated with stellate cells located in the ventral cochlear nucleus (Rhode *et al.*, 1983; Smith and Rhode, 1989). Stellate cells are found to reveal a chopping response during the first 10-15 ms of a pure tone stimulus with an individual chopping frequency that is not related to the stimulus (Smith and Rhode, 1989). Moreover, recorded rMTFs of stellate cells are found to be flat, while their tMTFs are found to be low pass at low stimulus levels and become increasingly more bandpass as the stimulus level increases (Frisina *et al.*, 1990; Kim *et al.*, 1990; Rhode, 1994a). Thus, the responses of the CR model units correspond well to the response properties of VCN stellate cells. Up to 32 CR units are simulated in the present neural circuit. In order to obtain small variations in the responses of different CR units, without the need of simulating the 50 AN fibers that provide input to each CR unit separately, the units are chosen to slightly differ in their membrane time constants τ_m and their spike thresholds Θ_{act} . Both sets of randomized parameters are chosen to follow a Gaussian distribution with a standard deviation of 5% of the mean values given in Table 3.1. The maximum deviation from the mean was restricted to $\pm 20\%$. The parameters were randomly permuted, before they served as parameters for the CR model units. Due to this slight randomization of parameters, small differences in the activity of the CR model units are obtained.

3.3.3 LP unit responses

Each LP unit of the model IC stage receives weak excitatory synaptic input from a different number of CR model units causing fast EPSPs (see Fig. 3.1. In addition, each LP unit receives strong inhibitory synaptic input from the EN model unit causing slow IPSPs. This choice of neural connectivity results in a modulation frequency selective rMTF of the LP model units. The rMTFs of two LP model units that receive input from 4 (triangles) and 8 (circles) model CR units are shown in the left panel of Fig 3.6 in response to 100% amplitude modulated 10-kHz tones with different modulation frequencies. Both rMTFs are characterized by two regions of enhancement that are interrupted by a region of suppression. The regions of suppression occur, if the inhibition from the EN model unit that reflects the stimulus modulation frequency exceeds the excitatory contribution, provided by the CR units. The more CR units project onto an LP unit, the higher the modulation frequency at which the region of suppression occurs. The first LP unit receiving input from 4 CR units (triangles) becomes suppressed at modulation frequencies between 70 and 100 Hz. In contrast, the response of the second LP unit that receives input from 8 CR units (circles) only becomes suppressed, if a stronger inhibition is provided by the EN unit. As the amount of inhibition reflects the stimulus modulation, a modulation frequency > 200 Hz is needed before the activity of this LP unit becomes suppressed. For modulation frequencies exceeding 600 Hz, at which the EN unit can not entrain to the fast stimulus fluctuation anymore and exhibits purely an onset response, the LP units are no longer suppressed and respond with a spike rate that reflects their CR input.

The lower left panel of Fig. 3.4 displays the PSTH of the LP model unit (8 CR input units) in response to a 10-kHz tone burst presented at 50 dB SPL. Since the PSTH of the EN unit shown in the upper left panel of the figure purely reveals one onset spike, this unit does not provide any input to the LP unit during the sustained stimulus portion. Thus, the sustained chopping found in its CR input is reflected in the sustained response of the LP model unit. Electrophysiological recordings from IC units with sustained pure tone PSTHs reveal that these units can show two regions of enhancement, interrupted by a region of suppression (Krishna and Semple, 2000). The right panel of Fig. 3.6 displays a recorded rMTF of a unit with a sustained pure-tone PSTH in response to an 100% amplitude modulated pure tone presented at 50 dB SPL, replot from Krishna and Semple (2000)). The carrier frequency of the AM stimulus was chosen to equal the unit's CF of 0.9 kHz. Although the recorded rMTF differs from the simulated rMTFs (Fig. 3.6) in its CF and in the frequency range at which the region of suppression occurs, it still displays a similar

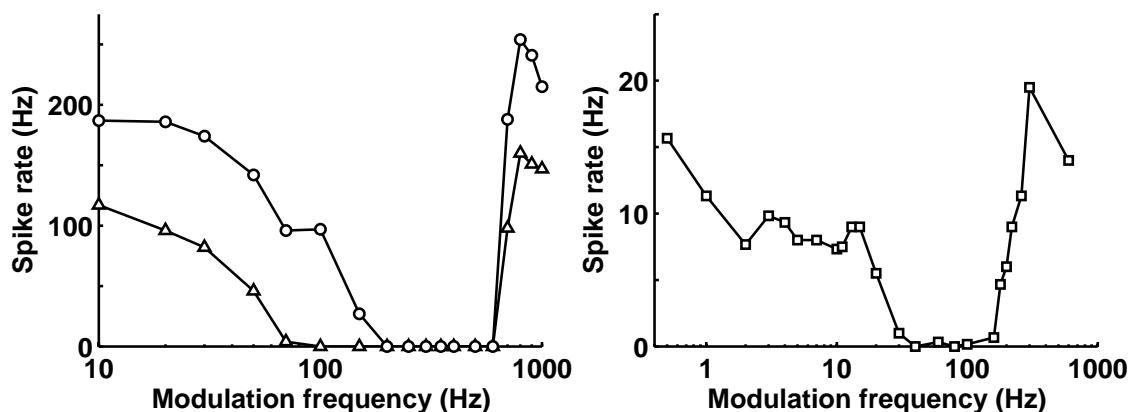


FIG. 3.6: Left: Simulated rMTF of two model LP units, receiving input from 4 (triangles) and 8 (circles) model CR units in response to 100% amplitude modulated 10-kHz tones with different modulation frequencies. Right: Recorded rMTF of a sustained IC unit (CF=0.9 kHz) as a function of 100% amplitude modulated 0.9-kHz tones presented at 50 dB SPL. Replot with permission from [Krishna and Semple \(2000\)](#).

characteristics. Thus, the response properties of the model LP unit are at least in good qualitative agreement with data obtained from sustained IC neurons.

3.3.4 BP unit responses

The frequency selectivity of the model LP units, reflected in the different modulation frequencies at which the region of suppression occurs in the rMTFs of different LP units, is transformed into bandpass shaped rMTFs at the model BP units. The bandpass shaped rMTF of a BP unit results from a weak excitatory synaptic input provided by the corresponding LP model unit and a strong inhibitory synaptic input from the adjacent model LP unit, as shown in Fig. 3.1. Compared to the LP unit that provides excitatory input to the model BP unit, the inhibitory LP unit is chosen to receive a smaller number of CR input such that the region of suppression in its rMTF occurs at a lower modulation frequency. The left panel of Fig. 3.7 displays the rMTF of the model BP unit that receives input from the two LP units shown in Fig 3.6, in response to a 100% amplitude modulated 10-kHz tone presented at 60 dB SPL. Weak excitatory input is provided by the LP unit receiving input from 8 CR units (circles), while strong inhibitory input is provided by the LP unit receiving input from 4 CR units (triangles). While the inhibitory LP unit suppresses the activity of the BP unit at low modulation frequencies, it provides no inhibitory contribution at modulation frequencies > 100 Hz. However, the contribution of the excitatory LP unit is not suppressed until the modulation frequency exceeds 200 Hz, resulting in a bandpass shaped rMTF at the BP unit. At modulation frequencies > 600 Hz, where both LP units are exclusively driven by the CR input, the contribution of the

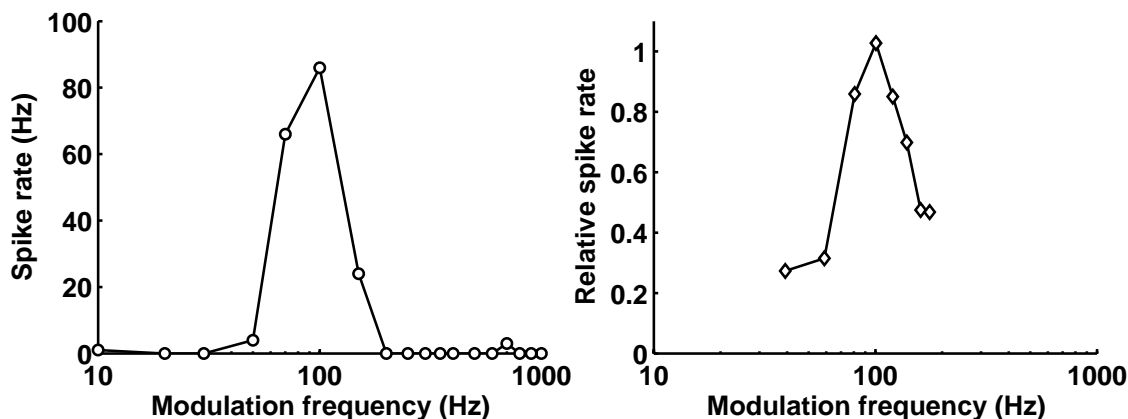


FIG. 3.7: Left: Simulated rMTF of the model BP unit that receives input from the two LP units shown in Fig. 3.6 (left), in response to a 100% amplitude modulated 10-kHz tone with different modulation frequencies. Right: Recorded IC bandpass rMTF in response to 100% amplitude modulated pure tones with different modulation frequencies. The carrier frequency of the AM stimulus was chosen to correspond to the unit’s CF of 1.8 kHz. The recorded rMTF was normalized by its BMF spike rate of 26 spikes/s. Replot with permission from [Langner and Schreiner \(1988\)](#).

inhibitory LP unit compensates for the excitatory LP unit input and the BP unit reveals no response.

The lower right panel of Fig. 3.4 displays the PSTH of the model BP unit shown in Fig. 3.7 in response to a 10-kHz tone burst presented at 50 dB SPL. In contrast to the sustained PSTH found in the model LP units (lower left panel of Fig. 3.4) the model BP unit reveals an onset PSTH. The right panel of Fig. 3.7 shows a recorded rMTF of an IC neuron in response to 100% amplitude modulated pure tones with different modulation frequencies and a carrier frequency that corresponds to the CF of the unit, replot from [Langner and Schreiner \(1988\)](#). The quality factor of a bandpass rMTF can be expressed as the BMF divided by the bandwidth of the rMTF 3 dB below its peak (Q_{3dB}). Since the -3 dB-bandwidth of the simulated 100-Hz bandpass is 51 Hz, it results a Q_{3dB} -value of 1.9. The bandwidth of the recorded bandpass is about 70 Hz, resulting in a Q_{3dB} -value of about 1.4. The simulated responses of the BP unit also correspond well to recorded data from [Krishna and Semple \(2000\)](#) who found that the rMTFs obtained from IC neurons that exhibit an onset response often reveal a bandpass shape.

3.3.5 Simulation of amplitude modulation filters

In order to obtain bandpass rMTFs with BMFs that cover a broad range of modulation frequencies, 32 CR units, receiving input from the same peripheral filter channel (CF=10.087 kHz), are simulated. The CR units differ slightly in their time constants τ_m and their spike thresholds Θ_{act} , which are chosen from a Gaussian distribution (as described in Sec. 3.3.2). The 32 CR units project onto different LP units, each

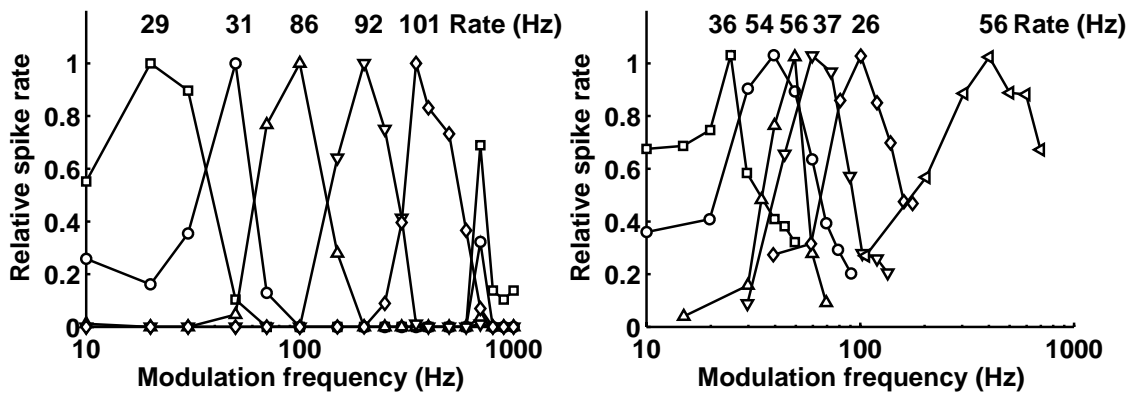


FIG. 3.8: Left: Simulated rMTFs of the five model BP units in response to 100% amplitude modulated 10-kHz tones with varying modulation frequencies. Each rMTF is normalized by its BMF spike rate (given above the rMTFs) that corresponds to the spike rate at the peak of the unit's rMTF. Right: Recorded IC rMTFs in response to 100% amplitude modulated pure tones with carrier frequencies that correspond to the individual CF of the recorded unit. Stimuli were presented 30 to 60 dB above the individual response threshold of a unit. Each rMTF is normalized by its BMF spike rate that is given above each rMTF. Replot with permission from [Langner and Schreiner \(1988\)](#).

of which receives input from a different number of CR units, ranging from 2^0 to 2^n , whereby $n = 5$. Thus, five model BP units are obtained that reveal bandpass shaped rMTFs with different BMFs. The left panel of Fig. 3.8 displays the simulated bandpass rMTFs of the five BP units, in response to 100% amplitude modulated 10-kHz tones with varying modulation frequencies ranging from 10 Hz to 1 kHz. Each rMTF is normalized by its individual maximum response rate (i.e. its BMF spike rate). The value of the BMF spikes rates are shown above the rMTFs. The right panel of Fig. 3.8 displays data obtained in IC recordings, replot from [Langner and Schreiner \(1988\)](#). Recorded data are obtained from 100% amplitude modulated pure tones with carrier frequencies that correspond to the individual CF of the recorded unit, presented between 30 and 60 dB above the individual response threshold of the units. The average Q_{6dB} -value (BMF divided by the bandwidth of the rMTF 6 dB below its peak) of 0.8 ± 0.3 reported by [Langner and Schreiner \(1988\)](#) differs from the simulated average Q_{6dB} -value of 1.3. However, the simulated Q_{6dB} -value is in the range of the Q_{6dB} -values derived from psychophysical modulation masking experiments ([Dau et al., 1997a,b](#); [Ewert and Dau, 2000](#)).

3.3.6 Level dependence and modulation depth

The level dependence of the simulated IC bandpass rMTFs is tested using the BP model unit with a BMF of 100 Hz. Figure 3.9 shows the rMTF of the 100-Hz BP unit in response to 100% amplitude modulated 10-kHz tones presented at 40, 60 and

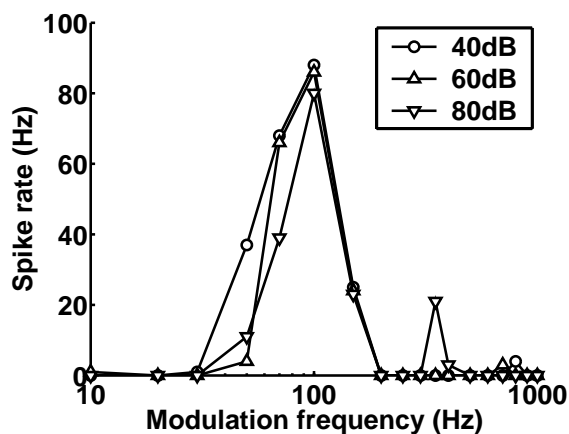


FIG. 3.9: Simulated rMTF of the 100-Hz BP unit (CF=10.087 kHz) as a function of the modulation frequency of 100% amplitude modulated 10-kHz tones presented at 40, 60 and 80 dB SPL.

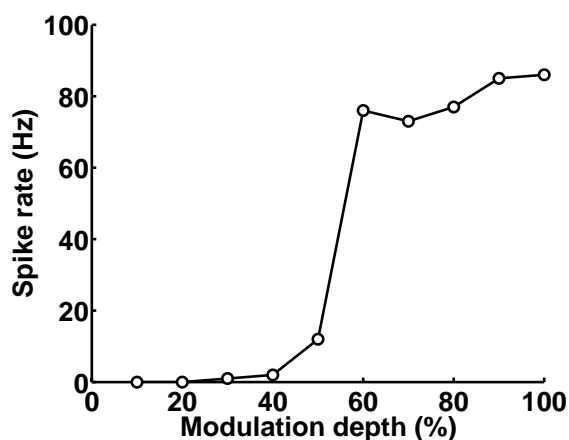


FIG. 3.10: Simulated spike rate of the 100-Hz BP unit (CF=10.087 kHz) as a function of the modulation depth of a 10-kHz tone amplitude modulated with 100 Hz and presented at a level of 60 dB SPL.

80 dB SPL. The bandpass shape of the rMTF is not affected by the stimulus level, and therefore represents a robust property of the model BP unit. The effect of stimulus modulation depth on the response of the same model BP unit is tested using a 10-kHz carrier modulated at a rate of 100 Hz with varying modulation depths presented at 60 dB SPL. Figure 3.10 displays the BMF spike rate of the 100 Hz bandpass when the stimulus modulation depth is varied from 10 to 100%. The simulated response exhibits a strong influence of the stimulus modulation depth on the BMF spike rate. While the unit essentially reveals no response at modulation depths smaller than 30%, its response rate increases rapidly between 30 and 60% before it saturates. Thus, the stimulus modulation depth can not be encoded by the spike rate of the model BP unit, as neither low stimulus modulation depths are encoded nor high modulation depths can be distinguished. This problem results inherently from the model EN unit that can not detect low stimulus modulation depths. However, a possible solution for this limitation of the present model is suggested in a companion model described in Chap. 4.

3.4 DISCUSSION

3.4.1 Biological plausibility of the present model

The pure-tone PSTH and the rMTF of each model unit have been compared to data from electrophysiological recordings, such that each unit could be associated with a physiological response type. The model EN unit, for example, is assumed to correspond to a PVCN octopus cell. These cells are found to receive convergent input from a large number of across-frequency AN fibers (Lieberman, 1993; Oertel *et al.*, 2000) and project to the superior paraolivary nucleus (SPN) and the ventral nucleus of the lateral lemniscus (VNLL). The influence of octopus cells on the IC is indirect and inhibitory as neurons in the SPN are GABAergic (Kulesza and Berrebi, 1999), and neurons in the VNLL that are innervated by octopus cells are glycinergic (Saint Marie *et al.*, 1997). The inhibitory influence of octopus cells on IC neurons corresponds well with the neural connectivity of the present model. Axons of VCN chopper neurons, assumed to be represented by the model CR units, have been found to project to the IC by way of synaptic terminals that are indicative of an excitatory neural connection (Smith and Rhode, 1989). Thus, the excitatory projections of the model CR units onto the LP units also correspond well to experimental findings.

Compared to the CN, little is known about cell types and neural connectivity in the IC. However, Krishna and Semple (2000) reported that IC neurons revealing rMTFs with a region of suppression exhibit a sustained pure-tone PSTH. In contrast, IC neurons that reveal a bandpass shaped rMTF, show an onset-type pure-tone PSTH. These findings agree well with the simulated responses of the IC model units. Although the reason that causes the region of suppression observed in recorded IC rMTFs is not known, the connectivity of the present model provides a possible mechanism by which these regions of suppression could be shaped. Moreover, it has been observed that if the stimulus modulation depth is gradually decreased, the region of suppression gradually turns into a region of enhancement until the rMTF reveals a low-pass shape (Krishna and Semple, 2000). In the present model, the region of suppression results from the inhibitory input provided by the EN unit. As this unit fails to entrain to stimuli modulated at a low modulation depth, it provides no inhibitory input to the LP model units. Thus, if low modulation depths are used the rMTFs of the LP model units do no longer show a region of suppression. This effect is also responsible for the dependency of the BMF spike rate of the model BP units on modulation depth as shown in Fig. 3.10. Since the bandpass shaped rMTF of the unit results from the different modulation frequencies at which the region of suppression occurs in the LP input units, its decreased spike rate at low stimulus

modulation depths results from the regions of suppression turning into regions of enhancement in the LP input units.

Since little is known about lateral connections between neurons in the IC, it can not be decided whether the ordered lateral inhibition among neighboring cells in the model IC stage is biologically plausible or not. However, the fact that the auditory midbrain appears to be extensively interconnected (Oliver and Huerta, 1991) does not seem to argue against the choice of lateral connections in the present model. The synaptic effectiveness of inhibitory synapses is chosen to be larger than the effectiveness of excitatory synapses in the present model. Additionally, inhibitory synapses are assumed to act on a longer time scale than excitatory synapses. However, since inhibition can act on a broad range of time scales extending to tens of milliseconds, the IPSP time constants (≤ 3 ms) used in the present model are biologically plausible.

3.4.2 Alternative mechanisms

Despite the biologically plausible response types of the units in the present model, the model provides a universal approach for the formation of bandpass filters in the IC. The different BMFs of bandpass neurons within one peripheral filter channel shown in Fig. 3.8 result from varying the number of CR input neurons in the present model. It is important that the spike rates of the CR model units are independent of the stimulus modulation frequency, i.e., that the CR model units reveal flat rMTFs. The simulated CR units of the present model exhibit chopper pure-tone PSTHs and thus can be associated with stellate cells. However, as 90% of the CN neurons are found to display flat or low pass rMTFs in response to amplitude-modulated signals (Backoff *et al.*, 1999), the constant-rate responses of the CR units could be represented by a number of different CN cell types. Moreover, the mechanism by which different BMFs of different model bandpass units are shaped, namely the different number of CR input units, can be exchanged by other mechanisms, that result in different input rates at different LP units. Such different input rates can, for example, be gained by varying the spike rates among different CR units. Differences in the effectiveness of synapses connecting CR units and LP units are another possible mechanism by which different BMFs could be shaped. Finally, a combination of these three possible mechanisms, i.e., a different number of input units, different spike rates and different synaptic effectiveness could also account for the formation of different BMFs. Which CN neuron type might represent the model CR units and which of the suggested mechanisms is involved can not be decided here. However, the suggested mechanism describing the formation of bandpass rMTFs

may provide a basic mechanism that is not depending on specific neural responses and could be realized in various ways.

3.4.3 Implications of the present model

The responses of the EN model unit have been found to correspond to O_I -unit responses observed in the VCN. This is a response type that is morphologically associated with PVCN octopus cells (Godfrey *et al.*, 1975). Due to their precise entrainment to click trains and AM stimuli with repetition/modulation rates < 800 Hz (Rhode and Smith, 1986; Rhode, 1994a; Oertel *et al.*, 2000), PVCN octopus cells are presumed to be the best encoders of AM stimuli among all major cell types in the CN (Frisina *et al.*, 1990; Rhode, 1994a; Winter and Palmer, 1995). Moreover, the ability of octopus cells to entrain to periodic stimuli has led to the assumption that these cells may play an important role in the processing of amplitude modulation and pitch information (Frisina *et al.*, 1990; Golding *et al.*, 1995; Evans and Zhao, 1997; Cai *et al.*, 2001). The present model is, to my knowledge, the first mechanism that employs simulated O_I -type responses in a neural circuit describing the formation of bandpass shaped rMTFs in the IC. Thus, the present model suggests a possible way of how the distinct O_I -unit responses could be used in higher-order auditory processing.

The different BMFs obtained in the BP units of the present model result from varying the input spike rate of the different LP model units. Thus, the formation of different BMFs is yielded by a rate-based mechanism and not by varying a temporal model parameter. This is in contrast to other existing models describing the formation of bandpass shaped rMTFs in the IC (Langner, 1981; Langner and Schreiner, 1988; Langner, 1997a,b; Hewitt and Meddis, 1994). These previous models are all based on varying a temporal parameter of the model in order to yield a representation of different BMFs at different IC neurons. In order to test the biological plausibility of these models, electrophysiological recordings have to reveal whether the range of temporal parameters that are needed to cover the wide range of modulation frequencies in these models really exist in biological neurons. This problem does not occur in the present model which describes a fundamentally different mechanism, based on the connectivity of biologically plausible unit responses. However, the present mechanism bears one problem. The small “dynamic range” of about 30% observed in the spike rate of the model BP unit in response to different modulation depths (Fig. 3.10) does not allow for a reasonable encoding of different stimulus modulation depths. Low modulation depths are not encoded whereas high modulation depths result in identical spike rates. This contrasts at least with psychophysical experiments in humans, where modulation depths as small as 3% can

be detected in amplitude modulated pure tones and a total dynamic range of about 97% has been observed [Kohlrausch *et al.* \(2000\)](#). The ability to distinguish between different modulation depths is also needed for the perception of complex AM stimuli and thus provides a crucial test for any neural AM model. Since the present neural model does not allow for encoding the range of modulation depths that can be distinguished perceptually, some aspects of the model need to be extended. Such an extended version of the model will be described in [Chap. 4](#).

3.5 SUMMARY AND CONCLUSION

A neural circuit was presented that allows for the transformation of temporal periodicity information, as a code of stimulus periodicity found at the level of the CN, into a rate-based periodicity code, assumed to represent stimulus periodicity at the level of the IC. The CN model stage employs two types of units that can be associated with neural response types found in the VCN: (i) the model EN units associated with ideal onset O_I units and (ii) the model CR units associated with sustained chopper C_S units. The temporal periodicity information provided by the model EN units is transformed into bandpass shaped rMTFs at the output units of the model IC stage. The different rate BMFs obtained in different model IC units simply result from varying the number of CR units that project onto the model IC units. Thus, in contrast to alternative models, describing the formation of bandpass shaped rMTFs between CN and IC, the present model employs no systematically varying temporal parameters like time constants or delay lines. Moreover, the bandpass shaped rMTFs simulated by the present neural circuit are independent of the presentation level of the AM stimulus. They might represent a neural implementation of the amplitude modulation filters suggested on the basis of psychophysical modulation masking data.

CHAPTER 4

AN ADVANCED NEURAL MODEL FOR THE PERIODICITY ANALYSIS OF COMPLEX SOUNDS

ABSTRACT

Masking experiments in the modulation frequency domain suggest a spectral frequency decomposition of the envelope of a complex stimulus by amplitude modulation filters (Bacon and Grantham, 1989; Houtgast, 1989; Dau *et al.*, 1997a,b). Although the neural circuit presented in Chap. 3 provides a possible mechanism by which a selectivity to the modulation frequency of sinusoidally amplitude modulated (SAM) pure tones might be shaped in inferior colliculus neurons, the neural circuit does not allow for a realistic description in the case of more general and more complex envelope waveforms. Moreover, the high sensitivity of detecting modulations in SAM tones found in human listeners (e.g. Kohlrausch *et al.*, 2000) and the resulting large dynamic range of audible modulation depths can not be encoded by the neural circuit presented in Chap. 3. Thus, an extended version of the neural circuit is presented here that employs a set of entrainment (EN) units, whose spike and release threshold potentials are systematically varied, such that they differ in their sensitivity to SAM depth. Within the extended model 10 EN units are used that shape each of the five simulated modulation filters. As a result, a linear relationship between the simulated model output and the modulation depth of an SAM stimulus is obtained. The extended model is tested using stimuli that reveal complex envelope waveforms, such as pure tones modulated by the sum of two sinusoids, narrowband Gaussian and low-noise noise and iterated rippled noise (IRN). The simulations are compared to results according to the psychophysically motivated envelope-power spectrum model (EPSM) (Ewert and Dau, 2000). The comparison reveals that the modulating

on frequency selectivity produced by the nonlinear neural circuit shows properties that are similar to those of the filterbank analysis within the EPSM. The present model is the first biologically motivated neural circuit that accounts both for the encoding of SAM depth over a large dynamic range and for modulation frequency selective processing of simple and complex sounds. The model may thus provide an important step towards an understanding of how amplitude modulation processing is performed by the auditory system.

4.1 INTRODUCTION

Information about periodic amplitude modulations (AM) as a physical feature of an acoustic signal is assumed to be transformed from a temporal periodicity code into a rate-based representation by auditory neural circuitry. This is motivated by electrophysiological recordings from auditory-nerve (AN) fibers (Rose, 1970; Evans, 1978) and cochlear nucleus (CN) neurons (Frisina *et al.*, 1990; Kim *et al.*, 1990; Rhode, 1994a; Rhode and Greenberg, 1994b) where AM information is found to be encoded in temporal neural activity patterns. In contrast, at the level of the inferior colliculus (IC), a subsequent stage of the CN along the ascending auditory pathway, neurons have been found that are selective to the modulation frequency of an AM stimulus in terms of their spike rate (Rees and Møller, 1983; Langner and Schreiner, 1988; Rees and Palmer, 1989; Krishna and Semple, 2000). The observed selectivity of IC neurons to different AM frequencies has led to the assumption that periodicity information is represented by a rate-based representation at the level of the IC (Schreiner and Langner, 1988, 1997). Such a rate-based representation is also motivated by the psychophysical concept of amplitude modulation filters that has been suggested based on masking experiments in the modulation frequency domain (Dau *et al.*, 1997a,b; Ewert and Dau, 2000).

The neural circuit proposed in Chap. 3 provides a mechanism of how temporal periodicity information might be transformed into a rate-based periodicity representation between the level of the CN and the IC. The temporal periodicity information is provided by an entrainment (EN) model unit localized at the CN stage of the neural circuit. This EN model unit responds to an AM stimulus by emitting exactly one spike per stimulus period. Electrophysiological recordings reveal that such entrained responses are observed in ideal onset (O_I) units (e.g. Rhode and Smith, 1986; Rhode, 1994a), a response type that is morphologically associated with octopus cells in the posteroventral cochlear nucleus (PVCN) (Kane, 1973; Godfrey *et al.*, 1975). Additionally, the CN stage of the neural circuit employs a set of constant-rate (CR) units that contrast the EN model unit by revealing a spike rate that is independent of the stimulus modulation frequency. Based on the sustained chopping observed in the CR model units in response to pure-tone stimuli these units can be morphologically associated with CN stellate cells (Frisina *et al.*, 1990; Kim *et al.*, 1990; Rhode, 1994a). Due to the neural connectivity chosen among the model units, bandpass shaped rate modulation transfer functions (rMTF), where spike rate is computed as a function of the stimulus modulation frequency, result at the bandpass (BP) units in the IC model stage. Since different BP model units reveal a maximum spike rate at different so-called best modulation frequencies (BMF) the neural circuit might account for the rate-based representation of AM frequencies assumed in the IC.

While the neural circuit presented in Chap. 3 performs well for the frequency-selective transfer functions with SAM tones when tested using a restricted range of modulation depths, it does not allow for an encoding of a large dynamic range of different SAM depths. Figure 3.10 in Chap. 3 revealed that modulation depths below 30% are not encoded at all while modulation depths above 60% can not be distinguished by the neural circuit. This is at least in contrast to psychophysical detection experiments in humans, where modulation depths as small as 3% can be detected in SAM pure tones (e.g. [Kohlrausch *et al.*, 2000](#)) resulting in a total dynamic range of 97% modulation depths.

Another interesting aspect that can not be accounted for by the neural circuit presented in Chap. 3 is the encoding of complex amplitude-modulated stimuli. The SAM pure tones, used to test the neural circuit, exhibit a simple temporal envelope structure. Natural sounds, however, often exhibit a more complex envelope structure reflected in a number of simultaneous AMs of different frequencies. The processing of more general AM stimuli has not been investigated by the two previous neural models of periodicity coding suggested by [Langner \(1981\)](#) (see also [Langner and Schreiner \(1988\)](#); [Langner \(1997a,b\)](#)) and [Hewitt and Meddis \(1994\)](#). The models suggest two alternative mechanisms of how temporal AM information might be transformed into a rate-based representation between CN and IC (see Sec. 3.1 of Chap. 3). Whether these models are capable of encoding complex AM stimuli is difficult to decide, since they have not yet been tested in complex conditions. The periodicity information in the neural circuit by [Langner \(1981\)](#) is provided by a so-called “trigger unit” whose response type resembles the entrainment unit of the neural circuit suggested in Chap. 3. Thus, it can be assumed that similar problems as found for the neural circuit suggested in Chap. 3 occur if the model by [Langner \(1981\)](#) is tested using AM stimuli with different modulation depths.

Masking experiments in the modulation-frequency domain have led to the assumption that the temporal envelope of a complex stimulus is spectrally decomposed by a bank of linear amplitude modulation filters ([Bacon and Grantham, 1989](#); [Houtgast, 1989](#); [Dau *et al.*, 1997a,b](#)). Based on the power-spectrum model (e.g. [Fletcher, 1940](#); [Zwicker *et al.*, 1957](#)) that accounts for masking effects in the audio-frequency domain, the envelope-power spectrum model (EPSM) can be used to explain a variety of psychophysical findings in the modulation frequency domain ([Ewert and Dau, 2000](#)). The EPSM assumes a linear limited-resolution frequency decomposition of the temporal envelope of the stimulus by computing the integrated envelope power of the spectral envelope components that fall into the passband of amplitude modulation filters tuned to different modulation frequencies.

In order to provide a mechanism that allows for the encoding of a large dynamic range of modulation depths in SAM tones as well as for an appropriate frequency-selective processing of complex sounds, the neural circuit suggested in Chap. 3 was extended. In the first part of the present study, the structure of the extended model is described. It follows an analysis of the model responses when tested with SAM tones with varying modulation frequencies presented at different levels and modulation depths. In the third part, simulation results obtained in response to complex stimuli, such as pure tones modulated by the sum of two sinusoids, narrowband Gaussian and low-noise noise, and iterated rippled noise (IRN) are compared to results according to the psychophysically motivated EPSM.

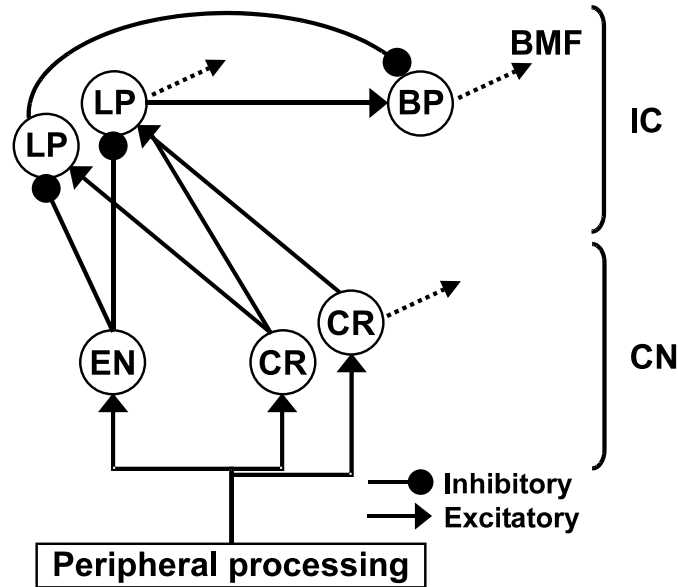


FIG. 4.1: Schematic representation of the neural connectivity within the model. Excitatory synaptic connections between model units are represented by arrows and inhibitory synaptic connections are represented by filled circles. The CN stage of the neural circuit consists of one entrainment (EN) unit and a number of constant-rate (CR) units. Each CN model unit receives input from the peripheral processing stages of the model. The IC stage of the neural circuit contains low-pass (LP) and bandpass (BP) units, with the latter representing the output units of the neural circuit. The neural connectivity corresponds to the neural circuit present in Chap. 3. For a detailed description see text.

4.2 MODEL STRUCTURE

The basic neural circuit of the present extended model is identical to the neural circuit presented in Chap. 3 in terms of its unit types and its neural connectivity. Since a detailed description of the neural circuit is given in Sec. 3.2 of Chap. 3 it will only be described briefly here. A schematic representation of the neural circuit is given in Fig. 4.1 where excitatory synaptic connections between different model units are represented by arrows and inhibitory synaptic connections are represented by filled circles. The present model is a cascade of three stages: (i) the peripheral processing stages that include basilar membrane filtering, inner hair cell transduction and the simulation of AN activity (bottom), (ii) the model CN stage (middle) and (iii) the model IC stage (top).

The CN stage of the neural circuit contains one entrainment (EN) unit and 2^n constant-rate (CR) units ($n = 5$). When stimulated with an AM stimulus, the EN unit entrains to the stimulus, i.e., it emits exactly one spike per stimulus period, such that its spike rate reflects the stimulus modulation frequency. In contrast, the spike rates of the CR units are independent of the modulation frequency of the stimulus. The IC stage of the neural circuit contains $n + 1$ low-pass (LP) units and n bandpass (BP) units. The LP units receive excitatory input from between

2^0 to 2^n CR units and inhibitory input from the EN unit of the model CN stage. This choice of connectivity results in a suppressive region in the rate modulation transfer function (rMTF) of each LP unit that occurs if the excitatory input from the CR units is exceeded by the inhibitory input from the EN unit. The modulation frequency at which the suppressive region occurs in different LP model units depends on the number of CR units providing its excitatory input. By way of excitatory and inhibitory projections of adjacent LP units onto the BP units, bandpass shaped rMTFs with different BMFs are obtained at different BP units of the neural circuit.

Although this neural circuit allows for a rate-based representation of modulation frequencies it does neither allow for encoding low modulation depths nor for distinguishing high modulation depths of an SAM stimulus. This was shown in Fig. 3.10 of Chap. 3 where the spike rate of a BP unit with a best modulation frequency (BMF) of 100 Hz was plotted as a function of the modulation depth of an 10-kHz tone, modulated at a rate of 100 Hz. At stimulus modulation depths below 30%, the BP unit essentially reveals no response to the stimulus modulation. If the modulation depth exceeds 30% the spike rate of the unit increases rapidly until it saturates at a modulation depth of 60%. The nonlinear manner in which the spike rate of the 100-Hz BP unit depends on the stimulus modulation depth results inherently from the all-or-none spiking behavior of the model EN unit. In other words, the EN unit can respond to AM stimuli only in two ways: if the modulation depth is large enough to be detected by the EN unit it entrains to the stimulus period; otherwise it exhibits an onset response.

In order to obtain a larger dynamic range of modulation depths, a set of EN units is introduced in the present extended model. These EN units differ in their sensitivity to different modulation depths by varying their two threshold potentials, i.e., the spike threshold and the spike-blocking release threshold. A schematic illustration of the extended model is shown in Fig. 4.2. In order to describe the model structure, a topological representation of different CFs, BMFs, and modulation depths, m , is indicated in the figure, with different peripheral channels being represented along the x-dimension of the figure. The Fig. 4.2 highlights the model structure for one peripheral channel ($x=\text{const}$). The set of CR units is represented along the y-dimension of the CN model stage. The different EN units are represented along the z-dimension of the CN model stage. The projections of EN and CR units result in a plane of LP units in the IC model stage, whose y-dimension represents the different number of CR unit inputs and whose z-dimension results from the different EN units of the CN model stage. Due to the LP unit projections, a plane of BP model units results where different BMFs are represented along the y-dimension and different modulation depths, m , are encoded along the z-dimension of the IC model

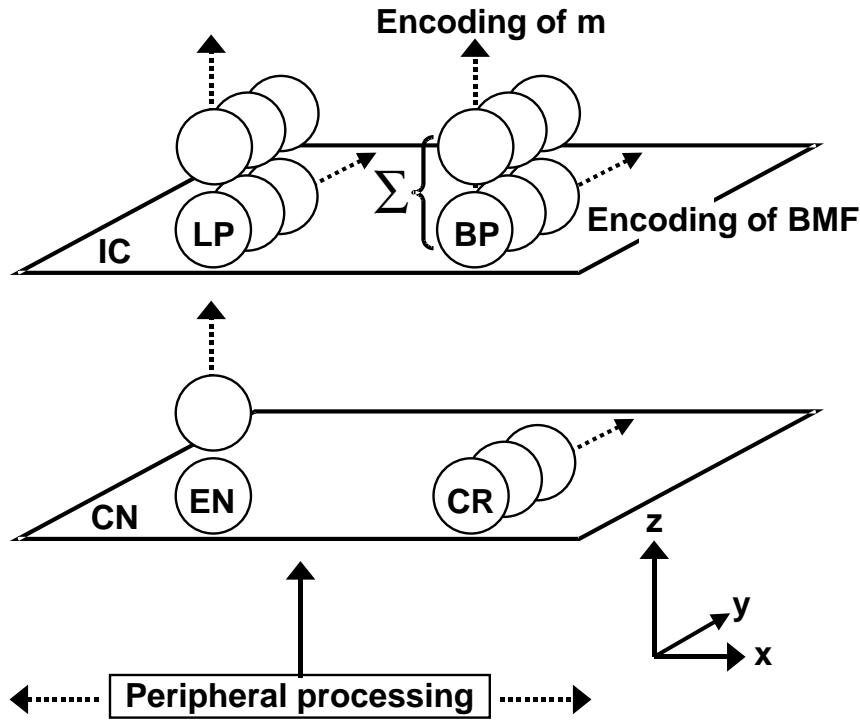


FIG. 4.2: The architecture of the extended model within one peripheral channel ($x=\text{const}$). The set of CR units is represented along the y -dimension axis in the CN model stage. The set of EN units is represented along the z -dimension in the EN model stage. The CN model units projections result in a plane of LP units IC model stage, whose y -dimension represents the different number of CR unit inputs and whose z -dimension represents the different number of EN unit input. The LP unit projections result in a plane of BP model units, where different BMFs are encoded along the y -dimension and different modulation depths, m , are encoded along the z dimension. The neural connectivity among different model units is shown in Fig. 4.1. For a detailed description see text.

stage. In order to obtain the model output, the activity of BP units with identical BMFs is summed along the “modulation dimension”. Finally, this summed activity is normalized in order to obtain the model output which is called the relative spike rate of the filters in the following.

4.2.1 Auditory periphery and Neuron dynamics

Since a detailed description of the peripheral processing stages of the model is given in Sec. 3.2.1 of Chap. 3 they are described only briefly here. The frequency decomposition performed on the basilar membrane and the subsequent transduction of mechanical into neural activity is simulated by a bank of fourth-order gammatone filters (Patterson *et al.*, 1988) and Meddis’ hair-cell model (Meddis, 1986, 1988; Meddis *et al.*, 1990). Based on the deterministic spike probability function, obtained from the hair-cell model, the auditory-nerve (AN) activity is simulated within each peripheral filter channel. While the large number of across-frequency AN input received by the EN units is simulated by using a noisy version of the hair cell spike

probability function, the AN input to the model CR units is obtained by simulating the individual spike trains of 50 peripheral fibers within one peripheral filter channel.

As described in Sec. 3.2.2 of Chap. 3, each unit of the present model is modeled as a point neuron with an integrate-to-threshold dynamic (Tuckwell, 1988). An integrate-to-threshold unit integrates each postsynaptic potential (PSP) evoked by a presynaptic spike by way of its membrane potential. If the membrane potential reaches its spike threshold, a spike is generated and the unit enters its refractory period. The refractory period of each unit consists of an absolute refractory period, with a fixed duration during which the emission of further spikes is prevented, and a relative refractory period with an input-dependent duration. With the exception of the EN model unit, the relative refractory period of the units is modeled by a dynamically changing potassium conductance (MacGregor, 1987; Arle and Kim, 1991). The relative refractory period of the EN model unit is modeled by a dynamic spike-blocking mechanism, a mechanism that has been suggested by Romand (1978) in order to account for the distinct response properties of onset units. The EN model units also differ from the other model units in the way their PSPs are modeled. While the PSPs within all other model units are represented by an “alpha-function”, the distinct temporal response properties of the EN units are simulated using an effective PSP that exhibits a biphasic shape. A detailed description of the dynamics of each model unit is given in Sec. 3.2.2 of Chap. 3.

In order to allow for the encoding of a large dynamic range of modulation depths in the present model, 10 different EN units are simulated that differ in their spike threshold Θ_{act} and their spike-blocking release threshold Θ_{rel} . While the spike threshold Θ_{act} determines the membrane potential at which the unit is sufficiently depolarized to generate an action potential, the release threshold Θ_{rel} determines the hyperpolarized potential at which the unit is released from spike-blocking (see Fig. 2.2 in Chap. 2). The threshold potentials chosen for the 10 EN units of the present model are shown in Fig. 4.3. With the exception of these two EN unit parameters, all other simulation parameters used in the present model correspond to the parameters of the neural circuit presented in Chap. 3 (see Table 3.1 and Table 3.2).

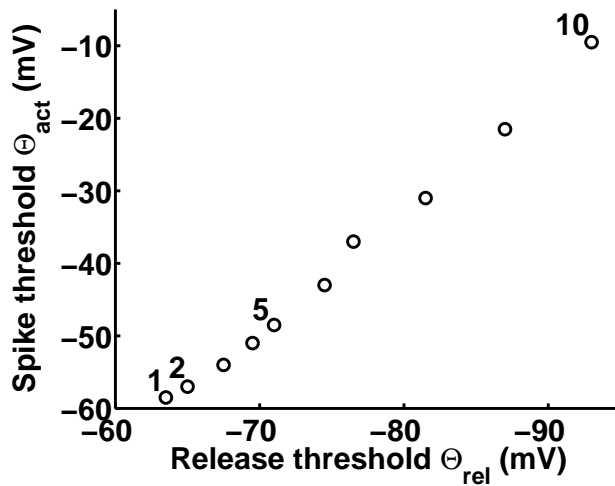


FIG. 4.3: The spike thresholds Θ_{act} of the 10 EN model units versus their spike-blocking release thresholds Θ_{rel} . The parameter combinations of the four EN units whose response properties are further examined in the following section are marked by the numbers 1,2,5 and 10.

4.3 SIMULATIONS AND DATA ANALYSIS

The neural circuit used in the simulations receives input from the peripheral filter channel centered at 10.087 kHz. The response properties of the different EN model units are characterized by their peri-stimulus time histograms (PSTH) obtained in response to a 100ms-10-kHz tone burst presented at 50 dB SPL, with 10 ms on- and offset ramps. PSTHs are gained from 250 representations of the high-frequency tone burst and binned with 0.5 ms. The temporal synchronization of the model EN units in response to 100% amplitude modulated 10-kHz tones with different modulation frequencies is analyzed using the synchronization coefficient (SC) (Goldberg and Brown, 1969). It is computed as the vector strength of the distribution of spikes (with SC=1 indicating perfect synchronization to the stimulus modulation and SC=0 representing no synchronization). Additionally, the rate modulation transfer function (rMTF), where spike rate is computed as a function of stimulus modulation frequency, is obtained for the EN model units in response to 100% amplitude modulated 10-kHz tones with different modulation frequencies.

The formation of bandpass modulation filters is tested by computing the relative spike rate of each model filter in response to 100% amplitude modulated 10-kHz tones as a function of modulation frequency. The relative spike rate of the model filters is obtained from the summed activity of all 10 model BP units with identical BMFs after dividing it by the so-called BMF rate. The BMF rate represents the average spike rate across all 10 BP units in response to a 100% amplitude modulated 10-kHz tone modulated at the BMF of the units and presented at a level of 60 dB SPL. Thus, a relative spike rate of 10 is obtained, if all 10 BP units within a certain model filter respond at their maximum spike rate. The respective BMF rates of the five model filters are given as numbers in the left panel of Fig. 4.6.

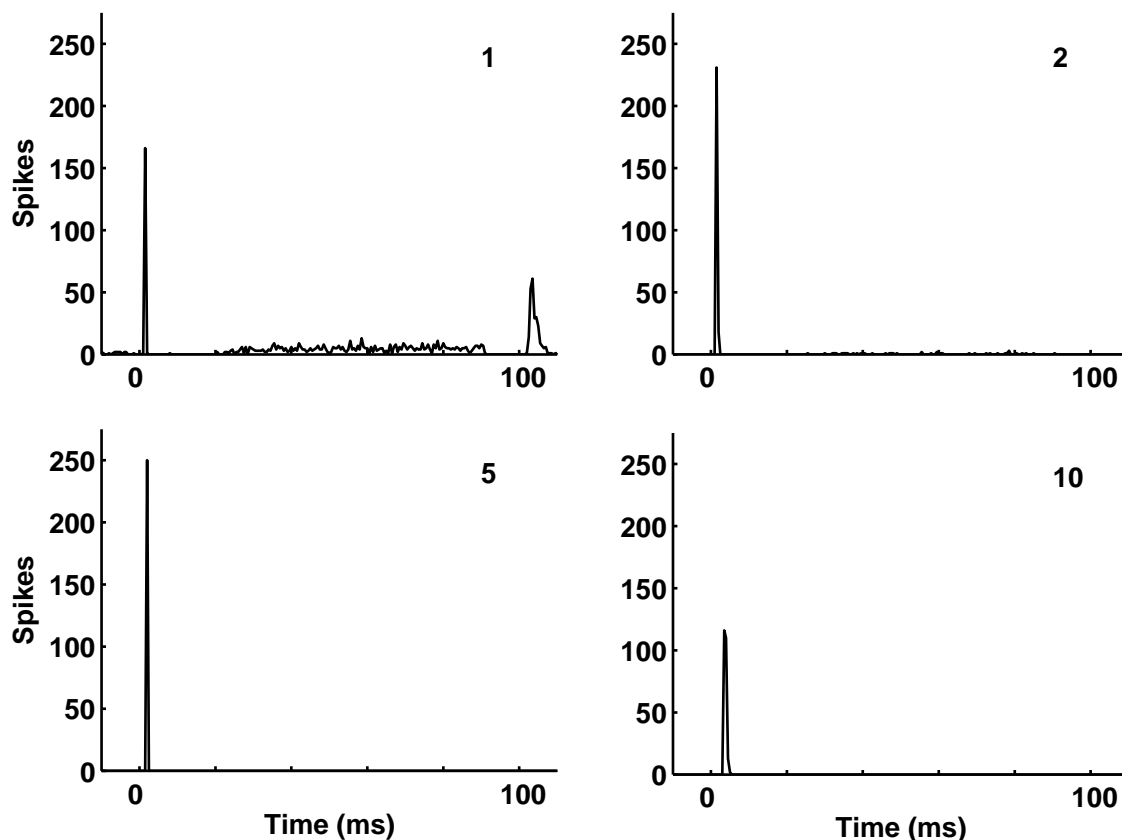


FIG. 4.4: The PSTHs of the four EN units with the threshold combinations 1, 2, 5 and 10 in Fig. 4.3 in response to a 10-kHz tone burst.

The relative spike rate of the model filters is also computed using complex stimuli, e.g., 10-kHz tones modulated by the sum of two sinusoids, narrowband Gaussian and low-noise noise, and iterated rippled noise (IRN). AM pure tones and complex stimuli are presented with a duration of 1.05 s with the initial 50 ms of a unit's response being excluded from the analysis, in order to avoid onset effects. If not stated otherwise, SAM tones and complex stimuli are presented at a level of 60 dB SPL. The model is further evaluated by comparing the simulated relative spike rates obtained in response to complex stimuli to the integrated envelope power at the output of each model filter.

4.3.1 The EN model units

Figure 4.4 displays the PSTHs of the four example EN units with the threshold potential combinations marked by the numbers 1, 2, 5 and 10 in Fig. 4.3. The PSTHs are obtained from a 10-kHz tone burst. Despite of their different threshold potentials, all EN units reveal a pure-tone PSTH that can be classified as onset. This agrees well with the EN unit of the neural circuit presented in Chap. 3 whose pure-tone PSTH was also classified as onset.

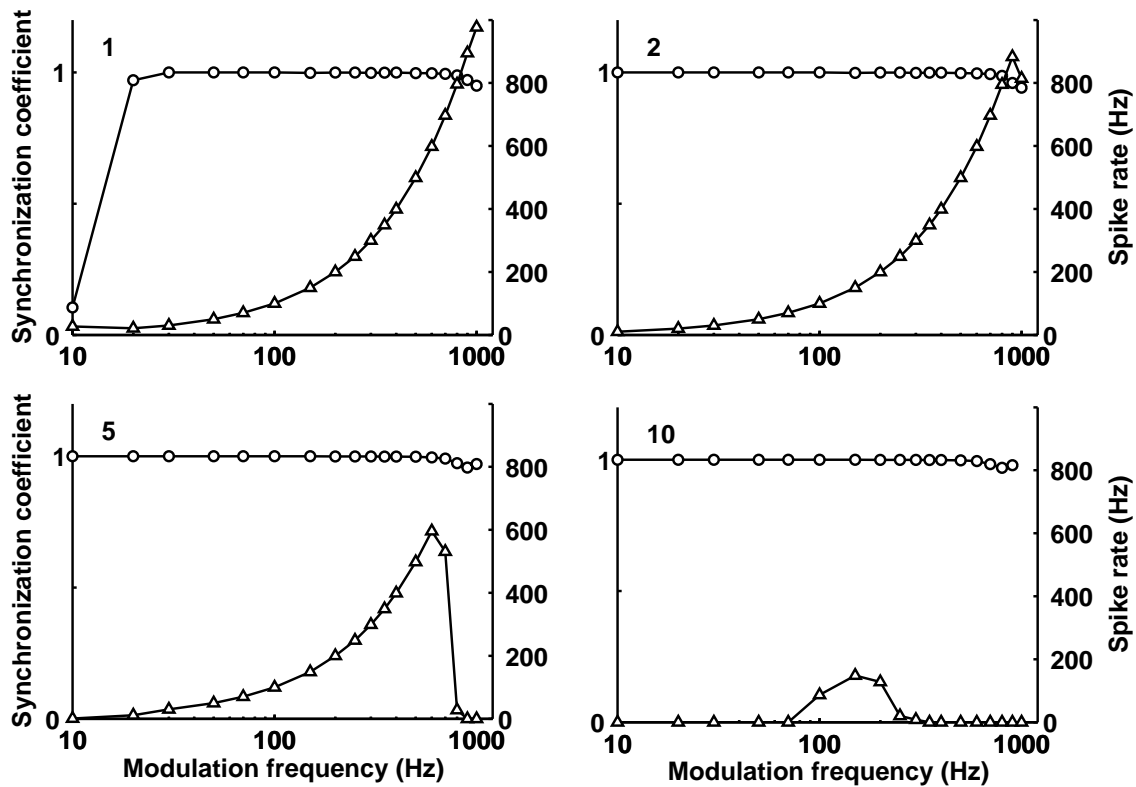


FIG. 4.5: Synchronization coefficients (left scale, circles) and rMTFs (right scale, triangles) of the four EN units with the threshold combinations 1, 2, 5 and 10 in Fig. 4.3. Simulation results are gained from 100% amplitude modulated 10-kHz tones.

Physiologically, onset units are commonly subdivided into three groups based on their PSTHs in response to high-frequency tone bursts presented at CF: onset with late or long-lasting activity (O_L), onset with chopping (O_C), revealing two or more onset peaks, and ideal onset (O_I), showing one precisely timed action potential at stimulus onset followed by no or little (< 10 spikes/s) subsequent activity (Godfrey *et al.*, 1975; Rhode and Smith, 1986; Winter and Palmer, 1995). Thus, according to the simulated PSTHs shown in Fig. 4.4, EN unit 1 (upper left panel) is classified as revealing an O_L -type response, while all other EN units reveal an O_I -type response. The low sustained activity in the PSTH of EN unit 1 results from the small potential difference between its spike and its release threshold (see Fig. 4.3). This small potential difference results in a high sensitivity of EN unit 1 to fluctuations in the stimulus amplitude such that even stochastic fluctuations in the AN activity are detected.

Figure 4.5 displays the synchronization coefficients (left scale, circles) and the rMTFs (right scale, triangles) of the same four EN model units in response to 100% amplitude modulated 10-kHz tones as a function of modulation frequency. Since EN unit 1 (upper left panel) exhibits the smallest potential difference between spike and release threshold, it is most sensitive to amplitude fluctuations. This high sen-

sitivity enables EN unit 1 to entrain to modulation frequencies even larger than 1 kHz as can be seen from its high synchronization coefficient and its spike rate that reflects the stimulus modulation frequency. However, at very low modulation frequencies (10 Hz) the synchronization coefficient is decreased and the spike rate exceeds the stimulus modulation frequency of 10 Hz. Thus, EN unit 1 fails to entrain to a modulation frequency of 10 Hz and instead exhibits a low spontaneous activity. EN unit 2 (upper right panel) and EN unit 5 (lower left panel) exhibit nearly perfect entrainment to the stimulus modulation frequency which can be seen from their high synchronization coefficient and their spike rates that reflects the stimulus modulation up to very high modulation frequencies. EN unit 10 (lower right panel) whose spike threshold differs largely from its release threshold, is prevented from detecting both, low modulation frequencies and modulation frequencies exceeding 250 Hz. Even though the unit exhibits the least sensitivity to fluctuations in the stimulus amplitude, its high synchronization coefficient reveals that if the unit responds to an AM stimulus, it does so in a highly synchronized manner. Since the different EN model units are supposed to cover a wide range of modulation depths, both EN unit 1 revealing low spontaneous activity and EN unit 10 exhibiting little sensitivity to AM stimuli are included in the analysis.

4.3.2 Characteristics of bandpass modulation filters

The left panel of Fig. 4.6 displays the relative spike rate of the five simulated model bandpass filters as a function of the modulation frequency of 100% amplitude modulated 10-kHz tones. The relative spike rate of the filters is obtained from dividing the summed activity of model BP units with identical BMFs by the corresponding BMF rate given as numbers in the figure. The bandpass filters obtained by the extended model version resemble the bandpass rMTFs shown in Fig. 3.8 of Chap. 3 in terms of BMFs and bandwidths. The estimated $Q_{6\text{dB}}$ -values (BMF divided by the bandwidth of the rMTF 6 dB below its peak) are given in Table 4.1.

TABLE 4.1: $Q_{6\text{dB}}$ -values of the model filters.

BMF (Hz)	$Q_{6\text{dB}}$
20	0.6
50	2.0
100	1.4
200	1.4
350	1.4

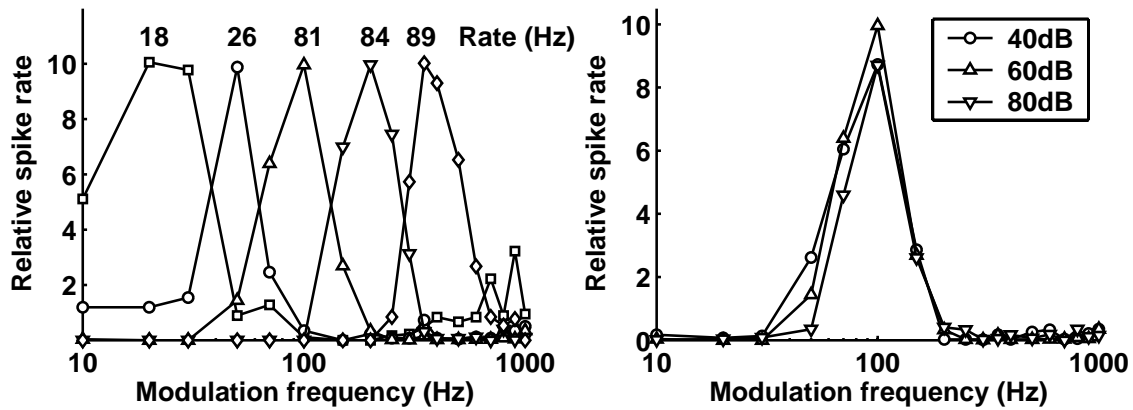


FIG. 4.6: Left: The relative spike rate of the model bandpass filters as a function of the modulation frequency of 100% amplitude modulated 10-kHz tones. The BMF rate used to gain the relative spike rate from the summed activity of all 10 model BP units with identical BMFs is shown above each filter. Right: The relative spike rate of the 100-Hz filter as a function of the modulation frequency of a 100% amplitude modulated 10-kHz tone presented at 40, 60 and 80 dB SPL.

The right panel of Fig. 4.6 displays the simulated relative spike rate of the 100-Hz filter as a function of the modulation frequency of a 100% amplitude modulated 10-kHz tone presented at different stimulus levels. Increasing the stimulus level from 40 to 80 dB yields only small changes in the relative spike rate of the 100-Hz filter indicating that the simulated bandpass filters are independent of stimulus presentation level in the tested range.

4.3.3 Coding of modulation depth

The dependency of the filter transfer characteristics on the stimulus modulation depth is examined using the 100-Hz bandpass filter. The left panel of Fig. 4.7 displays the relative spike rates of the four 100-Hz BP units that receive input from the EN model units corresponding to the threshold combinations 1, 2, 5 and 10 (see Fig. 4.3) as a function of AM modulation depth. The relative spike rates are obtained from a 10-kHz tone modulated at a rate of 100 Hz with different modulation depths. Each of the BP units is shown to encode only a limited dynamic range of modulation depths. Within the corresponding 100-Hz filter of the model a large dynamic range of modulation depths results from the summed activity of all 10 BP units. The right panel of Fig. 4.7 displays the relative spike rate of the 100-Hz filter as a function of the modulation depth of a 10-kHz tone, modulated at a rate of 100 Hz. The relative spike rate is essentially a linear function of the stimulus modulation depth, which is much different from the nonlinear behavior observed in the original neural circuit presented in Chap. 3 (see Fig. 3.10).

Figure 4.8 displays the 100-Hz filter transfer function for a 10-kHz tone amplitude modulated with depths of 20% (circles), 50% (triangles) and 100% (squares). The

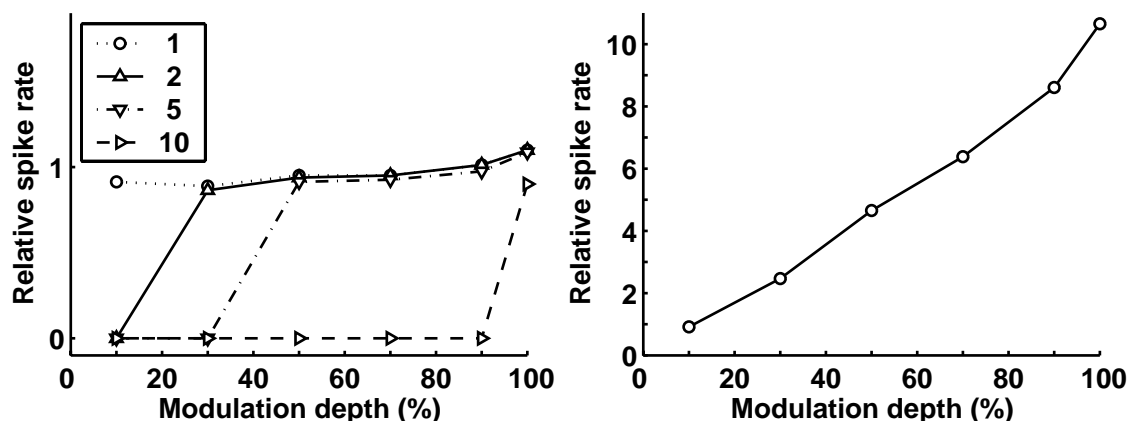


FIG. 4.7: Left: Responses of the 100-Hz BP units receiving indirect input from the four EN units with the threshold combinations 1, 2, 5 and 10 (see Fig. 4.3) as a function of the modulation depth of a 10-kHz tone modulated at a rate of 100 Hz (stimulus presentation level: 60 dB SPL). The simulated spike rate of each BP unit is divided by the BMF rate of the 100-Hz filter. Right: The relative spike rate of the 100-Hz filter as a function of the modulation depth of the same AM stimulus.

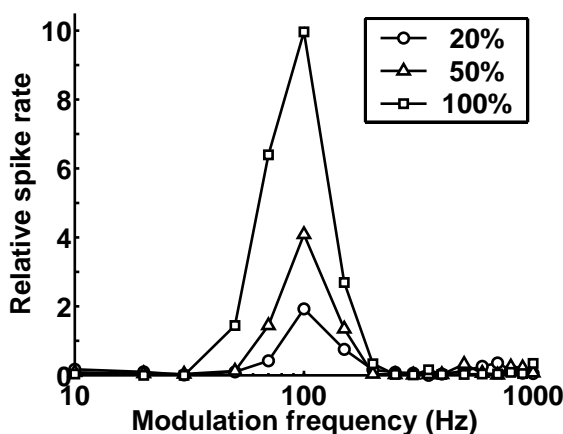


FIG. 4.8: The relative spike rate of the 100-Hz filter in response to amplitude modulated 10-kHz tones with different modulation frequencies and modulation depths (20%, 50% and 100%).

simulated filter functions reveal that neither the BMF nor the overall bandpass shape of the 100-Hz filter is affected by the modulation depth of the stimulus. Estimated $Q_{6\text{dB}}$ -values are $Q_{6\text{dB}} = 1.4$ for 100%, $Q_{6\text{dB}} = 1.6$ for 50% and $Q_{6\text{dB}} = 1.7$ for 20% modulation depth.

4.3.4 Processing of complex envelope waveforms

In order to evaluate whether the five modulation filters simulated in the present model can be associated with linear amplitude modulation filters, the simulated relative spike rates obtained in response to complex stimuli are compared to the integrated envelope power at the output of each model filter. This approach is based on the psychophysically motivated envelope-power spectrum model (EPSM) (Dau *et al.*, 1999; Ewert and Dau, 2000). Similar to the classical power-spectrum model of masking (e.g. Fletcher, 1940; Zwicker *et al.*, 1957) where the signal power at the

output of an auditory filter centered at the signal frequency is used to determine its detectability, the EPSM has been suggested to account for masking experiments in the envelope-frequency domain. According to the EPSM, a linear limited-resolution frequency decomposition of the stimulus envelope is performed by the auditory system.

In order to directly compare the simulation results obtained in response to complex stimuli with results according to the EPSM, the EPSM filter parameters are selected in a way that would match the predictions of both models in the case of 100% AM tone stimuli. Thus, the transfer functions of the modulation filters are obtained from a linear interpolation of the simulated filter data (see left panel of Fig. 4.6). At low modulation frequencies (<10 Hz), this interpolation was computed from the simulated relative spike rate in response to a 60 dB SPL 10-kHz tone. The EPSM results are obtained from extracting the envelope of the stimulus, computing the envelope power spectrum and calculating the power of the spectral envelope components that fall into the transfer range of each interpolated modulation filter. The envelope power spectrum, N , is computed from the Fourier transformation of the Hilbert envelope of the temporal stimulus waveform. The envelope power spectra of all stimuli are scaled such that their dc peaks are identical. The envelope power, $P_{env}(BMF)$, at the output of a specific modulation filter centered at BMF is yielded from multiplying the envelope power spectrum of the stimulus, N , with the squared transfer function of the filter $W_{BMF}(f_{env})$ and integrating across envelope frequencies f_{env} :

$$P_{env}(BMF) = \int_{f_{env}=0}^{\infty} N(f_{env})W_{BMF}(f_{env})df_{env}.$$

The squared transfer functions W_{BMF} of all model filters are assumed to be zero for $f_{env} > 1000$ Hz. As has been shown in Fig. 4.7 the simulated relative spike rate of a model filter is essentially a linear function of the modulation depth of an AM pure tone. In order to account for this linear dependency, the square root of the integrated power $P_{env}(BMF)$ at the output of each filter, that corresponds to the rms modulation depth for SAM tones, is compared to the simulated relative spike rates. All EPSM results are scaled by the same constant factor, in order to make the two measures directly comparable. This constant is obtained by dividing the sum of simulated relative spike rates of all model filters in all stimulus conditions by the corresponding sum of all EPSM results.

4.3.5 Processing of two-component AM

The amplitude modulated stimuli $s(t)$ used in the simulations consist of a pure tone carrier with carrier frequency $f_c=10$ kHz that is modulated by the sum of two

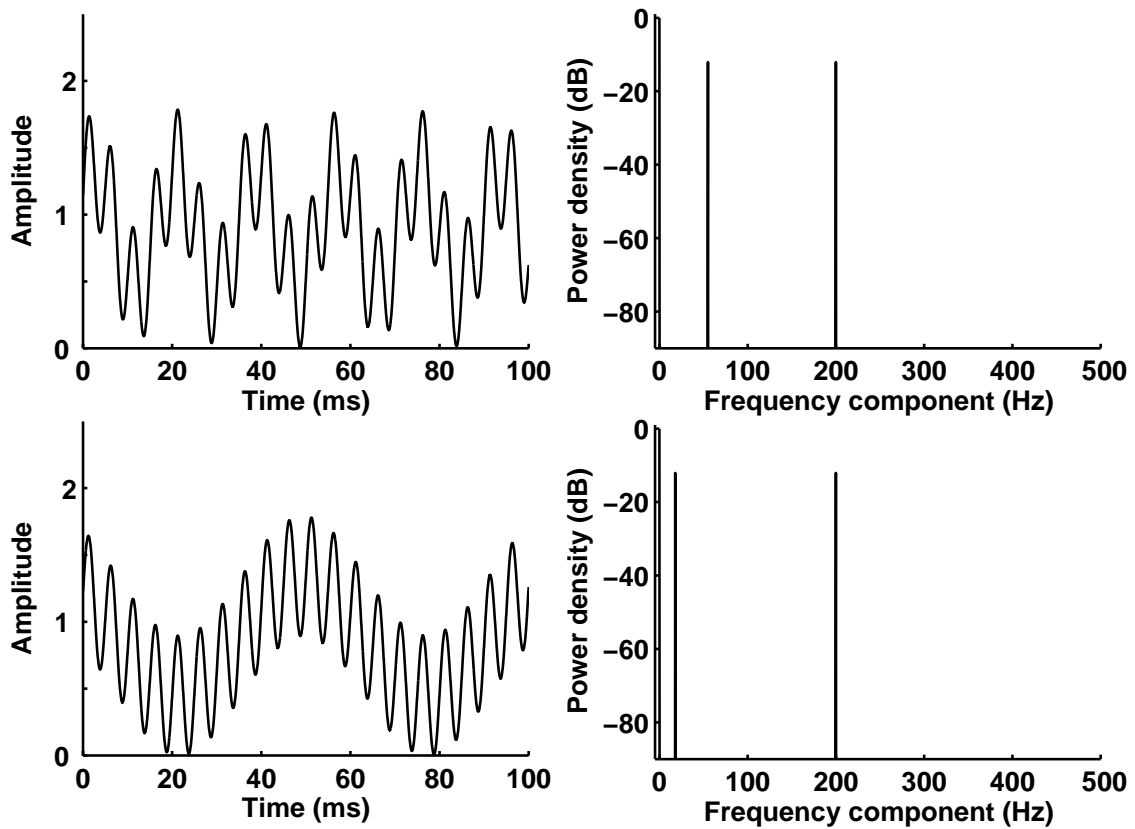


FIG. 4.9: Left: Temporal waveform of the envelope of a 10-kHz tone modulated by the sum of two sinusoids with modulation frequencies $f_{m1}=55$ Hz and $f_{m2}=200$ Hz (upper panel) and $f_{m1}=18$ Hz and $f_{m2}=200$ Hz (lower panel). Right: Corresponding envelope spectra of the two-component AM stimuli normalized such that the dc peak corresponds to 0 dB.

sinusoids, f_{m1}, f_{m2} , with modulation depths $m_1 = m_2 = 0.5$:

$$s(t) = \sin(2\pi f_c t)(1 + m_1 \sin(2\pi f_{m1} t) + m_2 \sin(2\pi f_{m2} t)).$$

Figure 4.9 displays the temporal envelopes of two complex AM stimuli with $f_{m1}=55$ Hz and $f_{m2}=200$ Hz (upper left panel) and $f_{m1}=18$ Hz and $f_{m2}=200$ Hz (lower left panel) presented at a level of 60 dB SPL. The corresponding envelope spectra, shown in the right panels of the figure, both reveal three spectral components, the dc component (peak at 0 Hz) and two components that correspond to the two modulation frequencies. The amplitudes of the spectral components are given in dB with respect to the dc peak which was chosen to correspond to 0 dB.

The left panel of Fig. 4.10 displays the simulated relative spike rates of the five model filters (circles) in response to the AM stimulus with modulation frequencies $f_{m1}=55$ Hz and $f_{m2}=200$ Hz. The EPSPM output that is represented by crosses is also shown in the figure. The right panel of Fig. 4.10 displays the simulation results (circles) and the EPSPM output (crosses) for the tone modulated at $f_{m1}=18$ Hz and $f_{m2}=200$ Hz. The simulation results are in good agreement with the EPSPM results. However, the simulated relative spike rate of the 20-Hz filter in response to the

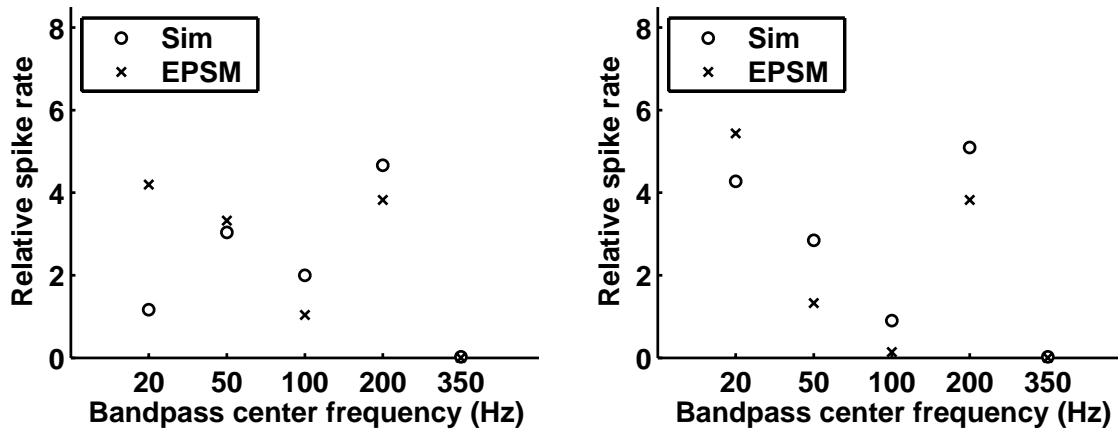


FIG. 4.10: Left: Simulated relative spike rates of the five model filters (circles) and EPSM output (crosses) in response to a 10-kHz tone modulated with $f_{m1}=55$ Hz and $f_{m2}=200$ Hz. Right: Simulated relative spike rates (circles) and EPSM output (crosses) in response to a 10-kHz tone with modulation frequencies $f_{m1}=18$ Hz and $f_{m2}=200$ Hz. Both stimuli are presented at a level of 60 dB SPL.

AM stimulus with $f_{m1}=55$ Hz and $f_{m2}=200$ Hz (left panel) clearly deviates from the EPSM output. Possible reasons for this discrepancy will be addressed in the discussion.

4.3.6 Processing of narrowband noise

The narrowband Gaussian noise used to test the present model is generated by setting the magnitude of the Fourier components of a broadband Gaussian noise to zero outside the desired passband of 100 Hz centered at 10 kHz. The left panel of Fig. 4.11 displays the temporal envelope of the narrowband noise stimulus and the right panel shows the corresponding envelope spectrum normalized to a dc peak of 0 dB. Besides the dc peak, the Gaussian noise exhibits a triangular continuous envelope spectrum if plotted on a linear scale, that decreases rapidly for spectrum components exceeding the bandwidth of the noise.

Figure 4.12 shows the simulated relative spike rate of the five model filters (circles) in response to the Gaussian noise presented at 60 dB SPL together with the EPSM results (crosses). The simulated relative spike rates agree well with the EPSM output. While the relative spike rates of filters with BMFs below the stimulus bandwidth reflect the triangular shape of the envelope spectrum, filters with BMFs that exceed the bandwidth of the stimulus essentially reveal no activity.

The low-noise noise is generated from a Gaussian noise with a bandwidth of 100 Hz centered at 10 kHz by 10 iterations of the following steps: The temporal waveform of the noise is divided by its temporal envelope on a sample-by-sample basis and the Fourier spectrum of the resulting waveform is restricted to its original

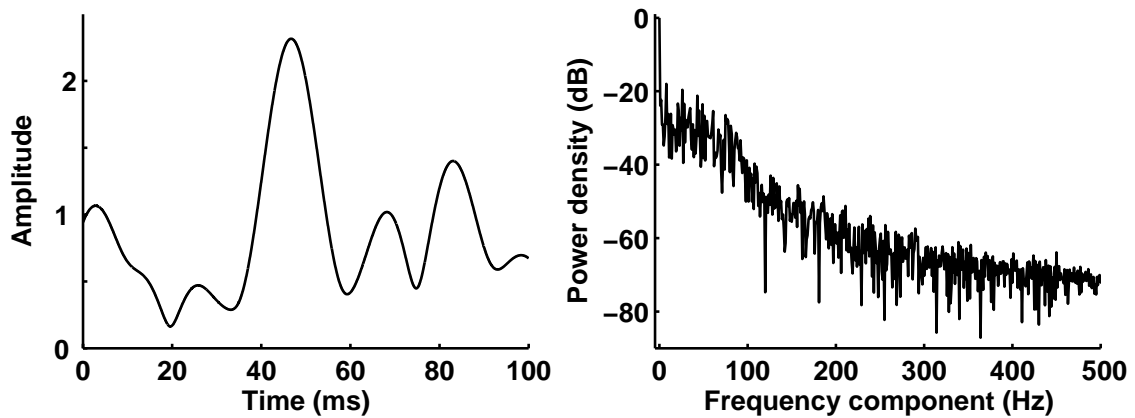


FIG. 4.11: Left: Temporal envelope of a narrowband Gaussian noise centered at 10 kHz with a bandwidth of 100 Hz. Right: Corresponding envelope spectrum normalized to a dc peak of 0 dB.

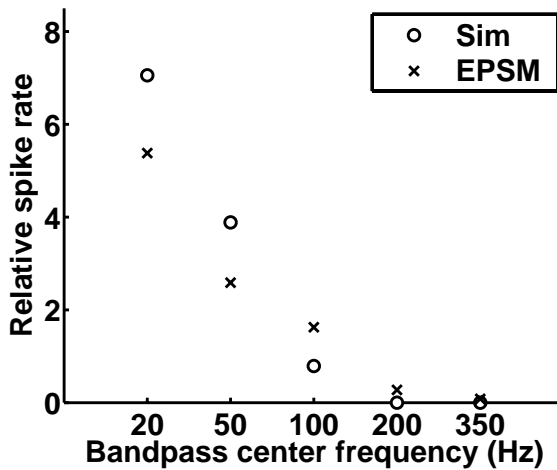


FIG. 4.12: Simulated relative spike rate of the five model filters (circles) in response to a narrowband Gaussian noise centered at 10 kHz with a bandwidth of 100 Hz and presented at a level of 60 dB SPL. The corresponding EPMSM output is represented by crosses.

bandwidth of 100 Hz. The resulting waveform exhibits a smooth temporal envelope. A more detailed description of this procedure is found in [Kohlrausch *et al.* \(1997\)](#). Despite of their identical bandwidths, the envelope spectra of low-noise noise (right panel of Fig. 4.13) and Gaussian noise (right panel of Fig. 4.11) exhibit a completely different shape. Moreover, since the envelope of low-noise noise is smoothed during the iterative procedure, its envelope spectrum contains much less energy than the envelope spectrum of Gaussian noise.

Figure 4.14 displays the simulated relative spike rates of the five model filters (circles) in response to a low-noise noise stimulus with a bandwidth of 100 Hz, centered at 10 kHz, together with results obtained from the EPMSM (crosses). The simulated relative spike rates agree well with the EPMSM output. As expected from comparing the overall amount of energy in the envelope spectra of narrowband Gaussian noise and low-noise noise, the spike rates of filters with BMFs below the bandwidth of the low-noise noise are generally smaller than those obtained in response to Gaussian noise of the same bandwidth (see Fig. 4.12). Filters with BMFs that

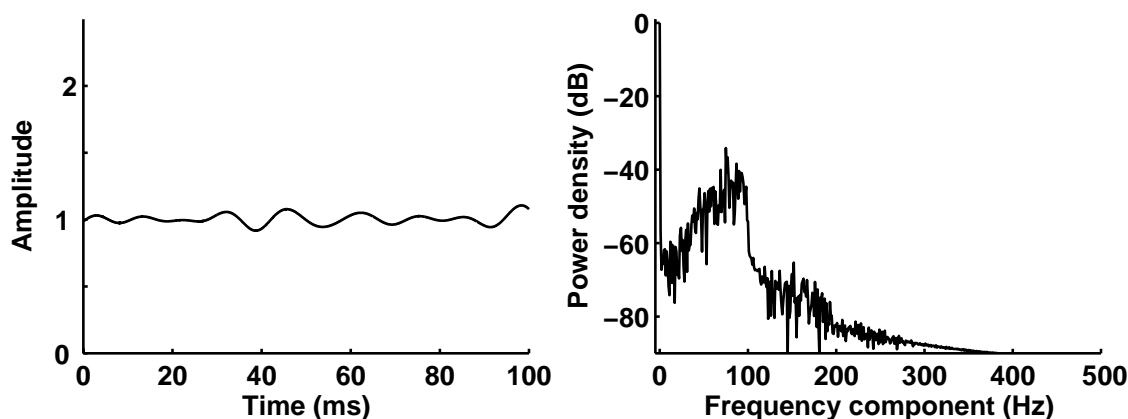


FIG. 4.13: Left: Temporal envelope of a low-noise noise centered at 10 kHz with a bandwidth of 100 Hz. Right: Corresponding envelope spectrum normalized to a dc peak of 0 dB.

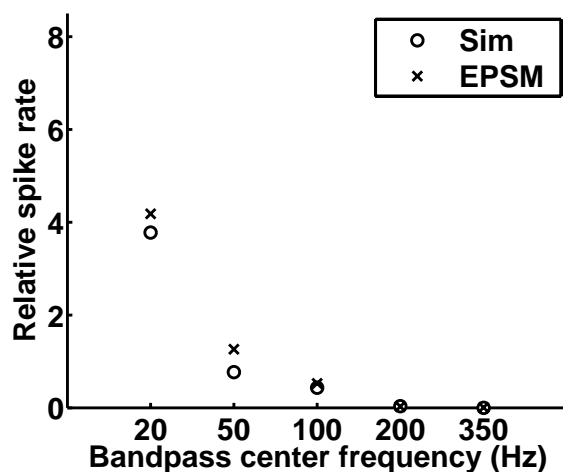


FIG. 4.14: Simulated relative spike rate of the five model filters (circles) in response to a low-noise noise centered at 10 kHz with a bandwidth of 100 Hz presented at a level of 60 dB SPL. The crosses correspond to the results obtained from the EPSM.

exceed the bandwidth of the low-noise noise reveal no response, as is also expected from the envelope spectrum of the stimulus.

4.3.7 Processing of iterated rippled noise

The iterated rippled noise (IRN) stimulus is generated from a broadband Gaussian noise. The noise is iteratively attenuated and delayed before being added to the original version of the noise. During the iteration process that results in a quasi periodicity of the stimulus, the output of one iteration stage serves as input to the next iteration stage. The process used here followed the “add same” configuration described in Yost (1996). The IRN stimulus is gained from $N = 16$ iterations using a delay, $\Delta = 20$ ms and a gain $g = 1$. While the narrowband stimuli used in the previous sections are not affected by the peripheral filter centered at 10.087 kHz, the broadband IRN stimulus is to be filtered before computing the EPSM output. The temporal envelope of the filtered IRN stimulus is shown in the left panel of Fig. 4.15 and the corresponding envelope spectrum is shown in the right panel of the figure. The amplitudes of the spectral envelope components are given in dB with

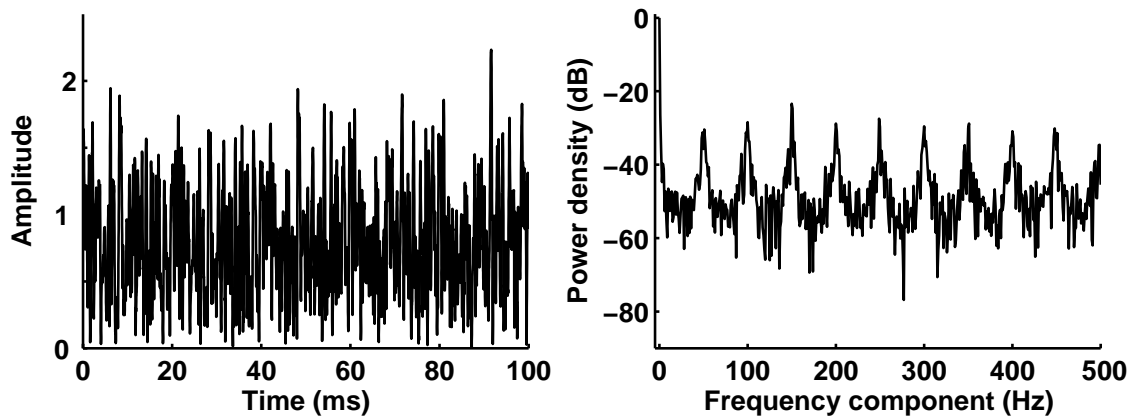


FIG. 4.15: Left: Temporal envelope of the IRN stimulus with $\Delta=20$ ms, $g=1$ and $N=16$. Right: Corresponding envelope spectrum normalized to a dc peak of 0 dB.

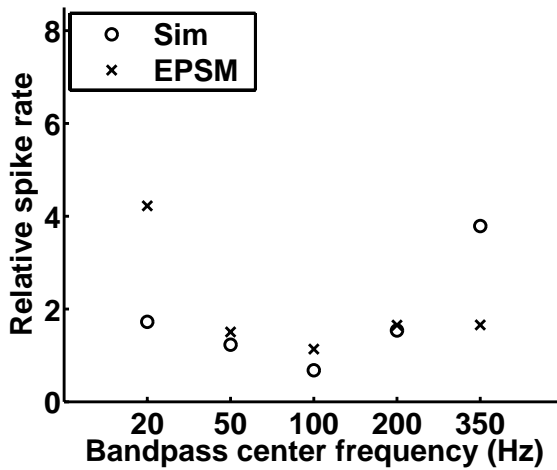


FIG. 4.16: Simulated relative spike rates of the five model filters (circles) and EPSM results (crosses) in response to IRN ($\Delta=20$ ms, $g=1$, $N=16$) presented at a level of 60 dB SPL.

the dc peak corresponding to 0 dB. The magnitude spectrum (not shown) as well as the envelope spectrum of the IRN reveal a rippled structure with peaks at integer multiples of 50 Hz, the reciprocal of the IRN delay $\Delta = 20$ ms.

Figure 4.16 displays the simulated relative spike rates of the five model filters (circles) in response to the IRN stimulus presented at 60 dB SPL. Additionally, the EPSM results are shown represented by crosses. Although they are in qualitative agreement, the relative spike rates and the EPSM results differ from one another. For example, the EPSM output for the 20-Hz filter is clearly larger than the simulated spike rate obtained for this filter. The opposite is observed for the 350-Hz filter, where the simulated spike rate exceeds the EPSM output. Possible reasons for this difference between simulated relative spike rates and EPSM results will be addressed in the discussion.

4.4 DISCUSSION

4.4.1 The model EN units

With the exception of the EN model units, the units employed in the present model are identical to the units employed in the neural circuit presented in Chap. 3. The neural connectivity of the present model is also identical to the connectivity of the neural circuit presented in Chap. 3. Since the biological plausibility of the different unit types as well as the neural connectivity between model units has already been discussed in Sec. 3.4 of Chap. 3, solely the assembly of EN units of the present model are discussed in the following.

The EN units of the present model were derived in such a way that they systematically differ in their two threshold potentials, namely the spike and the release thresholds. The specific choice of the EN threshold potentials (see Fig. 4.3) results in a linear relation between the simulated spike rate of a modulation filter and the modulation depth of an SAM stimulus (see right panel of Fig. 4.7). As can be seen from the PSTHs of the different EN model units (see Fig. 4.4), all EN units reveal an onset response despite of their different threshold potentials. However, while the EN unit with the smallest threshold potential difference (upper left panel of the figure) exhibits an O_L type response, the response of an EN unit becomes increasingly more O_I type as its threshold potential difference increases. Such a continuum of O_L and O_I -type responses appears plausible since the specific steady-state rate used to distinguish between the units is chosen somewhat arbitrary. A continuum of O_L and O_I responses is also assumed by Kalluri and Delgutte (2003b). However, as discussed in Sec. 2.4 of Chap. 2, this assumption contrasts the morphological and physiological differences observed in O_I and O_L units. While O_I units are associated with PVCN octopus cells (Kane, 1973; Godfrey *et al.*, 1975), it is not clear whether O_L -type responses also arise from octopus cells or whether they should be associated with bushy cells (Rhode *et al.*, 1983; Winter and Palmer, 1995). Moreover, as was also discussed in Sec. 2.4 of Chap. 2, the two onset response types are assumed to be shaped by fundamentally different mechanisms (Evans and Zhao, 1998). Although it can not be decided here whether the continuum of O_I and O_L responses, observed in the EN units of the present model, indeed results from the same mechanism implemented in the same morphological cell type, both EN unit response types are biologically plausible.

The required differences in the sensitivity of different EN model units to fluctuations in the stimulus envelope might, of course, also be obtained by a number of alternative implementations, for example, by exclusively varying the spike thresholds of the different EN units, by exclusively varying their release thresholds, or

their membrane time constants, etc. Thus, although the way in which the different EN units of the present model are implemented, is somewhat arbitrary, the general mechanism of the present model suggested to account for the processing of different modulation depths in SAM stimuli and complex envelope waveforms, is not affected by the implementation details of the EN units.

4.4.2 The modulation filters of the present model

In order to evaluate the present model simulation results obtained in response to complex stimulus conditions were compared to results according to the psychophysically motivated EPSM. In contrast to the EPSM that assumes a linear processing of AM information, the simulated spike rates of the biologically motivated model are obtained from a highly nonlinear mechanism, inherently resulting from the nonlinear responses of auditory neurons. Although the linear EPSM allows for explaining results from a large set of psychophysical modulation masking experiments, it does not address the question of how amplitude modulation filters might be shaped by auditory neural circuitry. A possible mechanism is suggested in the present model that performs reasonably well in spectrally decomposing complex envelope waveforms and gives similar results as the EPSM. No other neural periodicity model has so far been tested with such complex envelope waveforms.

In the present model, the simulated modulation filters with low BMFs, e.g., at 20 and at 50 Hz, reveal some activity even in response to unmodulated tones (not shown). This activity results from EN model units with small threshold potential differences that detect even stochastic fluctuations in the AN activity. Thus, these filters can not represent “true” bandpass filters where attenuation is indefinite at 0 Hz modulation frequency. However, the contribution of stochastic fluctuations in the AN activity is reduced when the EN model units are driven by an AM stimulus. This is in contrast to the deterministic EPSM where the dc peak of the stimulus envelope spectrum is passed due to the shape of the simulated model filters regardless of the stimulus that is presented. The stimulus driven response of the EN model units leads to deviations between the simulated relative spike rate and the EPSM output. The left panel of Fig. 4.10 where simulation results and EPSM results are shown in response to the two-component AM stimulus with modulation frequencies $f_{m1}=55$ Hz and $f_{m2}=200$ Hz displays one example where the stimulus driven response of the 20-Hz filter is decreased compared to the EPSM output that is enlarged by the dc peak of the stimulus envelope spectrum due to the shape of the 20-Hz modulation filter. Since the simulated modulation filters agree with the recorded IC rMTFs shown in Fig. 3.8 of Chap. 3, where filters with low BMFs also seem to exhibit no “true” bandpass shape, the stimulus driven response of neural

units might reflect a fundamental difference between auditory processing and the linear deterministic EPSM. However, one possible way of obtaining “true” bandpass filters even at low BMFs could be obtained by increasing the inhibitory contribution of the model LP units provided to the BP units.

4.4.3 Restrictions of the present model

The simulated relative spike rates obtained in response to complex periodic stimuli qualitatively agree with the results according to the EPSM. However, in some cases, the simulated relative spike rate differs from the EPSM output. Possible explanations for these differences are described in the following.

The stochastic fluctuations in the AN activity that serves as input to the units of the model CN stage lead to small deviations of the simulated relative spike rates from the deterministic EPSM results. In addition, small deviations might arise from the way the EN unit threshold potentials are varied: (i) While an EN unit with a low spike threshold exhibits an action potential after only a short integration time, the generation of action potentials in EN units with high spike thresholds requires a longer integration time. (ii) Model EN units with high spike thresholds can not detect the slowly rising slopes of stimuli modulated at a low frequency (see Fig. 4.5). Thus, BP units that receive input from EN units with high spike thresholds do not exhibit the 20 Hz bandpass in their rMTFs. Both, the increased delay in the EN unit activity and the reduced number of model subcircuits that take part in encoding low modulation frequencies might result in differences between the simulated relative spike rates and the results from the EPSM in filters with low BMFs. However, this problem could be avoided, if the EN units were chosen to possess the same low spike threshold and differed only in their release threshold. Thus, it is important to note that these deviations result from implementation details and do not represent a structural problem of the present model.

While the above mentioned EN unit features result only in small deviations between simulated spike rates and EPSM output, the main contribution to these deviations arises from the model mechanism itself, by which temporal periodicity information is mapped onto different BP model units. The temporal periodicity information that is most crucial for the present model is provided by the temporal activity patterns of the EN model units. As has been described before, the membrane potential of the EN model units integrates over a high-pass filtered version of the temporal stimulus waveform until the unit reaches its spike threshold and exhibits a spike. After a spike, the unit enters its spike-blocking mechanism and is prevented from emitting further spikes until it is released by its membrane potential falling below its release potential. Thus, while the EN model units differ in their

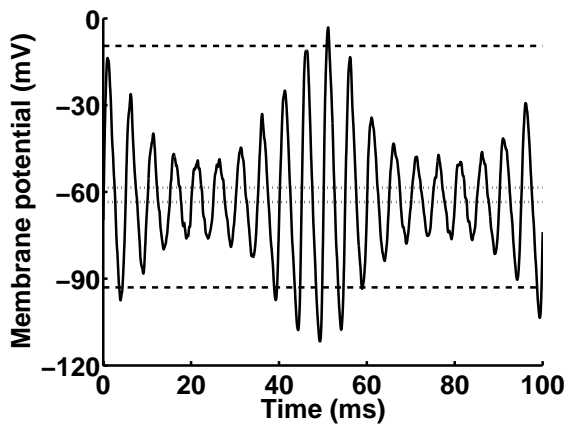


FIG. 4.17: Membrane potential of the EN model units in response to a 100% amplitude modulated 10-kHz tone modulated at 200 and 18 Hz. The dotted lines indicate the spike threshold ($\Theta_{act} = -58.5$ mV) and the release threshold ($\Theta_{rel} = -63.5$ mV) of EN unit 1. The dashed lines indicate the spike threshold ($\Theta_{act} = -9.5$ mV) and the release threshold ($\Theta_{rel} = -93$ mV) of EN unit 10.

spike and their release threshold, their membrane potentials are identical. Figure 4.17 displays the membrane potential common to all EN model units in response to the two-component AM stimulus with modulation frequencies of $f_{m1}=18$ Hz and $f_{m2}=200$ Hz. The dotted horizontal lines indicate the spike threshold ($\Theta_{act} = -58.5$ mV) and the release threshold ($\Theta_{rel} = -63.5$ mV) of the EN unit with the smallest threshold potential difference, i.e., EN unit 1 in Fig. 4.3. The dashed horizontal lines indicate the spike threshold ($\Theta_{act} = -9.5$ mV) and the release threshold ($\Theta_{rel} = -93$ mV) of the EN unit with the largest threshold potential difference, i.e., EN unit 10 in Fig. 4.3. While EN unit 1 (dotted lines) entrains to the fast modulation frequency of 200 Hz, EN unit 10 (dashed lines) entrains to the slow modulation frequency of 18 Hz. However, other EN units whose threshold potentials lie between the threshold potentials of EN unit 1 and EN unit 10 might respond with ISIs that do not correspond to one of the stimulus modulation frequencies. These units extract “erratic” periodicities that are not contained in the stimulus envelope waveform itself.

Whether these “erratic” periodicities represent a structural problem of the present model or whether they simply result from the way the EN model units are implemented is difficult to decide. However, the recorded synchronization coefficient of an O_I unit in response to 200% amplitude modulated pure tones with varying modulation frequencies, shown in the right panel of Fig. 2.9 in Chap. 2, indicates that the latter might be the case. The recorded synchronization coefficient of the O_I unit is close to 1 for all stimulus modulation frequencies. Although the simulated synchronization coefficient of the EN model unit, displayed in the left panel of the figure, agrees with the recorded synchronization coefficient when high modulation frequencies are used, it deviates from the recorded data at low modulation frequencies (e.g. 50 Hz) where the EN model unit also detects the small lobes of the 200% AM stimulus. Thus, the question must be raised, how O_I units can selectively follow low modulation frequencies without detecting the small lobes of a 200% AM

stimulus while still being sensitive to large stimulus modulation frequencies. If the different EN model units would be assumed to employ more complex, for example, adaptive mechanisms, they might also reveal such a selectivity to the modulation frequency of a 200% AM stimulus within the range of their overall sensitivity that is determined by their threshold potential difference. If the EN model units would be modeled such that they reproduced these findings “erratic” periodicities that are not contained in the stimulus waveform itself could possibly be reduced or even avoided.

4.4.4 Suggestions for physiological experiments

In order to further evaluate the present neural model, the simulated spike rates obtained in response to complex envelope waveforms should be compared to real responses recorded from IC neurons. Since such data are currently not available it is not clear how IC neurons with bandpass rMTFs respond to complex stimuli such as those used in the present study. Thus, the stimulus driven responses or the “erratic” periodicities observed in the BP units of the present model could possibly also be observed in recorded responses from auditory neurons. Moreover, it should be noted that the EPSM is just a basic functional model that accounts well for psychophysical modulation detection and masking experiments without specifying a way of how modulation filters might be shaped by the nonlinear units of the auditory system. Thus, recorded responses from IC neurons might also reveal small deviations from the corresponding EPSM results as observed in the present model. Since the present model depends crucially on the temporal information it receives from the EN model units, it would be interesting to know, whether the differences in modulation depth sensitivity suggested in the EN model units could be verified in electrophysiological recordings from onset units in the CN. Moreover, it would be interesting to know whether different CN onset units respond differently to the complex stimuli used in the present model.

4.5 SUMMARY AND CONCLUSION

The present model, which is an extended version of the neural circuit described in Chap. 3 provides a biologically motivated model of how temporal periodicity information is transformed into a rate-based periodicity representation. By employing a number of EN units, that differ systematically in their sensitivity to the modulation depth of an SAM stimulus, the present model allows for encoding a large range of modulation depths. Moreover, in contrast to the neural circuit presented in Chap. 3, the present model allows for a spectral decomposition of complex envelope waveforms, e.g., pure tones modulated by the sum of two sinusoids, narrowband Gaussian and low-noise noise, and iterated rippled noise (IRN). Simulation results in response to these complex envelope waveforms were compared to results according to the psychophysically motivated EPSM. The comparison revealed that the simulated spike rates obtained in different modulation filters of the present nonlinear neural model correspond to the linear limited-resolution frequency decomposition of the stimulus envelope that is assumed by the EPSM. Since the EPSM is a functional model that does not address the question of how modulation filters are shaped by the nonlinear neurons of the auditory system, this question might be answered by the neural circuit suggested in the present model. The present model is the first biologically motivated neural circuit that may represent a reasonable network for the processing and encoding of periodicity information in complex stimuli.

CHAPTER 5

SUMMARY AND CONCLUSION

The present thesis introduced a biologically motivated neural circuit for the processing of amplitude modulation in the auditory system. The model was motivated by findings from electrophysiological recordings that suggest a transformation of temporal periodicity information into a rate-based code represented by bandpass shaped rate modulation transfer functions (rMTF) with different best modulation frequencies (BMF) found in the inferior colliculus (IC) (e.g. [Langner and Schreiner, 1988](#); [Rees and Palmer, 1989](#)). Such a rate-based representation of periodicity information is also motivated by the psychophysical concept of amplitude modulation filters ([Dau *et al.*, 1997a,b](#); [Ewert and Dau, 2000](#)) that has been suggested based on masking experiments in the modulation-frequency domain. Previous neural models concerned with periodicity coding in the auditory system ([Langner, 1981](#); [Hewitt and Meddis, 1994](#)) are limited in their ability to simulate the psychophysically observed modulation frequency selectivity when tested in complex stimulus conditions. The model that was developed in the present thesis is the first neural model that allows for a modulation frequency decomposition of complex stimuli while employing findings from electrophysiological recordings. The model tries to bridge the gap between a description of electrophysiological data on the single-cell level and a description of behavioral data.

In Chap. 2, a new functional point-neuron model was developed that simulates the responses of ideal onset (O_I) units. Ideal onset responses are observed in units found in the posteroventral cochlear nucleus (PVCN) and are morphologically associated with octopus cells. The presented O_I -unit model that follows an integrate-to-threshold dynamic uses an effective postsynaptic potential (PSP) that exhibits a biphasic shape together with a dynamic spike-blocking mechanism. This functional model requires only a small set of 7 parameters while still being able to simulate a large variety of recorded O_I -unit responses. When tested with low-frequency pure tones and with 100% sinusoidally amplitude modulated (SAM) tones with modulation

frequencies <600 Hz, the model was shown to reveal reliable entrainment, i.e., the generation of exactly one spike per stimulus period, as observed in recorded O_I -unit responses. Moreover, the suggested model allows for simulating O_I -unit responses to a broad range of different stimuli, including high-frequency pure tones, polarizing current pulses, 200% SAM tones and harmonic tone complexes. Although octopus cells are viewed as coincidence detectors acting across a broad range of auditory-nerve fibers providing their input, the present O_I -unit model was found to account for octopus cell responses without explicitly assuming a coincidence detection mechanism. Thus, the suggested O_I -unit model provides an interesting alternative to coincidence-detector based approaches, like those suggested by [Kalluri and Delgutte \(2003a,b\)](#). Since the O_I -unit model accounts for a broad range of recorded O_I -unit responses while requiring only little computational power it might serve as a functional module that allows for investigating the role of O_I units in complex models of auditory processing.

In Chap. 3 a biologically motivated neural circuit was developed that provides a mechanism of how temporal periodicity information might be transformed into a rate-based representation between the level of the cochlear nucleus (CN) and the IC. In addition to well established peripheral processing stages (e.g. [Patterson *et al.*, 1988](#); [Meddis, 1986](#)) the model contains a CN and an IC stage. The model CN stage employs an entrainment (EN) unit, represented by the O_I -unit model suggested in Chap. 2 of this thesis, and a set of constant-rate (CR) units. The EN unit of the model CN stage entrains to the modulation frequency of an AM stimulus and thus provides the temporal periodicity information required by the present model. In contrast, the CR units of the CN model stage respond with a spike rate that is independent of the stimulus modulation frequency. The specific choice of the CN unit response properties and the neural connectivity between the model units result in bandpass shaped rMTFs at the bandpass (BP) units of the model IC stage. Different BMFs within the BP model units result from varying the number of CR units that project onto the different IC model units. Thus, in contrast to other existing neural models describing auditory periodicity coding ([Langner, 1981](#); [Hewitt and Meddis, 1994](#)), the present model does not require systematically varying temporal model parameters to allow for the formation of different BMFs within different IC model units. The neural circuit therefore may provide an interesting new mechanism by which temporal periodicity information might be transformed into a rate-based representation by the auditory system. Since the temporal periodicity information of the model is provided by units whose response properties can be associated with O_I -unit responses, the present model is the first to suggest a specific functional role of O_I -unit responses in AM processing. However, the evaluation of

the model revealed that the neural circuit does only encode a limited dynamic range of modulation depths in SAM tones which does not allow for a correct description of the processing of more complex stimuli consisting of more than one modulation-frequency component.

In Chap. 4 an advanced neural model of periodicity coding was therefore suggested. This model is an extension of the neural circuit presented in Chap. 3, whereby a set of EN model units were introduced that differ in their two threshold potentials, the spike and the spike-blocking release threshold. Apart from the EN model units, all other model units as well as their neural connectivity remained unchanged. When testing the response properties of the different EN model units, it was found that, despite of the differences in their threshold potentials, they can still be associated with CN onset units. The simulation results obtained in response to SAM tones of varying modulation depths revealed that the spike rates at the output of the model modulation filters depend linearly on the modulation depth of the stimulus. Thus, a large dynamic range of different modulation depths can be encoded by the advanced neural model. The model was evaluated using complex stimuli, such as pure tones modulated by the sum of two sinusoids, narrowband Gaussian and low-noise noise, and iterated rippled noise (IRN). The simulated spike rates in different model modulation filters obtained in response to complex stimuli revealed that the spectral frequency decomposition as performed by the present model qualitatively agrees to results according to the psychophysically motivated envelope-power spectrum model (EPSM) (Ewert and Dau, 2000). Although the linear EPSM allows for explaining a large set of data obtained from psychophysical modulation masking experiments, it does not specify how amplitude modulation filters might be shaped by the highly nonlinear auditory system. The present model might represent an important step towards answering this question since it provides the first biologically motivated neural circuit that allows for encoding a large dynamic range of SAM depths and also accounts for the spectral decomposition of complex envelope waveforms. The model may therefore lead to a better understanding of how AM information is processed by the auditory system.

In summary, the model developed in the present thesis suggests a robust coding scheme of modulation covering the range of perceptually relevant frequencies, while employing units whose responses can be associated with auditory neurons and a neural connectivity that is in line with findings from electrophysiological recordings. In more general terms, the mechanism by which amplitude modulation filters are shaped in the present model might provide a general concept that may also be suitable to describe filter concepts established to explain the neural processing in other sensory systems. The results obtained from the present thesis also provide cons-

straints for physiological experiments by which the model hypotheses can be tested and evaluated. Finally, neural models as the one presented here might be supplementary to the “effective” signal processing models used in technical applications to date. The expected interplay between neural models that include experimental data with experience from technical approaches might provide a deeper insight into the information processing strategies of the auditory system. This will eventually promote related applications, such as, robust speech recognition, digital hearing aids, or audio coding schemes.

REFERENCES

- Arle J. E., and Kim D. O. (1991). “Neural modeling of intrinsic and spike-discharge properties of cochlear nucleus neurons,” *Biol. Cybern.* **64**, 273–283.
- Backoff P. M., Palombi P. S., and Caspary D. M. (1999). “ γ -Aminobutyric acidergic and glycinergic inputs shape coding of amplitude modulation in the chinchilla cochlear nucleus,” *Hear. Res.* **134**, 77–88.
- Bacon S. P., and Grantham D. W. (1989). “Modulation masking: Effects of modulation frequency, depth, and phase,” *J. Acoust. Soc. Am.* **85**, 2575–2580.
- Bregman A. S. (1990). *Auditory scene analysis: the perceptual organization of sound*. MIT Press, Cambridge.
- Cai Y., Walsh E. J., and McGee J. (1997). “Mechanisms of onset responses in octopus cells of the cochlear nucleus: Implications of a model,” *J. Neurophysiol.* **78**, 872–883.
- Cai Y., McGee J., and Walsh E. J. (2000). “Contributions of ion conductances to the onset responses of octopus cells in the ventral cochlear nucleus: Simulation results,” *J. Neurophysiol.* **83**, 301–314.
- Cai Y., McGee J., and Walsh E. J. (2001). “Processing of pitch information in complex stimuli by a model of octopus cells in the cochlear nucleus,”. In Greenberg S., and Slaney M., editors, *Computational models of auditory function*. IOS Press, Amsterdam.
- Dau T., Kollmeier B., and Kohlrausch A. (1997a). “Modeling auditory processing of amplitude modulation. I. Modulation detection and masking with narrowband carriers,” *J. Acoust. Soc. Am.* **102**, 2892–2905.
- Dau T., Kollmeier B., and Kohlrausch A. (1997b). “Modeling auditory processing of amplitude modulation. II. Spectral and temporal integration in modulation detection,” *J. Acoust. Soc. Am.* **102**, 2906–2919.

- Dau T., Verhey J. L., and Kohlrausch A. (1999). "Intrinsic envelope fluctuations and modulation-detection thresholds for narrowband noise carriers," *J. Acoust. Soc. Am.* **106**, 2752–2760.
- De Boer E. (1976). "On the residue and auditory pitch perception,". In Keidel W. D., and Neff W. D., editors, *Handbook of Sensory Physiology*. Volume 3. Springer-Verlag, Berlin.
- Evans E. F., and Zhao W. (1997). "Onset units in guinea pig ventral cochlear nucleus: neuropharmacological studies," *Assoc. Res. Otolaryngol. Abstr.* **20**, 116.
- Evans E. F., and Zhao W. (1998). "Periodicity coding of the fundamental frequency of harmonic complexes: physiological and pharmacological study of onset units in the ventral cochlear nucleus,". In Palmer A. R., Rees A., Summerfield A. Q., and Meddis R., editors, *Psychophysical and Physiological Advances in Hearing*. Whurr Publishers Ltd, London.
- Evans E. F. (1978). "Place and time coding of frequency in the peripheral auditory system: Some physiological pros and cons," *Audiology* **17**, 369–420.
- Ewert S. D., and Dau T. (2000). "Characterizing frequency selectivity for envelope fluctuations," *J. Acoust. Soc. Am.* **108**, 1181–1196.
- Fletcher H. (1940). "Auditory patterns," *Rev. Mod. Phys.* **12**, 47–65.
- Frisina R. D., Smith R. L., and Chamberlain S. C. (1990). "Encoding of amplitude modulation in the gerbil cochlear nucleus: I. A hierarchy of enhancement," *Hear. Res.* **44**, 99–122.
- Godfrey D. A., Kiang N. Y. S., and Norris B. E. (1975). "Single unit activity in the posteroventral cochlear nucleus of the cat," *J. Comp. Neurol.* **162**, 247–268.
- Goldberg J. M., and Brown P. B. (1969). "Responses of binaural neurons of dog superior olivary complex to dichotic stimuli: Some physiological mechanisms of sound localization," *J. Neurophysiol.* **32**, 613–636.
- Golding N. L., Robertson D., and Oertel D. (1995). "Recordings from slices indicate that octopus cells of the cochlear nucleus detect coincident firing of auditory nerve fibers with temporal precision," *J. Neurosci.* **15**, 3138–3153.
- Golding N. L., Ferragamo M. J., and Oertel D. (1999). "Role of intrinsic conductances underlying responses to transients in octopus cells of the cochlear nucleus," *J. Neurosci.* **19**, 2897–2905.

- Hewitt M. J., and Meddis R. (1994). "A computer model of amplitude-modulation sensitivity of single units in the inferior colliculus," *J. Acoust. Soc. Am.* **95**, 2145–2159.
- Hewitt M. J., Meddis R., and Shackleton T. M. (1992). "A computer model of a cochlear-nucleus stellate cell: Responses to amplitude-modulated and pure-tone stimuli," *J. Acoust. Soc. Am.* **91**, 2096–2109.
- Houtgast T. (1989). "Frequency selectivity in amplitude-modulation detection," *J. Acoust. Soc. Am.* **85**, 1676–1680.
- Javel E. (1980). "Coding of AM tones in the chinchilla auditory nerve: Implications for the pitch of complex tones," *J. Acoust. Soc. Am.* **68**, 133–146.
- Joris P. X., and Yin T. C. T. (1992). "Responses to amplitude-modulated tones in the auditory nerve of the cat," *J. Acoust. Soc. Am.* **91**, 215–232.
- Kalluri S., and Delgutte B. (2003a). "Mathematical models of cochlear nucleus onset neurons: I. Point neuron with many weak synaptic inputs," *J. Comp. Neurosci.* **14**, 71–90.
- Kalluri S., and Delgutte B. (2003b). "Mathematical models of cochlear nucleus onset neurons: II. Model with dynamic spike-blocking state," *J. Comp. Neurosci.* **14**, 91–110.
- Kane E. C. (1973). "Octopus cells in the cochlear nuclei of the cat: Heterotypic synapses upon homeotypic neurons," *Int. J. Neurosci.* **5**, 251–279.
- Kim D. O., Sirianni J. G., and Chang S. O. (1990). "Responses of DCN-PVCN neurons and auditory nerve fibers in unanesthetized decerebrate cats to AM and pure tones: Analysis with autocorrelation/power-spectrum," *Hear. Res.* **45**, 95–113.
- Kipke D. R., and Levy K. L. (1997). "Sensitivity of the cochlear nucleus octopus cell to synaptic and membrane properties," *J. Acoust. Soc. Am.* **102**, 403–412.
- Kohlrausch A., Fassel R., van der Heijden M., Kortekaas S.R. van der Par, Oxenham A., and Püschel D. (1997). "Detection of tones in low-noise noise: Further evidence for the role of envelope fluctuations," *Acust. Acta Acust.* **83**, 659–669.
- Kohlrausch A., Fassel R., and Dau T. (2000). "The influence of carrier level and frequency on modulation and beat-detection thresholds for sinusoidal carriers," *J. Acoust. Soc. Am.* **108**, 723–734.

- Krishna B. S., and Semple M. N. (2000). "Auditory temporal processing: Responses to sinusoidally amplitude-modulated tones in the inferior colliculus," *J. Neurophysiol.* **84**, 255–273.
- Kulesza R. J., and Berrebi A. S. (1999). "Distribution of GAD isoforms in the superior paraolivary nucleus (SPON) of the rat," *Assoc. Res. Otolaryngol Abstr.* **22**, 70–71.
- Langner G., and Schreiner C. E. (1988). "Periodicity coding in the inferior colliculus of the cat. I. Neuronal mechanisms," *J. Neurophysiol.* **60**, 1799–1822.
- Langner G. (1981). "Neuronal mechanisms for pitch analysis in the time domain," *Exp. Brain Res.* **44**, 450–454.
- Langner G. (1997a). "Temporal processing of pitch in the auditory system," *Journal of New Music Research* **26**, 116–132.
- Langner G. (1997b). "Neural processing and representation of periodicity pitch," *Acta Otolaryngol* **532**, 68–76.
- Levy K. L., and Kipke D. R. (1997). "A computational model of the cochlear nucleus octopus cell," *J. Acoust. Soc. Am.* **102**, 391–402.
- Levy K. L., and Kipke D. R. (1998). "Mechanisms of the cochlear nucleus octopus cell's onset response: Synaptic effectiveness and threshold," *J. Acoust. Soc. Am.* **103**, 1940–1950.
- Liberman M. C. (1993). "Central projections of auditory nerve fibers of differing spontaneous rate. II: Posteroventral and dorsal cochlear nuclei," *J. Comp. Neurol.* **327**, 17–36.
- MacGregor R. J. (1987). *Neural and brain modeling*. Academic Press, Inc., San Diego, Cal.
- Meddis R., Hewitt M. J., and Shackleton T. M. (1990). "Implementation details of a computation model of the inner hair-cell/auditory-nerve synapse," *J. Acoust. Soc. Am.* **87**, 1813–1816.
- Meddis R. (1986). "Simulation of mechanical to neural transduction in the auditory receptor," *J. Acoust. Soc. Am.* **79**, 702–711.
- Meddis R. (1988). "Simulation of auditory-neural transduction: Further studies," *J. Acoust. Soc. Am.* **83**, 1056–1063.

- Oertel D., Bal R., Gardner S. M., Smith P. H., and Joris P. X. (2000). "Detection of synchrony in the activity of auditory nerve fibers by octopus cells of the mammalian cochlear nucleus," PNAS. National Academy of Sciences Colloquium on Auditory Neuroscience: Development, Transduction and Integration .
- Oliver D. L., and Huerta M. F. (1991). "Inferior and superior colliculi," . In Webster D. B., Popper A. N., and Fay R. R., editors, *The mammalian auditory pathway: Neuroanatomy*. Springer-Verlag, New York.
- Palmer A. R., and Winter I. M. (1993). "Coding of the fundamental frequency of voiced speech sounds and harmonic tone complexes in the cochlear nerve and ventral cochlear nucleus," . In Merchan M. A., Juiz J. M., Godfrey D. A., and Mugnaini E., editors, *The Mammalian Cochlear Nuclei: Organization and Function*. Plenum Press, New York.
- Palmer A. R. (1982). "Encoding of rapid amplitude fluctuations by cochlear-nerve fibers in the guinea pig," Arch. Otol. Rhinol. Laryngol. **236**, 197–202.
- Palombi P. S., and Caspary D. M. (1992). "GABA_A receptor antagonist Bicuculline alters response properties of posteroventral cochlear nucleus neurons," J. Neurophysiol. **67**, 738–746.
- Patterson R. D., Nimmo-Smith I., Holdsworth J., and Rice P. (1988). "An efficient auditory filterbank based on the gammatone function," 1988. APU report 2341, Applied Psychology Unit, Cambridge.
- Rees A., and Møller A. R. (1983). "Responses of neurons in the inferior colliculus of the rat to AM and FM tones," Hear. Res. **10**, 301–330.
- Rees A., and Palmer A. R. (1989). "Neuronal responses to amplitude-modulated pure-tone stimuli in the guinea pig inferior colliculus and their modification by broadband noise," J. Acoust. Soc. Am. **85**, 1978–1994.
- Rhode W. S., and Greenberg S. (1994b). "Encoding of amplitude modulation in the cochlear nucleus of the cat," J. Neurophysiol. **71**, 1797–1825.
- Rhode W. S., and Smith P. H. (1986). "Encoding timing and intensity in the ventral cochlear nucleus of the cat," J. Neurophysiol. **56**, 261–286.
- Rhode W. S., Oertel D., and Smith P. H. (1983). "Physiological response properties of cells labeled intracellularly with horseradish peroxidase in the cat ventral cochlear nucleus," J. Comp. Neurol. **213**, 448–463.

- Rhode W. S. (1994a). "Temporal coding of 200% amplitude modulated signals in the ventral cochlear nucleus of cat," *Hear. Res.* **77**, 43–68.
- Romand R. (1978). "Survey of intracellular recording in the cochlear nucleus of the cat," *Brain Res.* **148**, 43–65.
- Rose G. J., and Capranica R. R. (1985). "Sensitivity to amplitude modulated sounds in the anuran auditory nervous system," *J. Neurophysiol.* **53**, 446–465.
- Rose J. E. (1970). "Discharges of single fibers in the mammalian auditory nerve," . In Plomp R., and Smoorenburg G. F., editors, *Frequency analysis and periodicity detection*. A.W. Sijthoff, Leiden.
- Rosen S. (1992). "Temporal information in speech: acoustic, auditory and linguistic aspects," *Philos. Trans. R. Soc. London B Biol. Sci* **336**, 367–373.
- Saint Marie R. L., Shneiderman A., and Stanforth D. A. (1997). "Patterns of gamma-aminobutyric acid and glycine immunoreactivities reflect structural and functional differences of the cat lateral lemniscal nuclei," *J. Comp. Neurol.* **389**, 264–276.
- Schouten J. F., Ritsma R. J., and Cardoza B. L. (1962). "Pitch of the residue," *J. Acoust. Soc. Am.* **34**, 1418–1424.
- Schreiner C. E., and Langner G. (1988). "Periodicity coding in the inferior colliculus of the cat. II. Topographical organization," *J. Neurophysiol.* **60**, 1823–1840.
- Schreiner C. E., and Langner G. (1997). "Laminar fine structure of frequency organization in auditory midbrain," *Nature* **388**, 383–386.
- Smith P. H., and Rhode W. S. (1989). "Structural and functional properties distinguish two types of multipolar cells in the ventral cochlear nucleus," *J. Comp. Neurol.* **282**, 595–616.
- Stevens K. N. (1995). "Applying phonetic knowledge to lexical access," 1995. In: *Fourth European Conference on Speech Communication and Technology*. Volume 1. Madrid, Spain.
- Sumner C. J., Lopez-Poveda E. A., O'Mard L. P., and Meddis R. (2002). "A revised model of the inner-hair cell and auditory-nerve complex," *J. Acoust. Soc. Am.* **111**, 2178–2188.
- Sumner C. J., Lopez-Poveda E. A., O'Mard L. P., and Meddis R. (2003). "Adaptation in a revised inner-hair cell model," *J. Acoust. Soc. Am.* **113**, 893–901.

- Tuckwell H. C. (1988). *Introduction to theoretical neurobiology*. Volume 1. Cambridge University Press, Cambridge, England.
- Wenthold R. J., Zempel J. M., Parakkal M. H., Reeks K. A., and Altschuler R. A. (1986). "Immunocytochemical localization of GABA in the cochlear nucleus of guinea pig," *Brain Res.* **380**, 7–18.
- Wenthold R. J., Altschuler R. A., and Reeks K. A. (1987). "Glycine immunoreactivity localized in the cochlear nucleus and superior olivary complex," *Neuroscience* **22**, 897–912.
- Winter I. M., and Palmer A. R. (1995). "Level dependence of cochlear nucleus onset unit responses and facilitation by second tones or broadband noise," *J. Neurophysiol.* **73**, 141–159.
- Yost W. M. (1996). "The pitch of iterated rippled noise," *J Acoust Soc Am* **100**, 511–518.
- Zwicker E., Flottorp G., and Stevens S. S. (1957). "Critical bandwidth in loudness summation," *J. Acoust. Soc. Am.* **29**, 548–557.

CURRICULUM VITAE

Name Ulrike Dicke
Birth 22 May 1972 in Bremerhaven
Nationality German
Marital status Single

Education

since 06.2000 Work on doctoral thesis at the Carl von Ossietzky University of Oldenburg, Germany.

07.1999–11.1999 Research Assistant at the University of Bern, Switzerland.

03.1998–06.1999 Research Assistant at the Trinity College Dublin, Ireland.

1993–1997 Student of Physics at the University of Bremen, Germany.
Diplom (Master's Degree in Physics) in December, 1997.
(Title: "The development of a neural network model for the description of the effects of short-term plasticity in the mammalian somatosensory cortex")
Diplomvorprüfung (First Graduation in Physics) in July, 1994.

1991–1993 Student of Physics at the Technical University Carolo Wilhelmina zu Braunschweig, Germany.

1988–1991 Schulzentrum Bürgermeister Smidt (Gymnasium) in Bremerhaven, Germany.
Erwerb der allgemeinen Hochschulreife (Final examination) in June, 1991.

1984–1988 Wilhelm Raabe Schule (Gymnasium) in Bremerhaven.

1982–1984 Johann Gutenberg Schule (Orientierungsstufe) in Bremerhaven.

1978–1982 Fritz Husmann Schule (Grundschule) in Bremerhaven.

Experience

since 06.2000 Member of the "International Graduate School for Neurosensory Science and Systems" at the University of Oldenburg, supported by the Deutsche Forschungsgemeinschaft.

1998–1999 Fellow of the SMART II (Semi-autonomous Monitoring And Robotics Technology) project funded by the European Community within the TMR (Training and Mobility of Researchers) network at the Trinity College Dublin.

Meinen besonderen Dank...

...an Herrn Prof. Dr. Dr. Birger Kollmeier, der mir die Durchführung dieser Arbeit in der “Medizinischen Physik” der Universität Oldenburg ermöglicht hat. Er weckte mein Interesse für das Gebiet der neuronalen Periodizitätskodierung und gewährte mir den Freiraum, den ich benötigte, um neue Ideen zu entwickeln und die vorgestellten Modelle zu erarbeiten.

...an Herrn Prof. Dr. Volker Mellert für seine Bereitschaft, das Korreferat dieser Arbeit übernehmen.

...an Herrn Prof. Dr. Torsten Dau für sein Engagement bei der Betreuung dieser Arbeit. Besonders möchte ich ihm für seine motivierende Art danken und für seine unermüdliche Bereitschaft, diese Arbeit zu korrigieren.

...an Herrn Dr. Stephan D. Ewert für seine geduldige Hilfe und Ausgeglichenheit in unseren Diskussionen über die vorgestellten Modelle.

...an die Kolleginnen und Kollegen in der “Medizinischen Physik” sowie im “Internationalen Graduiertenkolleg Neurosensorik” für die gute Zusammenarbeit und die vielen anregenden Diskussionen.

...an meine Eltern und Geschwister dafür, dass sie immer für mich da sind und mich unterstützen.

Erklärung

Hiermit erkläre ich, dass ich die vorliegende Arbeit selbstständig verfasst und nur die angegebenen Hilfsmittel verwendet habe.

Oldenburg, den 4. November 2003

Ulrike Dicke